

**DYNAMICS AND CONTROL OF CHEMICAL WAVES
IN HETEROGENEOUS BZ REACTION**

Thesis

Submitted in partial fulfilment of the requirements for the degree of

DOCTOR OF PHILOSOPHY

by

Amrutha S V

Reg.No. 155070 PH15F01



**Department of Physics
NATIONAL INSTITUTE OF TECHNOLOGY KARNATAKA (NITK)
SURATHKAL, MANGALORE - 575 025
September 27, 2023**

DECLARATION

By the Ph.D. Research Scholar

I hereby *declare* that the Research Thesis entitled “**DYNAMICS AND CONTROL OF CHEMICAL WAVES IN HETEROGENEOUS BZ REACTION**”, which is being submitted to the *National Institute of Technology Karnataka, Surathkal* in partial fulfilment of the requirements for the award of the Degree of *Doctor of Philosophy* in *Physics* is a *bonafide report of the research work carried out by me*. The material contained in this thesis has not been submitted to any University or Institution for the award of any degree.


27/9/23

Amrutha S V

Register No.: 155070 PH15F01

Department of PHYSICS

National Institute of Technology Karnataka,
Surathkal

Place: NITK, Surathkal

Date: September 26, 2023

CERTIFICATE

This is to *certify* that the Research Thesis entitled “**DYNAMICS AND CONTROL OF CHEMICAL WAVES IN HETEROGENEOUS BZ REACTION**”, submitted by **Amrutha S V** (Register Number: 155070 PH15F01) as the record of the research work carried out by her, is *accepted* as the *Research Thesis submission* in partial fulfillment of the requirements for the award of degree of *Doctor of Philosophy*.

Dr T K Shajahan
Research Guide
Assistant Professor
Department of Physics
NITK Surathkal - 575025



27/5/23

Chairperson - DRPC
(Signature with Date and Seal)

Dr. N.K. UDAYASHANKAR
PROFESSOR & HEAD
DEPARTMENT OF PHYSICS
NITK SURATHKAL, SRINIVASNAGAR
MANGALORE - 575 025, INDIA

Dedication

To my well-wishers

Acknowledgements

This thesis would not have been possible without the valuable guidance of my supervisor, Dr. Shajahan T K. Thank you for the continued support at every step, starting from the conception of the project to the writing of this thesis, offering motivation, warnings and insight at all the right times.

Besides my advisor, I would like to thank the other members of my thesis committee, Dr. Beneesh P B and Dr. H. S. Nagaraja, for their guidance and encouragement during all the committee meetings. My sincere thanks go to Dr. Beneesh P B for the guidance in performing the experiments and the discussions whenever needed. My sincere thanks to Dr. Ajith K M for his encouragement and support.

I sincerely thank Mr. Sibeesh P P for helping me develop the experimental setup. I thank Mrs. Anupama Sebastian and Dr. Shreyas Punacha for carrying out all the numerical simulations required for my work. Furthermore, I would like to thank Mrs. Anupama Sebastian, for helping me develop the theory for unpinning spiral waves using electric fields. I thank all the master's students who worked in our lab.

I am thankful to my friends Dr. Ahmed Rizwan C L, Ms. Rajani K V, Mr. Safir T K, Dr. Siby Thomas, Mr. Ahmed Kasim K, Mrs. Sherin Thomas, and Dr. Sterin N S for their support.

I am thankful to all the staff of the Department of Physics for their cooperation during my research period. I am grateful for the financial support from the National Institute of Technology Karnataka Surathkal as a Ph.D. stipend and for covering the costs of conferences. I am thankful to the Department of Science and Technology, Science Education and Research Board of the Government of India for the financial support in setting up the laboratory.

I am grateful to my Father, Parameswaran V M, my Mother, S V Santha, and my Sister, Thulasi, who have provided me with moral and emotional support. Many thanks to my husband, Vineesh J, for his unconditional support and patience during all the tough times. I could not end without thanking my daughter Tanmaya, who suffered greatly from my increased stress.

I thank each and every one who has supported me along the way.

Statements of Contribution

1. This thesis is based on the following articles.
 - Amrutha, S.V, Sebastian, A., Sibeesh, P., Punacha, S., and Shajahan, T.K (2022). Mechanism of spiral wave unpinning in the Belousov–Zhabotinsky reaction with a dc electric field. *The Journal of Physical Chemistry C*.
 - SV, Amrutha, Anupama Sebastian, Puthiyapurayil Sibeesh, Shreyas Punacha, and T. K. Shajahan. Theory and experiments of spiral unpinning in the Belousov-Zhabotinsky reaction using a circularly polarized electric field. *Chaos* 33, 063157 (2023).
2. The publications not included in the thesis are listed at the end of the thesis under the section titled ‘publications.’
3. All the simulation details included in this thesis are performed by Anupama Sebastian and Dr. Shreyas Punacha in our laboratory. It is included in the thesis for the reason of continuity only.

ABSTRACT

The Belousov-Zhabotinsky (BZ) reaction is the prototype of a large class of systems that display excitation waves, including the physiological systems such as the heart, brain, and retina. Excitation waves in these systems exhibit similar spatiotemporal patterns, such as expanding target waves or rotating spiral waves. A characteristic feature of the rotating spiral waves is their tendency to pin to heterogeneities in the system. These stable pinned waves can cause fatal cardiac arrhythmias in systems like the heart. Hence the external control of rotating waves is an important requirement. Several studies proposed methods for controlling pinned waves using an external electric field. Field-induced unpinning in the cardiac system is well explored and found to be due to the secondary wave emission from the heterogeneities. The pinned chemical waves can also be unpinned with an electric field. However, secondary wave emission is not observed in the chemical medium. So the mechanism of unpinning is very different for the pinned waves in the BZ reaction as opposed to such waves in the cardiac tissue.

This thesis investigates the mechanism of spiral wave unpinning in the BZ reaction using static and rotating electric fields. The unpinning occurs if the applied field strength equals a particular threshold. Using different electric fields, we measured the unpinning phase of the spiral around the obstacle boundary. In a static DC field, independent of the initial phases, the spiral unpins at a fixed unpinning phase for a chosen field strength and chirality. When the initial phase is close to the unpinning phase, the unpinning happens with a fixed delay. Spirals with opposite chirality unpin mirror-symmetrically. In a rotating circularly polarised electric field (CPEF), the unpinning phase changes according to the initial phases and the rotational frequencies of both the field and the spiral. Not only a high-frequency CPEF but also a relatively slow-rotating CPEF or a CPEF with the same frequency as the spiral can induce unpinning if it possesses a threshold amplitude.

However, in every case, the spiral unpins as it propagates away from the anode. As the spiral propagates away from the anode, the electric force opposes its natural propagation. If the applied field strength is equal to a particular threshold, the opposition experienced in the spiral propagation leads to unpinning of the tip from the obstacle. The analytical formulae based on this assumption accurately predict the unpinning phase, and the values match well

with our observations. Such an unpinning by an opposing electric force is not seen in any other excitable medium. We conclude that, in the BZ medium due to the advective motion of the ions the chemical excitation waves interact with an applied electric field uniquely. We hope our work will provide a better understanding of the control of excitation wave dynamics using an external electric field.

Keywords: Excitable Medium, Spiral Waves, Chirality, Belousov-Zhabotinsky Reaction, Chemical waves, Unpinning, Electric Field

Contents

List of figures	vi
List of tables	vii
1 Introduction	1
1.1 Excitable media	2
1.2 The oscillating BZ reaction	4
1.3 Properties of chemical waves and their scope	8
1.4 Objectives of the Thesis	13
1.5 Organisation of the Thesis	17
2 Methods	19
2.1 Experiments on BZ reaction	19
2.2 Experimental Method	21
2.2.1 Chemicals and concentration	21
2.2.2 Method of wave generation	22
2.2.3 Experimental Design	25
2.2.4 Method of unpinning	27
2.3 The Oregonator model	30
3 Mechanism of spiral wave unpinning in the Belousov-Zhabotinsky reaction with DC electric field	35
3.1 Introduction	35
3.2 Methods	38
3.2.1 Experimental methods	38
3.2.2 Numerical methods	39

3.3	Results and discussion	40
3.4	Conclusions	49
4	Theory and experiments of spiral unpinning in the Belousov-Zhabotinsky reaction using a circularly polarized electric field	53
4.1	Introduction	53
4.2	Methods	55
4.2.1	Experimental Methods	55
4.2.2	Numerical methods	56
4.3	Results and Discussions	57
4.3.1	Anti-clockwise spiral	58
4.3.2	Clockwise spiral	66
4.4	Conclusions	68
5	Conclusions	71
	References	73
	List of publications	83

List of Figures

1.1	Concentration profile in BZ reaction	3
1.2	Action potentials	4
1.3	The BZ oscillation cycle	6
1.4	Oscillations and patterns	7
1.5	Spiral waves	10
1.6	Field interaction of target waves	11
1.7	Wave acceleration in electric field	12
1.8	Wave splitting in electric field	13
1.9	Spiral drift in an applied electric field	14
1.10	Spiral wave drift in BZ reaction	14
1.11	Unpinning Sutthiapod	16
2.1	Excitation waves in BZ reaction	23
2.2	Effect of temperature on BZ oscillations	23
2.3	Temperature effect on BZ patterns	25
2.4	Experiemntal arrangement	25
2.5	Camera and captured image	26
2.6	A free spiral wave in BZ reaction and the intensity-time series plot	27
2.7	Pinned spiral wave in BZ reaction	27
2.8	Angle measurement in GIMP	28
2.9	DAQ device	29
2.10	Experimental arrangement for electric field application	30
3.1	Spiral drift in a DC field	36
3.2	Schematic of Experimental set up	39
3.3	Defining unpinning	41

3.4	Unpinning sequence	42
3.5	Unpinning sequence with a glass rod	42
3.6	Unpinning at threshold	43
3.7	Unpinning phase with initial phase	44
3.8	φ_u with φ_0- comparison between spiral pinned to bead and rod	45
3.9	Effect of field direction on unpinning	46
3.10	Schematic of unpinning at threshold field	47
3.11	Verification of analytical formula	48
4.1	CPEF-Experiment setup	56
4.2	Unpinning sequence of an ACW spiral	58
4.3	Schematic diagram showing the mechanism of unpinning	59
4.4	Unpinning at $E_0 > E_{th}$	60
4.5	$(\varphi_u - \varphi_0)$ versus p for ACW spiral	62
4.6	Unpinning with different shaped obstacles	63
4.7	φ_u versus φ_0	64
4.8	Unpinning for $p = 1$	65
4.9	Unpinning sequence of a CW spiral	66
4.10	Unpinning of a CW spiral: $\varphi_u - \varphi_0$ versus p	67
4.11	Unpinning of a CW spiral for $p = 1$: $\varphi_u - \varphi_0$ versus φ_0	68

List of Tables

2.1	Belousov's recipe	20
2.2	Concentration and volume of reagents	22
2.3	Effect of temperature on pattern formation	24

Chapter 1

Introduction

Summary

This chapter briefly introduces the excitable media, focusing on the dynamics of spatio-temporal patterns in the oscillating Belousov-Zhabotinsky (BZ) reaction. It includes a detailed literature survey, scope, and research objectives. In the end, an organization of the thesis is also presented.

Oscillating or periodic phenomena such as the motion of the simple pendulum, the planetary motion, and biological clocks governing the life of living organisms are familiar to the scientific world. However, the scientific community largely disregarded the idea of oscillating chemical systems. It was thought that analogous to a simple pendulum, a chemical reaction must transit the equilibrium multiple times to carry out oscillations. However, according to the second law of thermodynamics, a chemical system cannot return from the equilibrium composition. Later in the 1970s, Prigogine and colleagues showed that the chemical oscillations never pass through the equilibrium but operate far from the equilibrium ([Prigogine and Lefever \(1968\)](#)). In chemical systems far from equilibrium, periodic oscillations can occur in the concentrations of intermediate species, but the initial reactant and final product concentrations do not oscillate. The field of nonlinear chemical dynamics was developed from this understanding.

G.T. Fechner reported oscillations in a chemical system in 1828. He explained the generation of an oscillating current in an electrochemical cell. The Liesegang rings, or patterns reported in 1898 by Raphael Liesegang, are another example of chemical oscillation ([Pechenkin \(2018\)](#)). In 1899, Ostwald noticed periodic variations in the chromium

dissolution rate in acid (Ostwald (1899)). All these systems were heterogeneous. Bray discovered the first homogeneous chemical medium, which exhibited oscillations in 1921 (Bray (1921)), and it is named the Bray-Liebhafsky (BL) reaction. In the BL reaction, iodate catalyzes the decomposition of hydrogen peroxide into oxygen and water. The modern era in the study of chemical oscillations began with an accidental discovery by the Russian chemist B. P. Belousov in 1958. In a homogeneous solution of bromate, citric acid, and cerium ions, Belousov observed periodic oscillation with continuous stirring. In a similar but unstirred system, chemical waves have appeared. However, his study was disregarded by the scientific community. Later, A. M. Zhabotinsky repeated Belousov's work and was able to publish the results (Zhabotinsky (1964); Zaikin and Zhabotinsky (1970)). Hence, the reaction is named the Belousov-Zhabotinsky (BZ) reaction.

Scientists noticed a close similarity in the dynamical behaviors observed in the oscillating chemical medium and biological phenomena, such as electrical impulse propagation in the heart and the brain and signaling waves in a group of social amoeba. The dynamical behaviors match so well that all these systems with identical qualitative features are grouped as excitable media. The characteristics of the excitable media are briefly explained in the following section.

1.1 Excitable media

Excitable media are a group of nonlinear dynamical systems, including various biological, chemical, and physical systems. An excitable system is continuously distributed in space. Each point in the system is excitable *i.e.*, the system possesses the property of excitability. Excitation is a rapid sequence of variations in a system-specific parameter in response to specific changes in the medium, known as the exciting stimulus. The element gets excited if the exciting stimulus reaches a certain threshold value. This excitation activated at a single element in the medium can spread from one element to another through local transport processes such as diffusion. This enables the propagation of excitation waves in the medium without damping. An excitation wave comprises two processes: the first one is a sudden transition from a stable rest state to an excited state. The second process involves a slow transition to the initial rest state. The time required for this transition is known as the refractory period. During the refractory period, the medium will not respond to any stimulus,

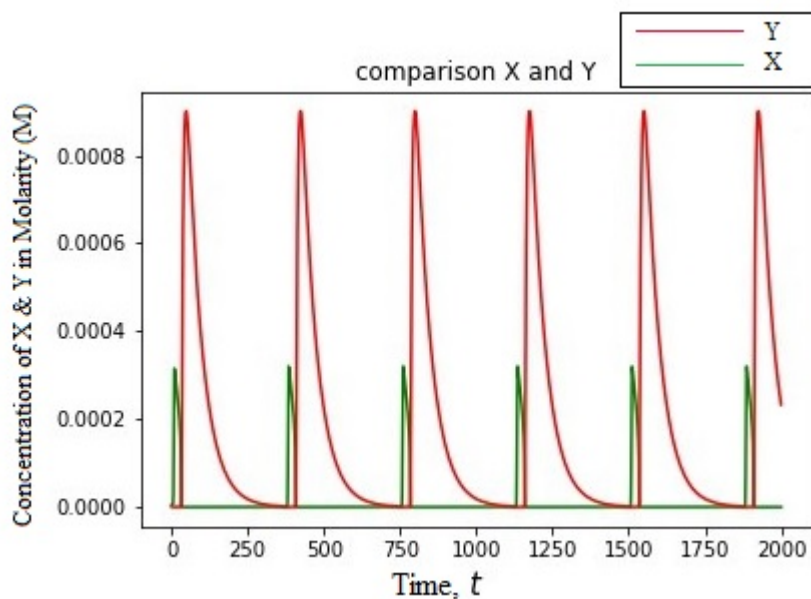


Figure 1.1: Concentration profiles of bromous acid and bromide ions: Each peak in the concentration profile of bromous acid corresponds to the excitation in BZ reaction

even above the threshold. A generic example of an excitable medium is a forest. A wildfire travels as a wave from the point of initiation. It transfers from vegetation to vegetation by burning the prior. It is impossible to fire a burnt spot again. In order to fire a burnt spot, the vegetation has to regrow in that area. Hence, the fire cannot propagate backward. The time required for the regrowth of the vegetation can be regarded as the refractory period of the system.

The autocatalytic production of $HBrO_2$ (Fig.1.1) corresponds to the excitation or action potential generation in the BZ reaction. The cardiac and neuronal action potential diagrams (Fig.1.2) look similar to the given concentration profile. In the BZ reaction, the exciting stimulus is a low concentration of bromide ions. The region between two successive chemical wavefronts is the refractory state. Due to the existence of the refractory state, the waves in excitable media undergo mutual annihilation on collision. The characteristic features of an excitable medium are:

- the existence of a stable rest state and an excited state
- a minimum threshold for excitation
- a refractory time period without any sort of excitation.

Before any excitation, there are no spatial or temporal patterns in an excitable medium, and the medium is said to have a spatio-temporal symmetry. Excitation (a localized disturbance of a specific threshold) at a particular spatial point breaks the symmetry by inducing excitation in the neighboring positions. The transport of excitation among the neighboring parts of the medium results in the formation of spatial patterns. Hence, these patterns are the result of the self-organization of the medium. The concentric wave patterns sometimes break, and they self-organize into rotating spiral wave patterns in two dimensions and scroll wave patterns in three dimensions.

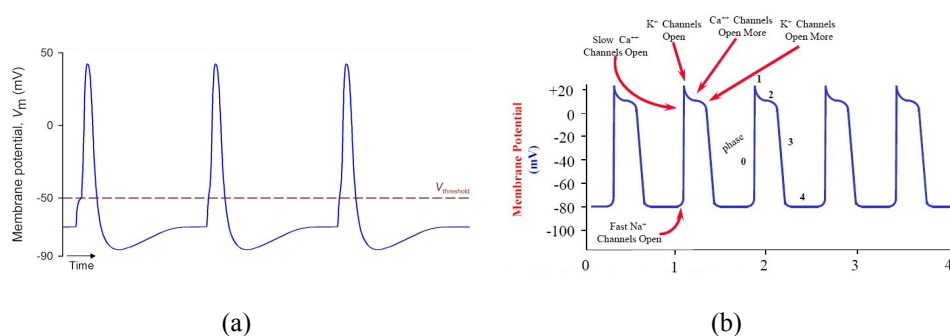


Figure 1.2: Action potential diagrams in (a) neuron and (b) heart.

Examples of excitable media include physiological systems such as cardiac myocytes ([Alonso et al. \(2016\)](#)), nerve cells, and pancreatic beta cells. Intracellular calcium waves in *Xenopus* oocytes ([Chatterjee and Sain \(2022\)](#)), cAMP waves in the colonies of starving slime mold amoeba ([Sawai et al. \(2005\)](#)), chemical waves in the Belousov-Zhabotinsky reaction ([Mikhailov and Showalter \(2006\)](#)), muscle contractions during childbirth in the uterine tissue, and patterns formed during the CO-oxidation reaction on Pt(110) surface ([Sadeghi et al. \(2012\)](#)) are examples of excitation wave propagation.

The work included in this thesis focuses on the dynamics and control of the chemical waves in the BZ reaction in an external electric field. Hence, in the next section, we discuss the mechanism of the BZ reaction and the process of chemical wave formation.

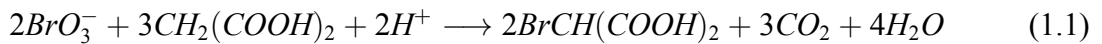
1.2 The oscillating BZ reaction

Belousov-Zhabotinsky reaction is a self-organizing chemical system that shows periodic oscillations in time and forms spatial patterns. The most common patterns are stationary

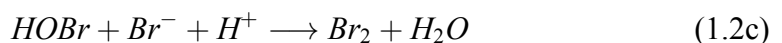
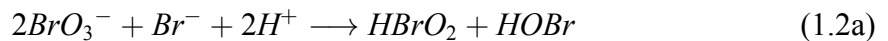
Turing patterns (Vanag and Epstein (2008)), target (concentric rings) (Zaikin and Zhabotinsky (1970); Zhabotinsky and Zaikin (1973)), spiral (Zhabotinsky and Zaikin (1971); Winfree (1972)), and scroll waves (three-dimensional spiral waves) (Winfree (1974)). In the decades that followed the discovery of the BZ reaction, scientists elucidated the central features of its chemical mechanism (Field et al. (1972)). Later studies found other chemical systems with similar dynamical behaviors (Sadeghi et al. (2012); Agladze and Steinbock (2000)). Based on the reaction mechanism, mathematical models describing the dynamics of the BZ system were developed (Field and Noyes (1974)). These models then found applications in studying the biological systems (Shanks (2001)).

The basic mechanism of the BZ reaction was elucidated by Field, Koros, and Noyes in 1972 (Noyes (1972)), and it was named the FKN mechanism. The FKN mechanism provides an abstract framework for understanding and modeling various spatio-temporal phenomena observed in the BZ system. However, the whole reaction mechanism of the BZ system is very complex. For example, Benini *et al.* (Benini et al. (1996)) proposed a model for the Ce(IV)/Ce(III)-catalyzed BZ reaction, which includes 80 elementary steps and 26 variables.

The BZ reaction typically involves the bromination of an organic acid. The important process in this reaction is the formation of bromous acid ($HBrO_2$) by an autocatalytic, nonlinear process. The main components of the BZ reaction are a one-electron metal redox catalyst (often Ce^{3+}/Ce^{4+} or Fe^{2+}/Fe^{3+}), a readily brominatable and oxidizable organic substrate (typically malonic or citric acid), and bromate ions. They are all dispersed in nitric or sulfuric acid. The whole reaction can be expressed as in Eq.1.1.



According to the FKN mechanism, the BZ reaction has three main processes. The reduction of BrO_3^- occurs in the first process. Along with that, malonic acid brominates in the first process.



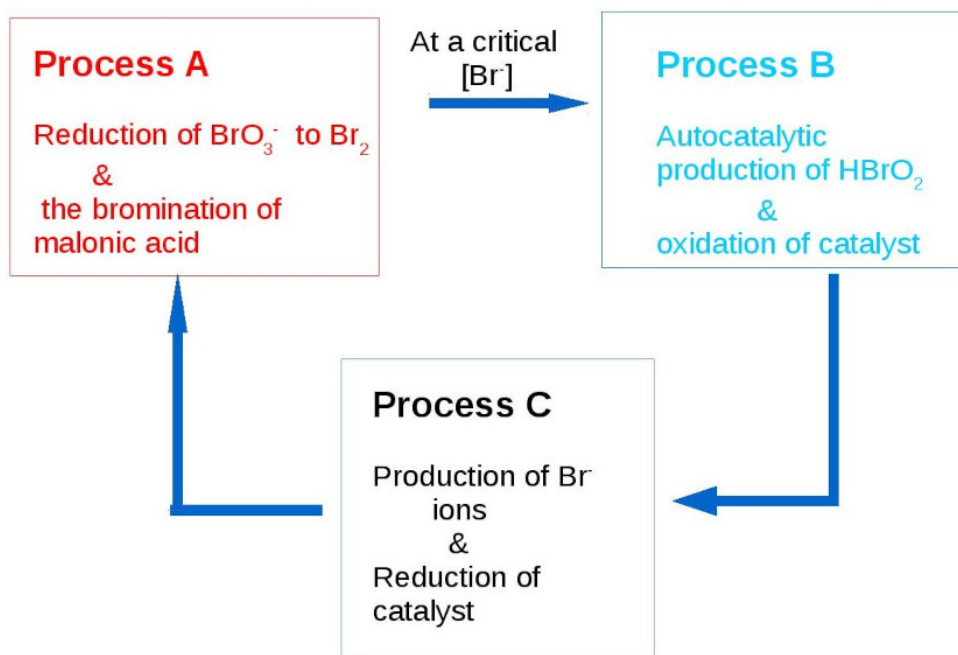
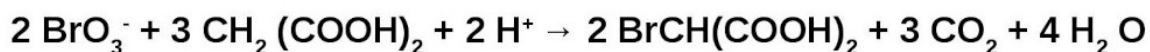
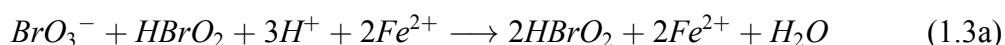
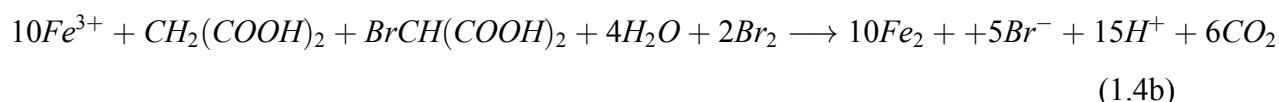
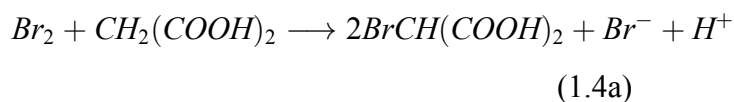


Figure 1.3: The BZ oscillation cycle: When Process A leads to a low critical concentration of bromide ions, Process B induces an autocatalytic production of the bromous acid. Process C occurs as the oxidized catalyst accumulates in the system. Process C produces bromide ions and regenerates ferrous ions.

Autocatalytic production of bromous acid and the oxidation of the catalyst happens in the second process.

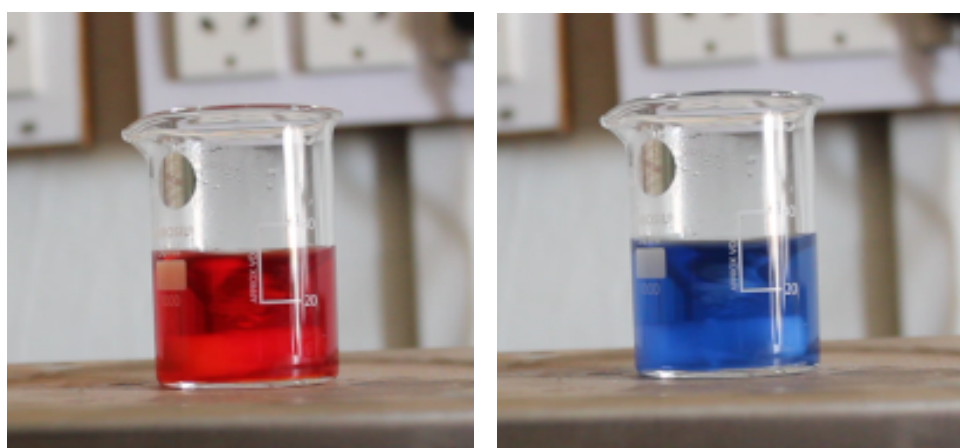


The catalyst reduction and the production of bromide ions occur in the third process.



The reaction cycle is represented in Fig.1.3. The concentration of bromide ions in the system is high at the beginning. In a slow reaction occurring in the first process, bromate

and malonic acid react and produce bromomalonic acid and water. Bromous acid is one of the reaction intermediates in this pathway. As the reaction proceeds, the concentration of bromous acid decreases. At this stage, the reaction medium remains red since the ferriin catalyst is in the reduced state (Fe^{2+}) (Fig.1.4a). As the reaction proceeds, the concentration of Br^- ions falls to a critical level where only a few bromous acid is available to start a reaction that results in bromomalonic acid and water. As the catalyst oxidizes, the reaction media turns blue (Fig.1.4b). In addition to the oxidation of the catalyst, an autocatalytic step occurs in which two moles of bromous acid are produced from one mole of bromous acid.



(a) BZ solution in red color

(b) BZ solution in blue color



(c) Excitation waves in BZ reaction

Figure 1.4: **Oscillations and spatial patterns in BZ reaction:** (a) Reduced BZ solution in red color at $t = 1.37$ minutes. (b) Oxidized BZ solution in blue color at 1.47 minutes after mixing the reagents. (c) Target waves formed in the BZ gel.

The third process begins when the oxidation of the catalyst is complete. Carbon dioxide and bromide ions are produced in the third process. The Fe^{2+} regenerates in the third process

by consuming bromomalonic acid, malonic acid, and ferric ions. Thus, the medium turns red and begins a new cycle. The oscillations occur until the system reaches the equilibrium state.

When the reaction occurs in an unstirred thin reactant film, the oscillations transform into traveling concentration disturbances known as chemical waves. The points where the waves initiate are called pacemaker sites. Concentric wave patterns propagate away from the pacemaker site (Fig.1.4c). A color contrast exists between the chemical waves and the medium because the catalyst possesses different colors for different oxidation states.

The chemical wave propagation is mainly due to the diffusion of bromous acid. The bromous acid diffuses ahead of the wavefront, and its autocatalytic production occurs just behind the advancing wavefront. Due to the autocatalytic process, the concentration of $HBrO_2$ suddenly increases by several orders of magnitude. The reactions occurring behind the wavefront inhibit the production of bromous acid. The region with a low bromous acid concentration corresponds to the refractory state of the medium, where wave does not exist. So, the waves can only propagate away from the pacemaker sites but not toward them.

Based on the FKN mechanism, an abstract mathematical model known as the Oregonator model is developed to explore the BZ dynamics. The actual chemistry behind the reaction has been significantly idealized and simplified in this model. The BZ reaction and the Oregonator model (Field and Noyes (1974)) have been used to explore various phenomena observed in excitable systems.

In the next section, we will discuss the dynamics and control of chemical waves in the BZ reaction and its applicability in other fields of excitable media.

1.3 Properties of chemical waves and their scope

In an unstirred BZ medium, the coupling of the reaction and diffusion process induces a beautiful set of propagating chemical waves. The spontaneous formation of chemical waves in the medium is related to a local decrease in the concentration of bromide ions. In a heterogeneous medium, the inhibitor bromide ions can be adsorbed on the surface of

the heterogeneity, resulting in a local decrease in its concentration (Zhang et al. (1992)). In a homogeneous chemical system, the fluctuations in the local reagent concentrations lead to the formation of pacemaker sites (Belousov (1973)). A target pattern is a group of concentric waves propagating from a single pacemaker site (Fig.1.4c). The early studies by Zhabotinsky (Zaikin and Zhabotinsky (1970); Belousov (1973)) and Winfree (Winfree (1972, 1973)) characterized the feature of target patterns (or traveling waves) in two-dimensional layers of unstirred BZ reaction solution. The velocity of wave propagation varies depending on the diffusion of the activating and inhibiting species, the time period of oscillations (dispersion relation), and the curvature of the wavefront (eikonal relation).

The idea of the spontaneous formation of traveling waves in a homogeneous system and its propagation in a single direction provides a method to construct self-propelled objects displaying functional motions in various biological and artificial systems (Suematsu and Nakata (2018); Kumar et al. (2021)). Chemical computing, a developing strategy used in information processing, is also based on chemical wave propagation. The interest in applications of the chemical excitable system for information processing (Igarashi et al. (2006); Gruenert et al. (2013); Oliver et al. (1996); Szymanski et al. (2011)) is motivated by similarities with signaling in neural systems. Achieving controllability over the chemical wave dynamics is essential to develop a programmable chemical computer using the BZ reaction.

If a concentric wave is broken mechanically or by interaction with heterogeneity, the free ends will curl and form counter-rotating spiral wave patterns (Winfree (1972)). The self-sustaining spiral waves rotate around its tip. The spiral tip is a phase singularity where the excitation front and the recovering tail come together. The circular area around which the tip rotates is called the spiral core. Generally, the spiral wave exhibits rigid rotation around its core. With the variations in the chemical concentrations, the tip can move in different trajectories like a circle, epicycle, or floral trajectories (Jahnke et al. (1989)). Winfree noted this motion as meandering. The spiral waves have a shorter period and higher stability than concentric waves. A spiral wave acts like an organizing center in a homogeneous medium and imposes its pattern throughout the medium. All the spirals in a given system possess the same frequency.

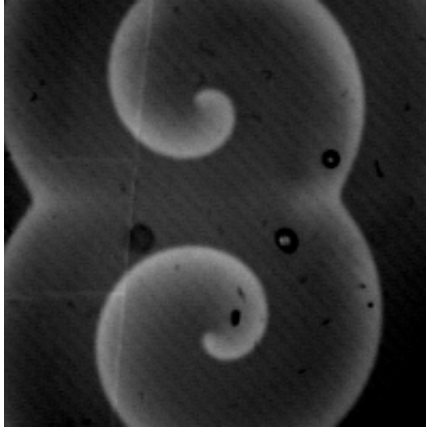


Figure 1.5: A counter-rotating spiral pair in the BZ reaction

Interactions of the spiral wave with heterogeneities induce stabilizing or destabilizing effects. The interaction between spiral waves and heterogeneities can cause wave breaks, forming multiple spirals and leading to turbulence. The tip of spiral waves can also pin or anchor to inexcitable obstacles present in the medium. This phenomenon is known as pinning. Pinning stabilizes the rotation centers and highly elongates the lifetime of rotating waves in the medium. In 1993, Steinbock *et al.* reported a systematic study about the pinning of spiral waves in the BZ reaction. The study was carried out in the photosensitive BZ reaction (Steinbock and Müller (1993)). The heterogeneity was created using a laser spot. As the size of the circular pinning heterogeneity increases, the wave period, wavelength, and velocity of the spiral also increase. In a three-dimensional BZ reaction, the intrinsic contraction of a scroll ring can be suppressed by pinning (Jiménez *et al.* (2009)). The studies on the rotating spiral waves and their pinning are influenced by their role in developing dynamic diseases in biological systems such as cardiac tissue; so do their unpinning by external means.

Motivated by many of the previously mentioned applications, numerous studies on controlling excitation wave dynamics are carried out in the BZ reaction. Varying chemical composition (Steinbock *et al.* (1993); Mahanta *et al.* (2018); Sibeesh *et al.* (2022)), medium temperature (Wood and Ross (1985); Teng *et al.* (2019)), and external field interaction (Ševčíková and Marek (1983); Agladze and De Kepper (1992); Schmidt and Müller (1997)) can alter the wave dynamics in the BZ medium.

As we have seen in the reaction mechanism of BZ reaction, the three fundamental chemical species which affect the wave propagation are Br^- ions, $HBrO_2$, and Fe^{3+} ions. The presence of mobile ionic species ensures a direct interaction between the chemical waves and the applied electric field. In the external electric field, the positive ions drift in the direction of the field, and the negative ions drift in the opposite direction. Hence, the external application of an electric field offers a flexible way to control the chemical wave dynamics.

The interaction of the target wave with a DC electric field leads to a variety of wave dynamics, including wave splitting (Fig. 1.8), reversal, and annihilation in the BZ medium (Feeney et al. (1981); Ševčíková and Marek (1983); Ševčíková et al. (1996)). The first experiments of the electric field influence on chemical waves in the BZ medium were reported by Feeney et al. (Feeney et al. (1981)) in 1981. The applied DC electric field caused a variation in the wave velocity and the annihilation of waves propagating toward the negative electrode in a threshold field. A new chemical wave with a crescent shape has been formed in the presence of an external field. The experimental observations match the theoretical predictions based on the FKN kinetics.

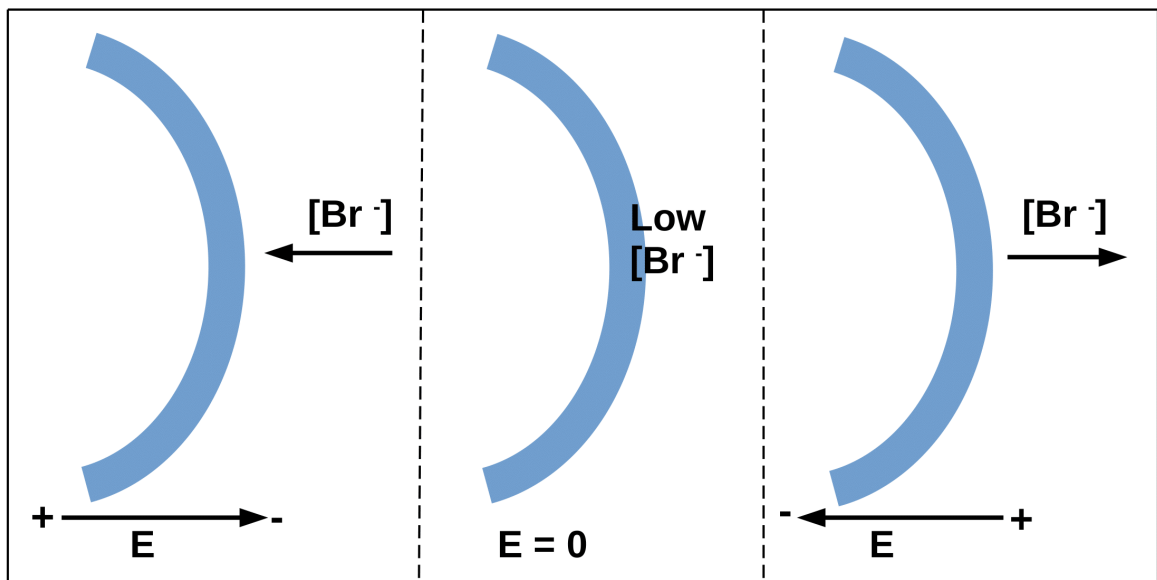


Figure 1.6: The interaction between the chemical wave and an electric field: In a zero-field ($E = 0$), the concentration of Br^- ions is low on a propagating wavefront and close in front of the wave boundary. If the electric field and the wave propagation are in the same direction, the Br^- ions diffuse against the wave. If the direction of the applied field is opposite to the wave propagation, the Br^- ions diffuse and move ahead of the wave.

As mentioned earlier, the decrease in the concentration of Br^- ions enables the autocatalytic production of $HBrO_2$. The autocatalytic production of $HBrO_2$ leads to the generation of an oxidation wave, high in concentrations of $HBrO_2$ and Fe^{3+} ions. The concentration of Br^- ions is low on a propagating wavefront and close in front of the wave boundary (Fig.1.6). Suppose that a chemical is propagating along the direction of the applied electric field. Then, the Br^- ions diffuse in a direction opposite to the wave propagation, causing an increase in its concentration close in front of the wave boundary. An increased bromide ion concentration causes retardation in the autocatalytic process and hence, a slowdown in the wave propagation. Suppose the applied field and the wave propagation are in opposite directions. Here, the Br^- ions diffuse and move ahead of the wave boundary. So, the bromide ion concentration in front of the boundary decreases faster than in the case of zero-field. A low bromide ion concentration in front of the wave boundary helps accelerate the wave. We applied a DC electric field to the BZ medium and measured the position of the wavefront traveling toward the anode and the cathode, respectively. The plot of position versus time shows an increase in the wave speed while moving toward the anode. The decrease in the wave speed while propagating toward the cathode is not observable; instead, the wavefront travels with a constant velocity (Fig.1.7). The wave velocity depends linearly on the intensity of the applied field (Ševčíková and Marek (1983)).

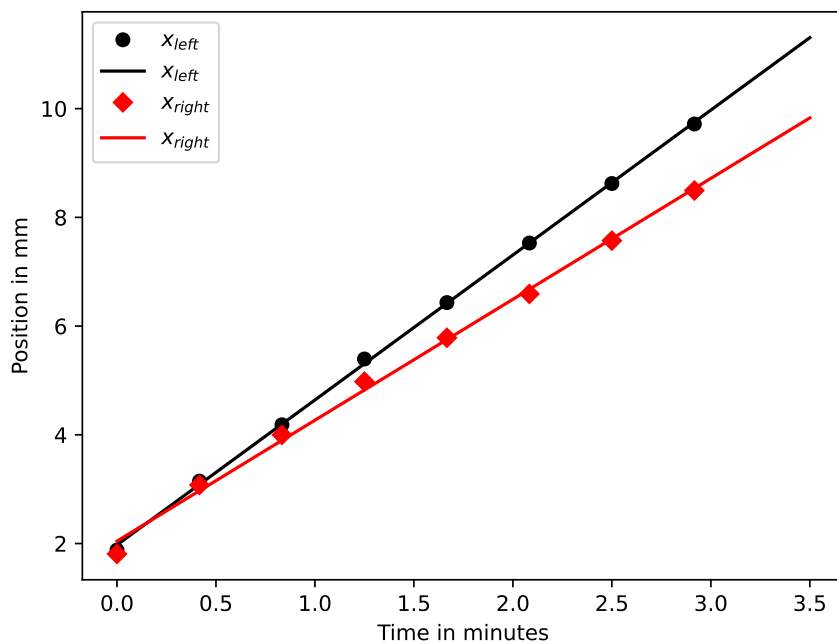


Figure 1.7: Wavefront positions of a target wave propagating toward the anode (black circles) and the cathode (red diamonds) are plotted against time, t . The anode and the cathode are placed on the left and right, respectively. The field strength is 2.0 V/cm.

The wave splitting and annihilation phenomenon can also be explained based on ionic migration. The wavefront with low bromide ion concentration widens at a larger positive electric field. When the area of low bromide ion concentration is sufficiently large, a new wave begins to form from the wave back. The newly created waves travel faster in the opposite direction. This is observed as wave splitting.

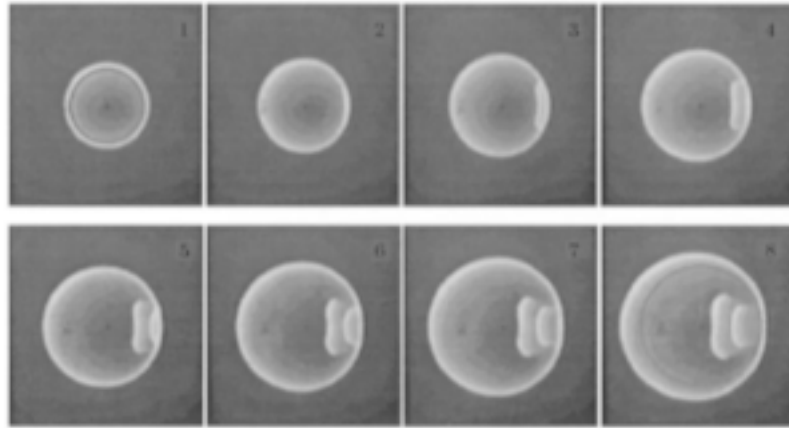


Figure 1.8: Two additional wave segments split and propagate away from the circular wave in an applied electric field. The field intensity is 4.06 V/cm. The electric field directs from left to right (Ševčíková et al. (1996))

Wave annihilation occurs due to the increased concentration of bromide ions in front of the leading wave boundary. Then, the autocatalytic production of bromous acid gets suppressed, and the concentration of Fe^{3+} decreases. Hence, the wave became extinct.

1.4 Objectives of the Thesis

In this thesis, we work on the spiral wave of chemical activity in the BZ medium. The spiral waves drift in a constant DC electric field (Agladze and De Kepper (1992); Steinbock et al. (1992); Schmidt and Müller (1997)). The spiral drifts with two velocity components. One of the two components is parallel to the electric field, and the other is perpendicular to the field. The parallel component always directs toward the anode. The perpendicular drift direction varies according to the spiral chirality (Fig.1.9).

The term chirality represents the direction of spiral rotation. A spiral wave can have either clockwise or anti-clockwise chirality. A higher field induces a more significant drift of the spiral wave.

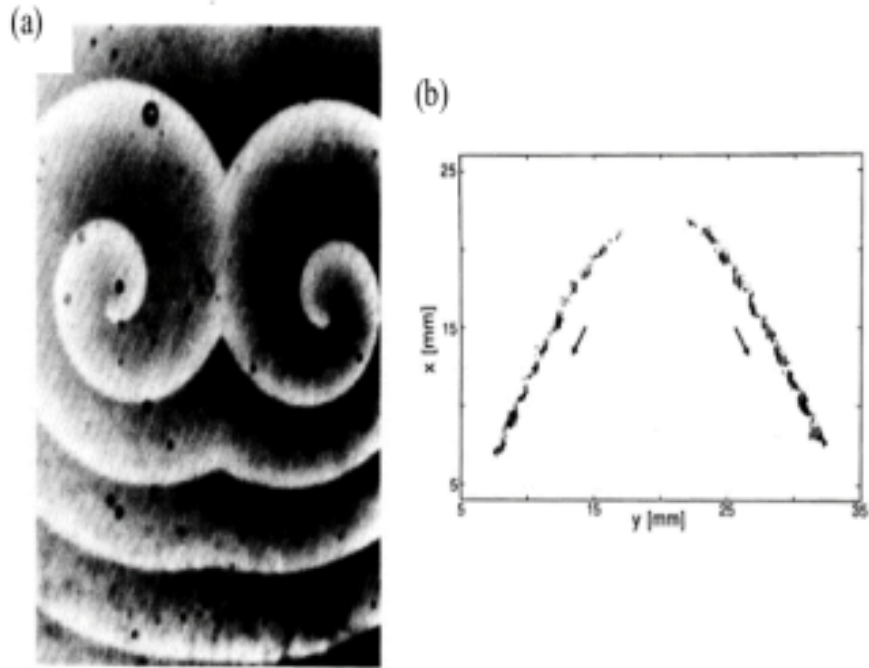


Figure 1.9: A spiral wave drifts toward the anode with a perpendicular velocity component. The direction of the perpendicular drift is decided by the spiral chirality (Schmidt and Müller (1997))

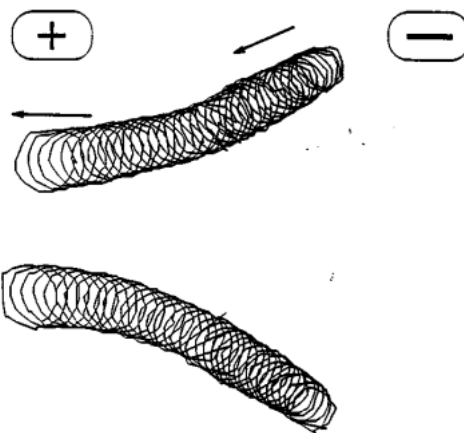


Figure 1.10: The upper clockwise-rotating spiral and the lower counterclockwise-rotating spiral are pulled together in a field directed along the positive X-axis (Schmidt and Müller (1997))

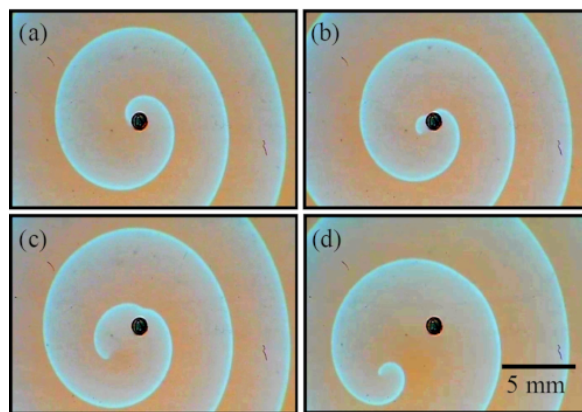
An external electric field changes the speed of spiral propagation. The wave propagation, as well as the tip rotation, slows down while moving toward the negative electrode. The spiral tip rotates around a large core as the spiral slows down. The tip rotates more quickly around a small core when propagating toward the positive electrode (Steinbock et al. (1992)). A repulsing force exists between a counter-rotating spiral pair. This force depends on the distance between the cores. However, the spirals annihilate each other after reaching

a minimum inter-core distance. In Fig. 1.10, the electric field is directed along the positive X-axis. The upper spiral rotates in a clockwise direction, and the lower spiral rotates in a counterclockwise direction. The counter-rotating spirals are pulled together in the applied field (Fig. 1.10). By reducing the mutual distance, this effect can force an interaction between the spirals (Schmidt and Müller (1997)).

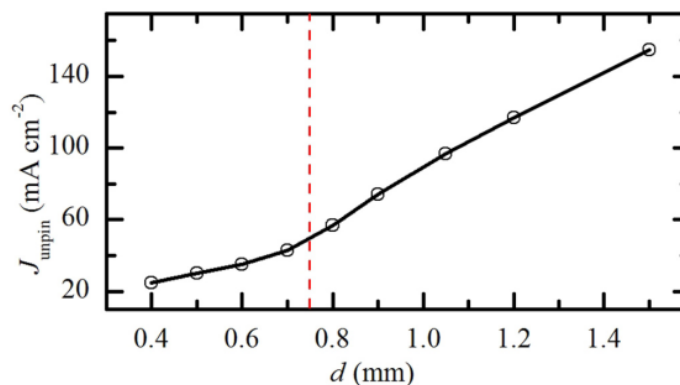
Apart from the DC electric field, many groups studied the response of free spirals to AC and polarized electric fields (Li et al. (2017)). The spiral waves in the BZ reaction experience a directional drift in an AC electric field of frequency twice that of the spiral rotation (Munuzuri et al. (1994)). The spiral drift direction continuously changes when the phase difference between the spiral and the electric field changes from 0° to 180° . The theory of spiral drift in AC and polarized electric field has been studied in numerical simulations using the response function theory (Li et al. (2017)). The interaction of the spiral wave with a rotating electric field is studied by considering the fact that the spiral waves and the electric field possess rotation symmetry. A circularly polarised electric field (CPEF) rotates at a constant rate with constant magnitude. Hence, CPEF is spatially uniform. So, a CPEF can simultaneously control the dynamics of multiple spiral waves in a medium similarly. An applied CPEF is said to be co-rotating if it rotates along the same direction as the spiral rotation. The term counter-rotation is used to represent the rotation in opposite directions. In a high-frequency co-rotating CPEF, the spiral drifts the fastest (Chen et al. (2006)), and a counter-rotation between the two locks the spiral. A co-rotating CPEF with a frequency near the spiral frequency can synchronize the spiral rotation with an entrainment ratio of 1:1 (Chen et al. (2009)). Rotating waves of a particular chirality can be chosen in a medium by tuning the frequency of the applied CPEF (Li et al. (2014)). Experiments in the BZ reaction have shown that spiral turbulence can be successfully controlled with CPEF (Ji et al. (2013)). The applied CPEF with a higher frequency than the turbulent system synchronizes multiple spirals. The high-frequency spirals become dominant in the system and thus control the turbulence.

Elimination of the spiral waves has a life-saving motivation since they cause lethal ventricular fibrillation. As mentioned earlier, controlling pinned rotating vortices is more challenging to achieve. To eliminate them, first, they have to be unpinned from the heterogeneities. Numerous experimental and computational studies have reported the ability of an applied

electric field to unpin a pinned spiral from the heterogeneity. The mechanism of unpinning in the cardiac excitable system is well explored. In the cardiac system, secondary wave emission occurs from the heterogeneity in the presence of an electric field with threshold amplitude. The induced waves have higher frequencies than the pinned waves. These high-frequency secondary waves lead to unpinning in such systems. This method of unpinning in the cardiac system is known as the wave emission from heterogeneities (WEH) (Pumir et al. (2007)). A good number of studies show the unpinning of pinned spiral waves by WEH with pulsed electric field (Luther et al. (2011); Punacha et al. (2019)) and rotating circularly polarized electric field (Feng et al. (2014); Pan et al. (2016); Punacha et al. (2020)). Unpinning by the method of WEH using a CPEF has shown to be more effective in the case of an excitable cardiac system.



(a) Spiral unpinning in the BZ reaction



(b) Plot of threshold current density with obstacle size

Figure 1.11: (a) Snapshots of field-induced spiral unpinning in the BZ reaction. The field is directed along the positive x-axis. (b) The threshold current density linearly increases with the obstacle size (Sutthiopad et al. (2014)).

With an external electric field, the chemical waves in the BZ reaction can also be unpinned. The existing unpinning studies in the BZ reaction have used only unidirectional (DC) electric fields. Sutthiopad *et. al* (Sutthiopad et al. (2014)) shown that spiral unpinning is possible in the BZ reaction if the applied current is above a threshold value (Fig.1.11). This threshold increases linearly with the radius of the pinning heterogeneity (Porjai et al. (2016)). Unpinning spiral waves pinned to larger obstacles are more difficult because of the high critical threshold (Sutthiopad et al. (2014)). The unpinning of scroll rings in the BZ reaction, pinned to two unexcitable spheres, occurs when a DC electric field is applied to a three-dimensional system (Jiménez et al. (2013)). However, a secondary wave emission is not observed in the chemical excitable medium. So, the mechanism of field-induced unpinning in the BZ reaction must be different and has not been addressed so far.

Therefore, we propose to find out the mechanism of unpinning in the BZ reaction with an applied electric field. Also, we try to perform experiments of spiral unpinning in BZ reaction with a rotating circularly polarized electric field (CPEF).

Thus, the objectives of this study are as follows:

- To provide a mechanism for the field-induced unpinning of spiral waves in the BZ reaction using a DC electric field.
- To perform the unpinning of pinned spirals using a rotating circularly polarized electric field (CPEF) in the BZ reaction by changing different medium and field parameters and to address the mechanism of spiral unpinning.

1.5 Organisation of the Thesis

The work included in this thesis concerns the dynamics and control of chemical excitation waves using external electric fields. We use the excitable BZ reaction for the study. The field-induced unpinning is explained based on the diffusion of ionic species in the BZ system.

The thesis consists of four chapters. Chapter 1 briefly introduces the excitable media in general, focusing on the dynamics and control of two-dimensional rotating waves in the BZ medium through external means. This chapter also includes the relevant literature survey,

the research scope, and the research objectives. At the end of this chapter, an organization of the thesis is also presented.

Chapter 2 presents the experimental methods and the mathematical model necessary to understand this study. This chapter briefly details the experimental setup and numerical techniques used in this work.

Chapter 3 is based on the mechanism of spiral unpinning in the BZ reaction in a constant DC electric field. Here, we systematically investigate the process of unpinning experimentally for spiral waves having different chirality. The experimental result is compared with simulations performed using the Oregonator model. (The co-authors Anupama Sebastian and Dr. Shreyas Punacha carry out all the numerical work in this thesis.)

Chapter 4 presents the unpinning of spiral waves using a circularly polarized electric field (CPEF). Here, we discuss the mechanism of unpinning spiral waves with CPEF of different frequencies and validate the experimental observations with numerical results.

Chapter 5 summarizes the research work presented in this thesis. It also includes concluding remarks and the scope for future research in these areas.

Chapter 2

Methods

Summary

This chapter briefly describes the experimental methods and numerical model necessary to understand the concepts presented in this thesis.

2.1 Experiments on BZ reaction

Belousov found that oscillations could be generated in a liquid state homogeneous system while developing a model of the Krebs cycle (Field (1985)). In living cells, the chemical energy adenosine triphosphate (ATP) is produced through the Krebs cycle. The cell utilizes ATP for a variety of biological functions, including the production of proteins and the contraction of muscles. The ion citrate is a significant reaction intermediate in the Krebs cycle. Hence, along with bromate and Ce^{4+} salts, Belousov used citric acid as the substrate for his model reaction. He noticed color oscillations from yellow to clear in a stirred reaction solution. He explained the color change based on the changes in the oxidation states of cerium ions. The reduced cerium ions Ce^{3+} do not have any color, but the oxidized state (Ce^{4+}) possesses a yellow color. The chemical reagents used by Belousov are shown in Table 2.1. Zhabotinsky developed the reaction by replacing the cerium catalyst with ferroin complex and the citric acid with malonic acid (AM (1964)). He obtained an oscillating chemical system with noticeable color variations, and it is now frequently employed as a model system in nonlinear dynamics.

Table 2.1: Concentrations of reagents used by Belousov

Reagent	Concentration
Cerium(IV) sulfate (CeSO ₄)	0.04 M
Potassium bromate (KBrO ₃)	0.01 M
Sulfuric acid (H ₂ SO ₄)	0.80 M (approx.)
Citric acid (C ₆ H ₈ O ₇)	0.87 M

Several different Belousov-Zhabotinsky reaction recipes have been employed until now (Jahnke and Winfree (1991)). Generally, all the BZ systems are catalyzed by transition metal ions such as cerium, iron, manganese, and ruthenium complexes. Using Ru(II/III) complexes as the catalyst makes the system photosensitive (Steinbock et al. (1993)). Many systems have also used Co, Cu, Cr, Ag, Ni, and Os complexes. Systems with different catalysts have distinct behaviors since the catalyst affects the oscillation frequency of the system. Hence, developing a generalized model (Ganaie and Peerzada (2009); Körös (1974); Hu et al. (2006)) is difficult. Both high- and low-reduction potential couples are used as catalysts in the BZ reaction. Each type provides a different chemical mechanism for oxidizing the organic substrate (Körös et al. (1974); Ganapathisubramanian and Noyes (1982)). In general, the catalyst for the BZ reaction can be a transition metal ion with a single valence electron and a standard redox potential in the range 0.9 to 1.6 V (Vavilin et al. (1969)).

In most common cases, malonic acid is used as the substrate in the BZ reaction because it provides a more contrasted environment for studying chemical waves rather than citric acid, which was initially used in Belousov's experiments. It is possible to use a variety of oxidizable organic substrates in the BZ reactions. For example, bromomalonic acid (Benini et al. (1998)), 1,4-cyclohexadione (Hamik et al. (2001); Kurin-Csörgei et al. (1996)), oxalic acid (Krüger et al. (1995)), tartronic acid, mesoxalic acid (Krüger et al. (1995)), resorcinol (Ganaie and Peerzada (2009)), xylose (Rastogi et al. (2004)) and aldoses (Sevcik and Adamcikova (1985)) can replace malonic acid.

The pattern formation studies in the BZ reaction can be performed using gels (Yamaguchi et al. (1991)), membranes (Winston et al. (1991)), beads of ion exchange resin (Maselko and Showalter (1989)), and mesoporous glasses (Amemiya et al. (1995)). The reaction can be performed either in both open or closed reactors. In open reactors (e.g., continuously fed

tank reactors - CFTR) (Tam et al. (1988)), the required far-from-equilibrium conditions can be maintained indefinitely with the continuous supply of reactants. However, in a closed system like a Petri dish, the reaction runs for a fixed time period, depending on the initial conditions.

2.2 Experimental Method

Our experimental medium is an unstirred autocatalytic chemical system based on the typical BZ reaction. The unstirred BZ reaction exhibits various dynamic behaviors than the stirred system, including spatial patterns and propagating waves. We use malonic acid as the organic substrate and ferroin as the catalyst. The oxidizing agent is sodium bromate. Sulfuric acid is the source of hydronium (H^+) ions in our system. We use a closed system taken in a Petri dish. The reaction medium is immobilized using agar gel to avoid hydrodynamic perturbations. A single gel layer of thickness 3 mm is considered a two-dimensional system, and studies about the spiral dynamics are carried out in it.

2.2.1 Chemicals and concentration

Chemicals

- Sulfuric acid (H_2SO_4): a strong diprotic acid that makes the BZ reaction medium acidic.
- Sodium Bromate ($NaBrO_3$): an effective inorganic oxidant that brominates malonic acid.
- Malonic acid ($CH_2(COOH)_2$): It is a dicarboxylic acid. It has two acidic α -hydrogens. The α -hydrogens facilitate its bromination during the BZ reaction.
- Ferroin ($[Fe(o-phen)_3]SO_4$): 1,10-Phenanthroline iron(II) sulfate complex is known as ferroin. Its cation $[Fe(o-phen)_3]^{2+}$ can be oxidised to $[Fe(o-phen)_3]^{3+}$. The redox potential is 1.06V in 1M H_2SO_4 . The reduced ferroin is red, and in the oxidized state, it is blue.
- Agar ($C_{12}H_{18}O_9$): A polysaccharide used for gel preparation.

Concentration

The concentration and volume of each chemical reactant to prepare 25 ml of the BZ reaction gel is tabulated below Table 2.2.

Table 2.2: Concentration and volume of reagents

Reagent	Concentration (M)	Volume (ml)
H_2SO_4	0.5	8.0
$NaBrO_3$	1.0	1.0
Malonic Acid	1.0	1.0
Ferroin	0.025	0.5
Deionized water	-	14.5
Agar (only for gel)	1.4% w/v	

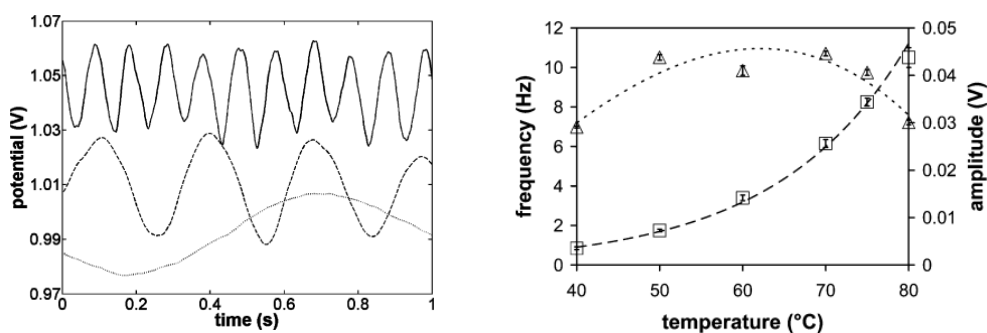
2.2.2 Method of wave generation

The gel medium to perform the experiments is prepared by mixing 0.20g of agar powder in 14.5 ml of deionized water. This mixture is kept for stirring and heating on a magnetic stirrer with a hot plate. When the solution starts boiling, it is transferred to a room-temperature heating plate, allowing it to cool. Reagents are added to this solution while stirring at 400 to 420 rpm. After one complete color oscillation (Fig. 1.4a,b), the solution is poured into a Petri dish and allowed to gel. The gel surface is touched with a silver wire to induce the pacemaker sites for excitation waves (Fig. 2.1). The silver reacts with the bromide ions, resulting in a local reduction of the inhibitor concentration. Hence, an oxidation wave will be generated from the point of contact. Spiral waves are generated by breaking a propagating circular wavefront using a stainless steel pin.



Figure 2.1: Target and spiral waves formed in the BZ gel.

The typical BZ oscillators driven by bromide ions sensitively depend on medium temperature. The first study about the temperature dependence of BZ oscillations was reported in 1974 by Koros. It was reported that the oscillatory frequency of the medium depends on the temperature (Körös (1974)). Many efforts have been made since then to comprehend the temperature-dependent oscillatory dynamics. Bansagi et al. have reported that high-frequency oscillations can be obtained in a homogeneous reaction medium by heating (Bánsági Jr et al. (2009)). The oscillatory frequency generally increases with an increase in temperature. With temperature, the BZ rate constants vary according to the Arrhenius law (Wood and Ross (1985)). The wavelength of chemical waves in the BZ reaction decreases linearly with the temperature (Teng et al. (2019)).



(a) Effect of temperature on oscillatory behavior (b) [Effect of temperature on frequency and amplitude

Figure 2.2: **(a)** The oscillatory behavior of the BZ reaction is plotted for three temperatures: dotted line for 40 °C, dashed line for 60 °C, and solid line for 80 °C **(b)** squares and triangles represent the initial oscillatory frequencies and amplitudes, respectively (in the temperature range 40-80 °C) (Bánsági Jr et al. (2009))

It is clear from the previous studies that the medium temperature has a major effect on the reaction behavior. We varied the cooling time of the boiled agar solution and measured the medium temperature before adding the reagents. The reaction behavior in a temperature range of 38°C to 53°C is recorded (Table 2.3). Room temperature varies from 28°C to 32°C . The cooling time varies according to the room temperature.

Table 2.3: Effect of temperature on pattern formation

Cooling time of boiled agar solution	Temperature of the solution when adding the reagents	The behavior of unstirred solution layer
10 minutes	Around $40 - 42^{\circ}\text{C}$	Colour oscillation is most prominent. No regular patterns (Fig.2.3a)
2minutes	Around 55°C	Oscillations occurred only during gelation. Regular patterns are observed (Fig.2.3b)
5minutes	Around 52°C	Possible to induce patterns at desired positions (Fig.2.3c)

For an average of 10 minutes, the temperature drops to $40 - 42^{\circ}\text{C}$. In this condition, the reaction medium oscillates through red and blue even after transferring to a Petri dish. For an average cooling time of 2 minutes, the medium showed several excitation patterns, including concentric and spiral waves. We can not induce patterns at desired positions in both cases. Hence, to optimize the temperature conditions, we repeated the experiments at temperatures between the above values. The reaction layer prepared after a cooling time of 4-6 minutes (temperature drops to $50 - 52^{\circ}\text{C}$) allows for inducing patterns at required positions.



(a) No excitation patterns (b) Many patterns at random positions (c) Central pattern

Figure 2.3: Snapshots of BZ reaction medium performed at different temperatures

2.2.3 Experimental Design

The experimental setup is shown in the Fig.2.4 given below.



(a) Experimental setup

(b) Stainless steel box

Figure 2.4: (a) the whole experimental arrangement and (b) stainless steel box to keep the petri dish and light source

The camera is kept above the glass petri dish containing the reaction solution. It is fixed on a tripod head (Vanguard Aluminium Tripod Espod CX203 AGH) and connected to a PC. A stainless steel box is designed to keep the petri dish and light source. The box has multiple slots to hold a plain glass sheet. The glass sheet is covered with a light-diffusing cloth. We placed the petri dish over this glass sheet (Fig.4.1b). A white light source (3 W and 8 W LED light) is kept below to illuminate the system.

Ferriin catalyst undergoes striking color changes, from red to blue, during each excitation cycle. The color variations make the optical detection of the excitation waves possible. Pattern formation in the reaction continues for 2-3 hours, and images are taken every 2 seconds.

We used a CCD camera to record the spatio-temporal patterns in the experimental medium (mvBlueCougarX120bC - Fig.2.5a). The lens of the camera is covered using a blue filter to enhance imaging. The captured image is in Fig.2.5b.

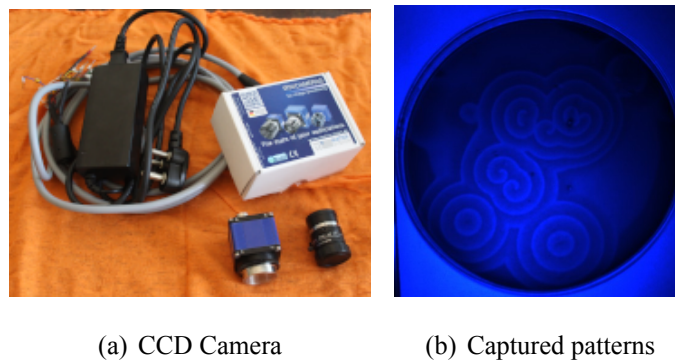


Figure 2.5: CCD camera (mvBlueCougarX120bC) and the captured image

Cameras with CCD sensors produce high-quality images with low noise. Our CCD camera can be connected to a computer through an Ethernet port. We can inspect, evaluate, and identify still or moving images through the computer. Such a device is known as a machine vision system. The main advantage of such machine vision cameras is that they expose all pixels simultaneously. So, a CCD camera gives an image undistorted by motion, which is better for making measurements from it. We use LabVIEW software (a virtual instrumentation platform from National Instruments) for data acquisition. LabVIEW (Laboratory Virtual Instrument Engineering Workbench) provides various features and tools. LabVIEW uses a graphical, general-purpose programming language known as G. For over two decades, NI-LabVIEW has been used to develop sophisticated test, measurement, and control applications. We have developed an image acquisition code in LabVIEW. The experimental data analysis mainly consists of image processing. The image data obtained from the LabVIEW program is processed with Python. The intensity-time series (Fig.2.6) plotted with the Python program helps determine the period of wave propagation.

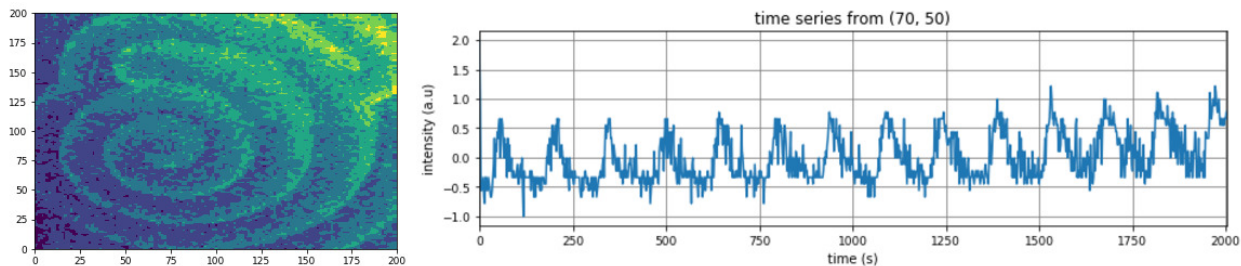


Figure 2.6: Pseudocolor image of a free spiral wave in the BZ reaction and the corresponding intensity-time series plot. The image is plotted in a 200×200 grid. The time series is plotted corresponding to the intensity variations at the point 70×50 .

2.2.4 Method of unpinning

For pinning to occur, the diameter of the heterogeneity must be comparable with the diameter of the spiral core. Also, pinning occurs only when the heterogeneity is inserted precisely at the spiral tip. We used glass beads with diameters varying from 1-5 mm as pinning heterogeneity (Fig.2.7). Cylindrical glass rods with similar diameters are also used as heterogeneity. Pinning of the spiral tip to the glass bead is confirmed only after 2-3 complete spiral rotations.

We induce the spiral wave only on the surface of the gel by touching it with the tip of a silver wire. The spherical glass bead is partially inserted into the medium so that the spiral tip on the gel surface gets pinned to the great circle of the sphere. Since the thickness of our medium (3 mm) is of the order of the spiral wavelength (3.696 mm), we expect a spherical bead to behave similarly to a cylindrical rod inserted vertically across the medium.

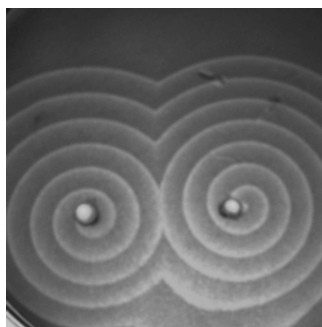


Figure 2.7: A counter-rotating spiral pair in the BZ reaction: The spiral on the left is pinned to a spherical bead, and the one on the right is free-rotating.

Silicate glass surfaces acquire a negative surface charge density when immersed in water. It is due to the dissociation of silanol groups. Behrens *et al.* (Behrens and Grier (2001))

estimates this is the order of mC/m^2 in deionized water. In electrolytes, this charge density decreases due to the screening effect of positive ions in the medium. The charge on the glass bead used in our experiment would be less than a few milli-Coulombs (mC) per glass bead due to the screening effect in an acidic medium. The negatively charged Br^- ions, which diffuse across the wavefront, possess a significant role in deciding the spiral propagation. Spiral pinning is possible only if the bromide ions overcome the repulsion from the acquired negative charge. Since pinning occurs successfully, it can be assumed that the induced charge is not significant enough to affect the experimental results.

For data analysis, we use the angular position of the pinned spiral around the obstacle boundary, denoted as the spiral phase. The software GIMP (GNU Image Manipulation Program) measures the spiral phase from the captured images. Fig.2.8 shows how to measure the angle using the software GIMP. The resolution of our camera is $0.07 \text{ mm}/\text{pixel}$. The maximum error in the measurement of the unpinning angle of the spiral in experiments shown in Fig.2.8 is ± 6 , which arises from the least measurable angle value, which in turn depends on the resolution of the camera. The minimum angle measured around a spherical bead of radius 0.6 mm is 6.7° . The minimum measurable angle for $r=0.75 \text{ mm}$ is 5.35° , and that for $r=0.9 \text{ mm}$ is 4.46° .

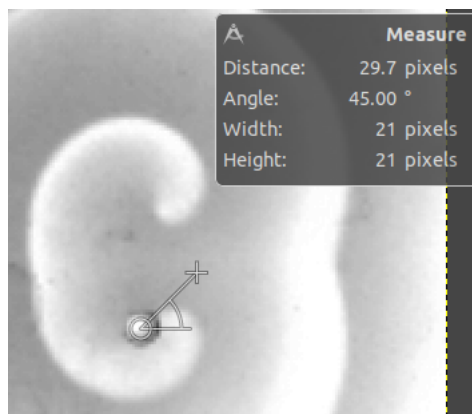


Figure 2.8: Angle measurement in GIMP: Angle (φ) is measured from the $+x$ -axis with the obstacle center as the origin.

Unpinning experiments will be performed in a constant DC and circularly polarized (CPEF) field. The input voltage signal is taken from a data acquisition device (NI USB-6343, X Series Multifunction DAQ from National Instruments - Fig.4.8).



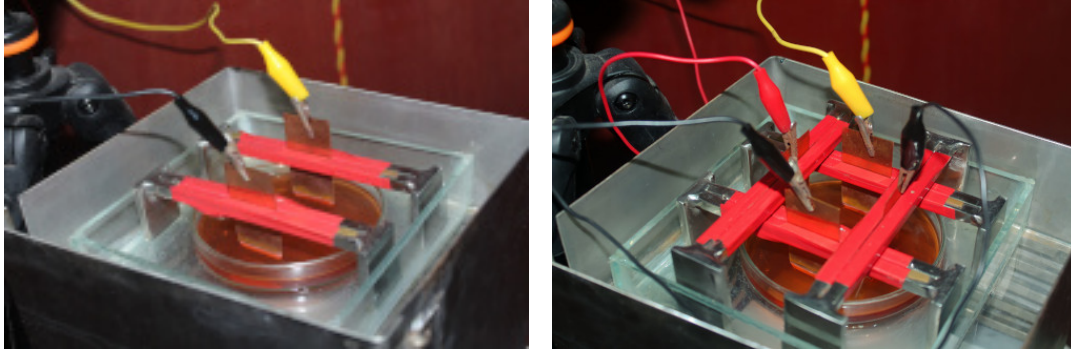
Figure 2.9: Data Acquisition device - DAQ (NI USB-6343, X Series Multifunction DAQ from National Instruments)

The DAQ is devised to measure or generate physical signals such as voltage. It initially gathers the signals from measurement sources. Then, the gathered signals are digitized for storage, analysis, and display on a personal computer. The maximum signal amplitude (V) obtained from the DAQ is 10 V. The field strength can also be controlled by changing the distance between the electrodes (d), according to the relation $E = \frac{V}{d}$.

Copper (Jiménez et al. (2013)), platinum (Ji et al. (2013)), and stainless steel (Ševčíková et al. (1996)) are used as electrodes in experiments of BZ reaction to apply an external electric field. We used copper electrodes because of their large availability at a lower cost.

In the case of copper, prolonged application of the electric field (more than 30 minutes) may result in a brown deposit around the anode. The deposition could be due to the oxidation of the copper electrode. Since the medium is immobilized in agar gel, the oxidation products can not diffuse into the observation area. Compared to the distance between the electrodes (5 cm), the observation area (1.5 cm × 1.5cm) is small, so the reactions near the electrode do not immediately affect the spiral wave. Moreover, the spiral unpins within one period of its tip rotation, around 4 minutes. Thus, the effect of electrode oxidation can be neglected in our experiments.

We applied the DC electric field through a pair of copper electrodes of dimension 5 cm x 2.5 cm x 0.25 mm each (Fig.2.10a). The rotating field is realized by applying two AC electric fields through two pairs of copper electrodes (Fig.2.10b). The ohmic heating can lead to a temperature rise in the reaction medium. We kept the whole reaction medium in a water bath to reduce the effect of ohmic heating.



(a) DC

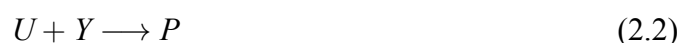
(b) CPEF

Figure 2.10: Electrode arrangement for (a) DC field and (b) CPEF

The two AC signals for generating the CPEF are applied to the medium with a phase difference of $\frac{\pi}{2}$. The frequency of the AC voltage signals is decided according to the frequency of spiral rotation in the medium. The frequency of the spiral wave is calculated with the relation $f_{spiral} = \frac{1}{T_{spiral}}$, where T_{spiral} is the time period of spiral rotation obtained from the intensity-time series plot (Fig.2.6).

2.3 The Oregonator model

The reaction mechanism developed by Field, Koros, and Noyes (the FKN model) forms the foundation for modeling studies of the BZ reaction (Field et al. (1972)). A three-variable model known as the Oregonator model encapsulates the vital characteristics of the FKN process. (Field and Noyes (1974)). This model explains how the chemical state changes over time. The Oregonator model works backward by initially understanding the idealized BZ mechanism to a mathematical abstraction that preserves the dynamical phenomena. The details of the actual chemistry underlying the reaction have been greatly idealized and simplified in this model. The Oregonator model can be understood from the following five chemical steps:





where $A = B = [BrO_3^-]$, $U = [HBrO_2]$, $Y = [Br^-]$, $V = 2[Fe^{3+}]$, P, Q=waste-product concentrations, and f is a stoichiometric factor whose value may vary. The rate equations can be written based on this model as follows:

$$\frac{dU}{dt} = k_1AY - k_2UY + k_{3,4}BU - 2k_5U^2 \quad (2.6)$$

$$\frac{dY}{dt} = -k_1AY - k_2UY + fk_6V \quad (2.7)$$

$$\frac{dV}{dt} = k_{3,4}BU - k_6V \quad (2.8)$$

where k_i 's ($i = 1$ to 6) are the rate constants.

Nonlinear dynamics often control excitable systems. These equations demonstrate the nonlinear dynamical nature of the Oregonator model. These differential equations can be expressed as follows using the parameters q, s, w and dimensionless variables u, y, v, τ :

$$\frac{du}{d\tau} = s(y - uy + u - qu^2) \quad (2.9)$$

$$\frac{dy}{d\tau} = \frac{1}{s}(-y - uy + fv) \quad (2.10)$$

$$\frac{dv}{d\tau} = w(u - v) \quad (2.11)$$

Here,

$$u = \frac{k_2}{k_1A}U \quad (2.12)$$

$$y = \frac{k_2}{k_{3,4}B} Y \quad (2.13)$$

$$v = \frac{k_2 K_6}{k_1 k_{3,4} AB} V \quad (2.14)$$

$$\tau = \sqrt{k_1 k_{3,4} AB} t \quad (2.15)$$

$$q = \frac{2k_1 k_5 A}{k_2 k_{3,4} B} \quad (2.16)$$

$$s = \sqrt{\frac{k_{3,4}}{k_1 A}} \quad (2.17)$$

$$w = \frac{k_6}{\sqrt{k_1 k_{3,4} AB}} \quad (2.18)$$

The stability of the steady-state solutions is used to analyze the dynamical behavior of the system. For the steady state, $\frac{du}{d\tau} = \frac{dy}{d\tau} = \frac{dv}{d\tau} = 0$. The steady state solutions are

$$v_0 = u_0 \quad (2.19)$$

$$y_0 = \frac{f u_0}{1 + u_0} \quad (2.20)$$

$$q u_0^2 + [q - (1 - f)] u_0 - (1 + f) = 0 \quad (2.21)$$

In the stationary state, the value of y can be related to u as $y = \frac{f u}{1 + u}$. Substituting this in the previous equations will reduce the three-variable model to a two-variable model.

$$\frac{du}{d\tau} = s \left(\frac{f u}{1 + u} - \frac{f u v}{1 + u} \right) + u - q u^2 \quad (2.22)$$

$$\frac{dv}{d\tau} = w(u - v) \quad (2.23)$$

By examining the stability of stationary state solutions, oscillations in the chemical system can be explained.

When the medium is not disturbed, the BZ reaction exhibits wave propagation and the formation of spatiotemporal wave patterns. Depending on the reagent concentration, the

medium can produce target and spiral waves in two dimensions and scroll waves in three dimensions. These patterns are produced due to the coupling between the reaction and diffusion processes. Consider a two-variable system (Eqs. 2.22 and 2.23) in the context of an oscillating stirred BZ medium, where u and v represent the concentrations of the autocatalytic and inhibitory species, respectively. The pattern formation, in this case, is the outcome of the coupling of the chemical processes $f(u, v)$ and $g(u, v)$, as well as the diffusion of the chemical species u and v . The rate equations are given by:

$$\frac{du}{d\tau} = f(u, v) + D \frac{\partial^2 u}{\partial x^2} \quad (2.24)$$

$$\frac{dv}{d\tau} = g(u, v) + D' \frac{\partial^2 v}{\partial x^2} \quad (2.25)$$

Here, D and D' denotes the diffusion coefficients for u and v respectively. These equations form a system of reaction-diffusion (RD) equations. Depending on the system dimensions, various wave patterns will emerge in the system. An external electric field can be added to the model equations as an advection term.

Chapter 3

Mechanism of spiral wave unpinning in the Belousov-Zhabotinsky reaction with DC electric field

Summary

In this chapter, we study the mechanism of spiral wave unpinning in the Belousov-Zhabotinsky (BZ) reaction with a DC electric field. We systematically analyze the unpinning by varying the chirality of spiral rotation, the initial phase of the spiral, the size of the pinning obstacle, the direction, and the strength of the applied electric field. We conclude from our observations that a retarding ‘electric force’ on the chemical wave is responsible for the unpinning in the BZ medium.

3.1 Introduction

According to previous studies, chemical waves are significantly affected by an applied electric field. In the beginning, the effects of electric fields on the chemical wave were studied theoretically using models based on the FKN kinetics ([Schmidt and Ortoleva \(1977, 1979, 1981\)](#)). The theoretical predictions were later confirmed in BZ experiments by [Sevcikova and Marek \(Ševčíková and Marek \(1983\); Sevcik and Adamcikova \(1985\)\)](#). It was found that in the presence of an external electric field, wave propagation velocity varies according to the field intensity and direction. The diffusion of chemical species in response to the applied electric field causes variations in the chemical wave dynamics. The three important chemical species that control the wave propagation in the BZ medium are Br^- ions,

$HBrO_2$, and Fe^{3+} ions. The Br^- and Fe^{3+} ions can directly interact with the applied electric field. In an external electric field, the Fe^{3+} ions drift in the direction of the field, and the Br^- drift in the opposite direction. Depending on the diffusion of ionic species, the propagation of chemical waves alters. A DC electric field applied in the BZ reaction can also cause annihilation and splitting of the waves (Feeney et al. (1981); Ševčíková and Marek (1983)).

The dynamics of spiral waves can also be controlled by an applied electric current (Agladze and De Kepper (1992); Steinbock et al. (1992); Pérez-Muñuzuri et al. (1992); Schmidt and Müller (1997)). Studies on how the electric field affects chemical waves have revealed that waves moving toward the anode are accelerated, while those moving toward the cathode are decelerated. This effect would cause a rotating spiral to move toward the anode. Experimental studies have been done on the influence of an electric field on a spiral wave and observed a directional drift towards the anode as expected.

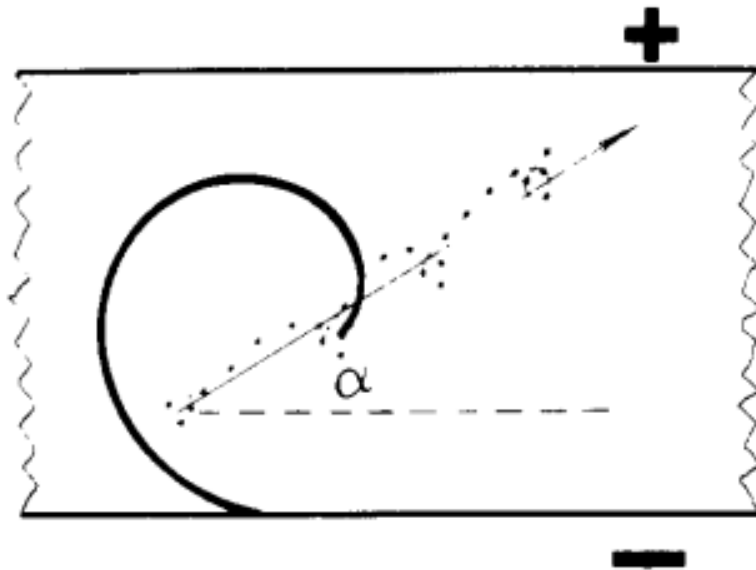


Figure 3.1: Spiral drift in an external electric field: The spiral wave drifts toward the anode with some angle α . The drift angle depends on the field intensity (Agladze and De Kepper (1992)).

Agladze *et al.* have given a simple mechanism to explain the drift of spiral waves in a unidirectional electric field (Fig.3.1). Each spiral rotation cycle in the presence of an electric field can be split into two halves depending on the orientation of the spiral tip. One half of the rotation is towards the anode and the other towards the cathode. According to the previous results, the wave propagation slows down when it propagates toward the cathode. As a result, the rotation of the tip slows down, and it rotates around a large core. On the other hand, in

the other half, when the tip is oriented towards the anode, its rotation speeds up, and the spiral rotates around a small core. The consequence is the drift of the spiral tip in an entire cycle, as depicted in the picture (Fig.3.1). The tip shifts faster if the difference between the core size is larger.

The increase of the spiral wave core observed by Perez-Munuzuri *et al.* (Pérez-Muñuzuri *et al.* (1992)), in a circular electric field centered at the core, can be explained by the large and small core effect of the electric field. When a positive constant voltage is applied to the central electrode, the period, wavelength, and core size of the spiral wave increase by a factor of up to three, but a negative voltage does not affect the spiral wave characteristics. A low-frequency alternating current affects the spiral wave as a direct current does. The observed results were explained by assuming an electrostatic interaction around the electrode at the spiral core. Near the central electrode, the concentration of inhibitor bromide ions increases with voltage. The increase in the bromide ion concentration delays the autocatalytic process and, hence, the excitation in the medium.

According to the observations, there exists an unexpected perpendicular spiral drift component to the field direction. The perpendicular drift component is comparable to, or even greater than, the parallel drift component. The direction of the perpendicular drift component is determined by the chirality of the spiral (Agladze and De Kepper (1992); Steinbock *et al.* (1992); Schmidt and Müller (1997)). Munuzuri *et al.* (Muñuzuri *et al.* (1993)) suggested that the spiral dynamics in an electric field strongly depend on the contraction and elongation of the spiral tip. The width, w , of a spiral wave, is related to its velocity as $w = \tau V$, where τ is the wave duration. According to the relation, the electric field also affects the width of the wave. The width of the rotating tip modulates periodically; it increases or decreases when the tip propagates to the positive or negative electrode. The elongation of the tip caused by changes in w produces a perpendicular drift component whose direction is determined by the chirality of the rotating spiral.

It is well known that the tip of a rotating spiral wave can pin to inhomogeneities present in the medium. Pinning alters the wave parameters such as the wave period, wavelength, and velocity depending on the size of the pinning obstacle (Lim *et al.* (2006); Sutthiopad *et al.* (2015)). An electric field can unpin a pinned spiral wave if the applied current is above a

threshold current density (Sutthiopad et al. (2014)). This threshold increases linearly with the size of the pinning heterogeneity (Sutthiopad et al. (2014); Porjai et al. (2016)). A study in a three-dimensional BZ system demonstrated that pinned scroll waves could also be unpinned by external electric fields (Jiménez et al. (2013)). However, the mechanism of unpinning is very different for the pinned waves in the BZ reaction as opposed to such waves in the cardiac tissue. Because the chemical waves in the BZ reaction are constituted of charged ions, they can directly interact with the external electric field (Agladze and De Kepper (1992); Enderlein and Kuhnert (1996); Li et al. (2017)). Unpinning in the physiological system is possible with carefully delivered secondary excitation generated by the electric field, which is absent in the chemical medium (Luther et al. (2011); Shajahan et al. (2016); Punacha et al. (2019)). The mechanism of field-induced unpinning has yet to be addressed so far. In this chapter, we investigate the field-induced unpinning of chemical waves.

To understand the unpinning of chemical waves in an electric field, we must study how the pinned wave leaves heterogeneity. This chapter reports a detailed investigation of the location at which the spiral wave leaves the pinning obstacle in the BZ reaction as a function of the chirality of spiral rotation, the initial phase of the spiral, the size of the pinning obstacle, direction, and the strength of the applied electric field. We study unpinning in the experiments and numerical simulations of the Oregonator model. From the observations, we deduce a relationship between the phase of unpinning, the size of the pinning obstacle, the strength, and the direction of the electric field.

3.2 Methods

3.2.1 Experimental methods

We performed experiments in uniform thin layers of ferroin-catalyzed Belousov-Zhabotinsky (BZ) reaction. The initial concentrations of reagents in the medium are: $[H_2SO_4] = 0.16$ M, $[NaBrO_3] = 40$ mM, $[Malonic\ acid] = 40$ mM, and $[Ferroin] = 0.5$ mM. The procedure for solution preparation and spiral generation is explained in detail in the chapter Methods.

A glass bead is inserted partially across the gel surface by gently pushing it into the agar gel so that the spiral tip on the surface pins to the great circle of the spherical bead. A pinned

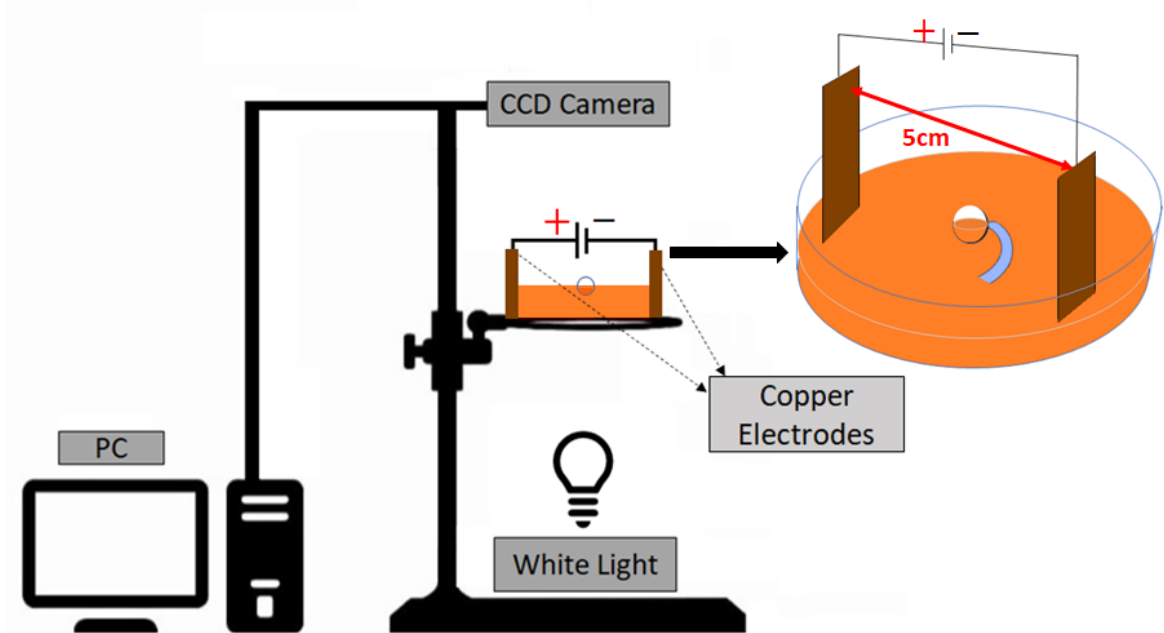


Figure 3.2: Schematic representation of the experimental setup: Images of BZ reaction are recorded with a CCD camera controlled by LabVIEW software. The system is illuminated from the bottom with white light. Electrode positions in the medium with respect to the obstacle are illustrated in the inset. The white circle at the center of the reaction medium represents the pinning obstacle. (Not to scale.)

spiral wave takes 4.17 minutes to rotate around a bead of radius 0.6 mm in the absence of an applied electric field. The time period for the spiral pinned to obstacles of radii $r = 0.75$ mm and 0.9 mm is 4.58 and 5.04 minutes, respectively. The error in the time measurements is 0.5 seconds. The rotation period increases with the size of the pinning obstacle, as reported earlier (Lim et al. (2006)). A schematic diagram of the experimental setup is shown in Fig.3.2. Unpinning experiments are performed in the presence of a constant DC electric field. We applied the field through a pair of copper electrodes (of dimension $5 \text{ cm} \times 2.5 \text{ cm} \times 0.25 \text{ mm}$ each) kept 5 cm apart. For comparison, we have performed experiments using a cylindrical rod.

3.2.2 Numerical methods

In simulations, the unpinning studies are carried out using the three-variable Oregonator model. The coupling of chemical reactions (Eqns. 2.9-2.11) with the diffusion of corresponding chemical species results in the formation of patterns in the medium. The following

are the model equations (Schmidt and Müller (1997)):

$$\frac{\partial u}{\partial t} = \frac{1}{\varepsilon}(qw - uw + u(1 - u)) + D_u \nabla^2 u \quad (3.1)$$

$$\frac{\partial v}{\partial t} = u - v + D_v \nabla^2 v + M_v(\vec{E} \cdot \nabla v) \quad (3.2)$$

$$\frac{\partial w}{\partial t} = \frac{1}{\varepsilon'}(-qw - uw + fv) + D_w \nabla^2 w + M_w(\vec{E} \cdot \nabla w) \quad (3.3)$$

where u , v and w represent the re-scaled, dimensionless concentrations of $HBrO_2$, Fe^{3+} , and Br^- respectively. Values of the parameters used are $q = 0.002$, $f = 1.4$, $\varepsilon = 0.01$, and $\varepsilon' = 0.0001$. In Eq.3.2 and Eq.3.3, the applied electric field \vec{E} along $+x$ -axis, is added as an advection term. Since u is non-ionic, the electric field does not affect its diffusion. The mobility values of u , v , and w are $M_u = 0$, $M_v = -2$, and $M_w = 1$ respectively. The computation domain is 300×300 grids of size $dx = dy = 0.1$ spatial units (s.u). The numerical scheme is the explicit forward Euler method with a time step of $dt = 0.0001$. No-flux boundary conditions are imposed on the domain and the obstacle boundaries. An obstacle of radius r is created by reducing the value of D_u to 0.0001 at the center. D_v and D_w are kept constant across the simulation domain. The phase-field approach sets no-flux boundary conditions at the obstacle boundary. The obstacle radii range from 0.75 to 1.5 s.u. The electric field is initiated at 18 different initial phases of the spiral.

3.3 Results and discussion

Previous studies have shown that the propagation of a chemical excitation wave can be controlled with an external electric field (Feeney et al. (1981); Ševčíková and Marek (1983)). A free-rotating spiral wave in an external electric field moves from its initial position along a trajectory at an angle to the electric field. The direction of this trajectory is determined by the strength of the applied field and the chirality of the spiral (Agladze and De Kepper (1992); Steinbock et al. (1992); Li et al. (2017)). It was also shown that the field could detach a pinned spiral wave from an inexcitable obstacle in the reaction medium (Sutthiopad et al. (2014)). In light of these results, we investigated the mechanism of unpinning by observing the position of the spiral unpinning with respect to the direction of the applied field. We used the experimental BZ reaction and the Oregonator model to systematically study the

unpinning by an external electric field.

As long as the spiral tip stays pinned to the obstacle, the spiral core traced by the tip strictly follows the obstacle boundary. Whenever the spiral core starts to deviate from the obstacle boundary, we consider it as unpinning see Fig.3.3.

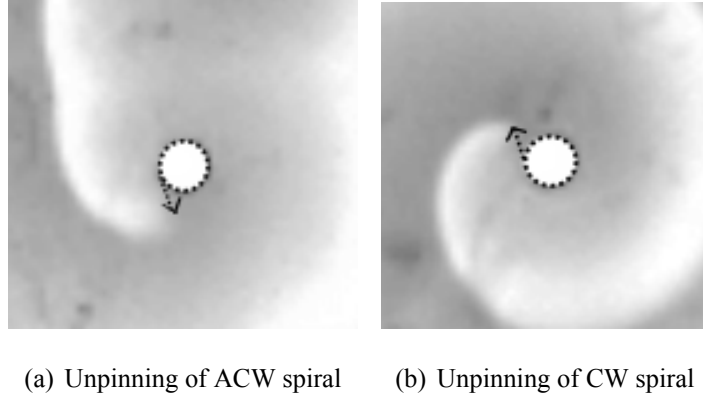


Figure 3.3: The dotted circle represents the obstacle boundary, which is the same as the core of the pinned spiral wave (in Fig.3.4). As the tip unpins from the obstacle, it traces a different path marked by the arrows.

We measured the position of the spiral tip around the obstacle boundary at the time of unpinning in degrees from the $+x$ -axis, and it is denoted as the unpinning phase (φ_u) of the spiral. Here, the applied field is oriented along the x -axis. In experiments, the angle at which the rotating wave detaches from the glass bead is determined from the images using the software GIMP (GNU Image Manipulation Program). Experimental images have a resolution of 0.07 mm/pixel, which gives us a resolution of 6.67° in angle measurements for a bead of radius 0.6 mm. In simulations, the spiral tip is defined as the intersection of two contours $u = 1/2$ and $F(1/2, v) = 0$, where F is given by reaction term in Eq.3.1 (Barkley (1991)).

We observed that the spiral tip unpins from the obstacle only when the field strength is above a threshold (E_{th}). We determined E_{th} by systematically ramping up the field strength to find the minimum field required to get the wave unpinned within one rotation of the spiral. Fig.3.4 shows the unpinning of anti-clockwise (ACW) and clockwise (CW) rotating pinned spirals subjected to a uniform DC electric field of strength greater than E_{th} . It was found that both ACW and CW spirals detach near the anode as the tip propagates away from the anode.

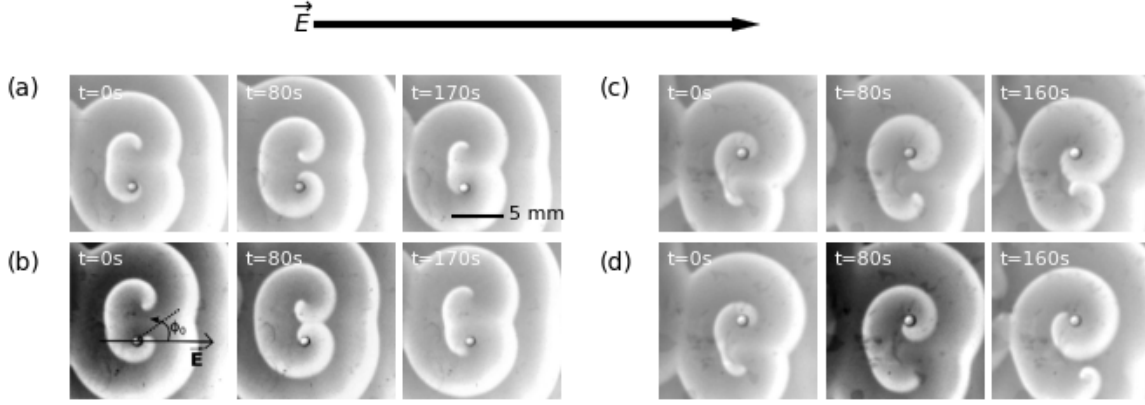


Figure 3.4: Unpinning of the spiral wave with DC electric field: (a) An anti-clockwise (ACW) rotating spiral pinned to an obstacle of radius 0.6 mm without an external electric field. (b) An anti-clockwise rotating spiral with initial phase $\varphi_0 = 45^\circ$ unpinned at $\varphi_u = 203.6^\circ$ in an electric field of strength $E = 2.40$ V/cm. (c) A clockwise (CW) rotating spiral pinned to an obstacle of radius 0.6 mm without an external electric field. (d) A clockwise rotating spiral with initial phase $\varphi_0 = 315^\circ$ unpinned at $\varphi_u = 151.43^\circ$ in an electric field of strength $E = 2.40$ V/cm. The bold black arrow represents the field direction.

For an electric field applied along the $+x$ -axis (*i.e.*, for the anode situated at 180°) in Fig.3.4, the CW spiral detached around 135° , and the ACW spiral detached around 225° . After unpinning, the tip drifts at an angle from the direction of the anode, as the free spiral drifts in an electric field (Agladze and De Kepper (1992); Steinbock et al. (1992); Schmidt and Müller (1997)). A spiral pinned to a cylindrical glass rod of length more than the thickness of the medium also unpins similarly (Fig.3.5).

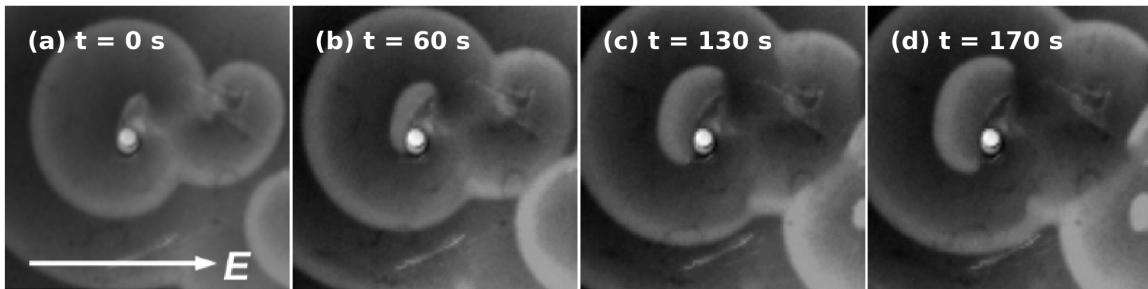


Figure 3.5: Spiral pinned to a cylindrical glass rod of diameter 1.0 mm is unpinned at $\varphi_u = 206.47^\circ$ with a DC electric field $E = 2.40$ V/cm for $\varphi_0 = 45^\circ$. $E_{th} = 0.76$ V/cm. From the equation, $\varphi_u = 198.46^\circ$.

According to Sutthiopad *et al.*, the critical threshold (E_{th}) increases with the size of the pinning obstacle (Sutthiopad et al. (2014)). We determined the E_{th} for obstacles with radius $r = 0.6$ mm, 0.75 mm, and 0.9 mm in experiments (Fig.3.6a). Regarding the spiral wavelength

($\lambda = 3.696$ mm), these radii are 0.162λ , 0.202λ , and 0.243λ , respectively. From Fig.3.6b - 3.6d, it is clear that at $E = E_{th}$, the unpinning phase of spirals with similar chirality is constant irrespective of the obstacle size.

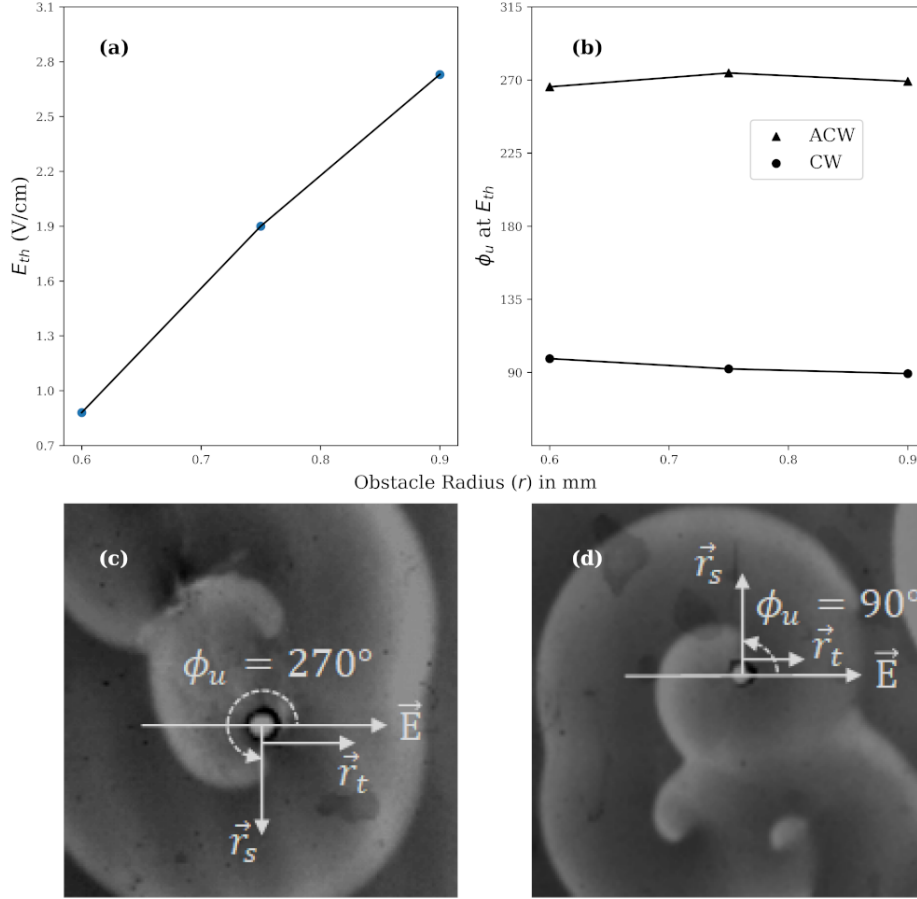


Figure 3.6: Unpinning of the spiral wave as a function of the radius of the obstacle: (a) Threshold field strength (E_{th}) for unpinning spiral from obstacles having different radii are plotted. The critical threshold for unpinning increases linearly with the obstacle size. The radius is measured in millimeters (mm). (b) ϕ_u is plotted against the obstacle radius. At $E = E_{th}$, (c) ACW spiral always unpins at 270° (circles) while (d) CW unpins at 90° (triangles). \vec{E} represents the field direction and \vec{r}_t is the tangential propagation vector at ϕ_u . In both (c) and (d), the obstacle radius = 0.6 mm and $E = 0.8$ V/cm.

To find the factors influencing the unpinning phase, we applied the electric field at different initial phases of the spiral. The initial phase of a spiral, ϕ_0 , is the phase of the spiral tip on the obstacle boundary at the time of field initiation.

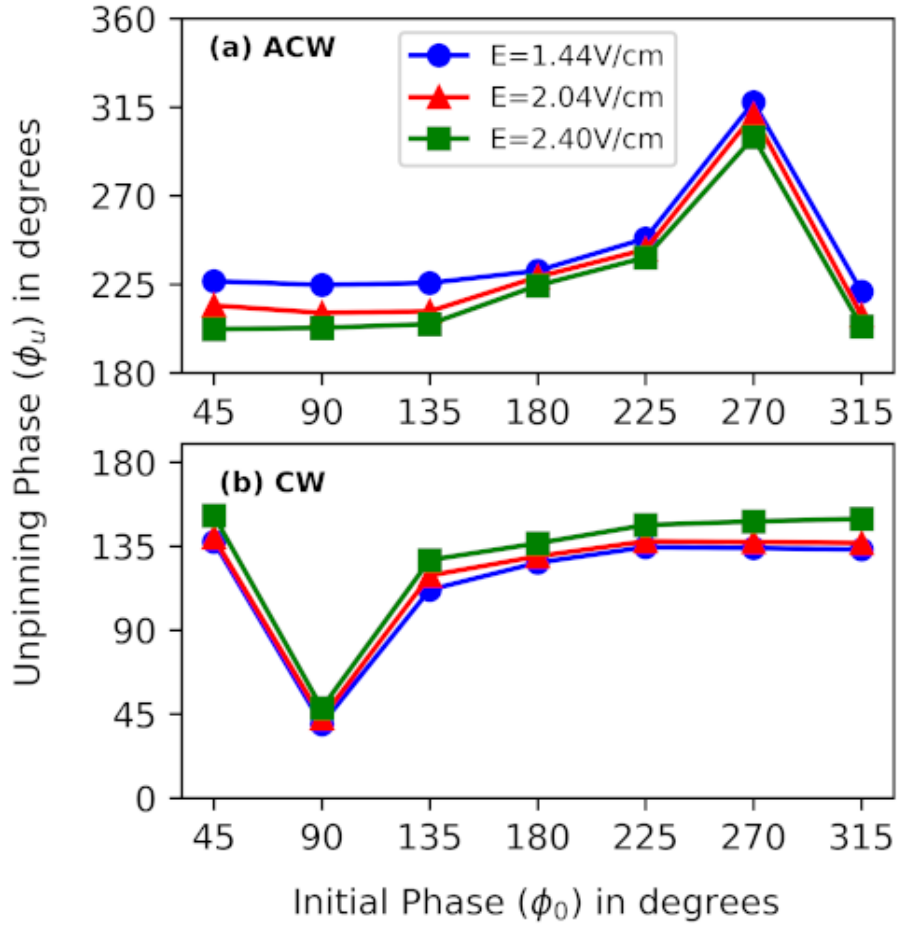


Figure 3.7: Unpinning phase as a function of the initial phase of the spiral: (a) In the experiment, the detachment phase for the ACW spiral is plotted for different initial phases. ϕ_0 is varied in the steps of 45° , for different $E = 1.44, 2.04, \text{ and } 2.40 \text{ V/cm}$. $E_{th} = 0.8 \text{ V/cm}$, and the obstacle radius is 0.6 mm . (b) same as in (a) for CW spiral.

For different ϕ_0 , the spiral unpins with a constant ϕ_u , except when ϕ_0 is close to the expected unpinning phase. In such situations, the wave is unpinned with a fixed delay (Fig.3.7). A comparison between the unpinning of a spiral pinned to a spherical bead and a cylindrical rod (Fig.3.8) reveals that this observation is common for both.

Another parameter that can influence the unpinning is the direction of the applied field, θ_E . For $\theta_E = 0^\circ$ (along $+x$ -direction), a CW spiral unpins between 90° and 180° . When the field direction is reversed, *i.e.*, for $\theta_E = 180^\circ$ (along $-x$ -direction), the CW spiral unpins in between 360° and 270° . An ACW spiral unpins in between 180° and 270° for $\theta_E = 0^\circ$, and in between 0° and 90° for $\theta_E = 180^\circ$ (Fig.3.9). Despite the difference in the phase values, the unpinning phase is always symmetrical to the field vector.

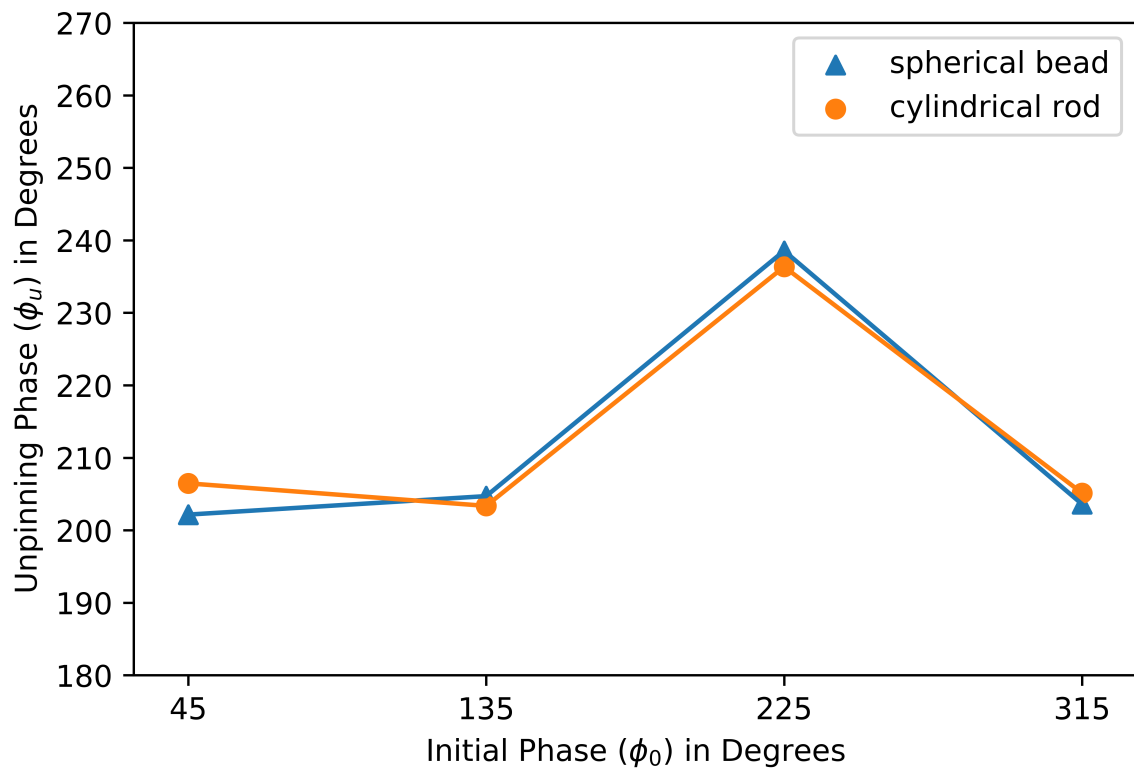


Figure 3.8: Comparison of unpinning with spherical bead and cylindrical rod as an obstacle: (a) Spiral pinned to a spherical glass bead of radius 0.6 mm is unpinned with $E = 2.40$ V/cm for different spiral initial phases. $E_{th} = 0.80$ V/cm. From the equation, $\phi_u = 199.47^\circ$. (b) Spiral pinned to a cylindrical glass rod of radius 0.5 mm is unpinned with $E = 2.40$ V/cm for different spiral initial phases. $E_{th} = 0.76$ V/cm. From the equation, $\phi_u = 198.46^\circ$.

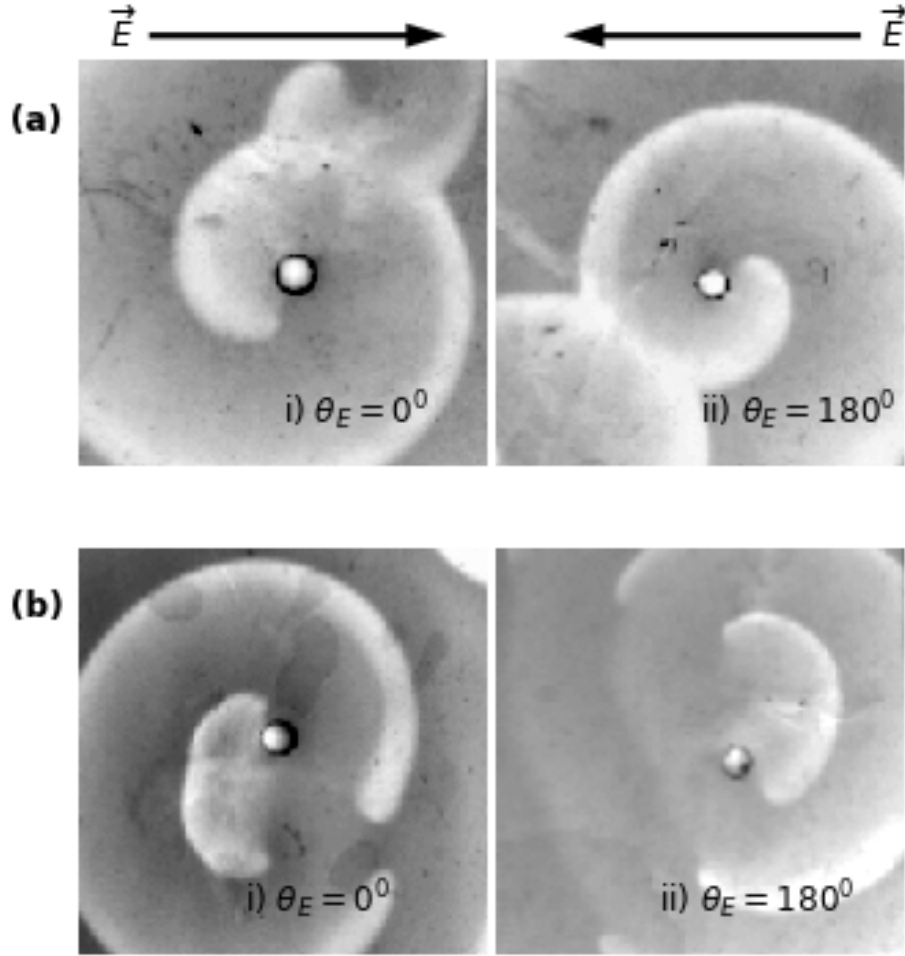


Figure 3.9: Effect of field direction (θ_E) on unpinning: (a) For $\theta_E = 0^\circ$, (i) an ACW spiral unpins in between 180° and 270° (ii) a CW spiral unpins in between 90° and 180° . (b) For $\theta_E = 180^\circ$, (i) an ACW spiral unpins in between 0° and 90° (ii) a CW spiral unpins in between 270° and 0° . The electric force exerted toward the anode influences the spiral detachment position. The obstacle radius is 0.6 mm, and $E = 2.40$ V/cm.

From these observations, we hypothesize that the unpinning happens because of the slow down in the spiral tip velocity due to the electric field. The wave unpins when the electric force opposing the tip movement is above the critical threshold. The direction of the spiral tip velocity at each phase φ_s around the obstacle boundary is represented by \hat{r}_t (Fig.3.6c and 3.6d). The orientation of \hat{r}_t is $(\varphi_s + 90^\circ)$ for ACW spiral and $(\varphi_s - 90^\circ)$ for CW spiral. With $E = E_{th}$, the wave unpins when the field vector and \hat{r}_t align parallel to each other as in Fig.3.6c and Fig.3.6d. Fig.3.10 schematically represents the alignment of the spiral with respect to the applied field of threshold strength during unpinning.

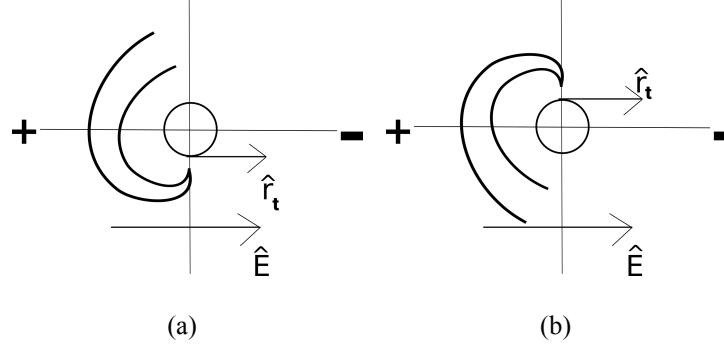


Figure 3.10: Schematic representation showing the orientation of \vec{E} and \hat{r}_t during unpinning with a field of threshold field strength: (a) for ACW spiral and (b) for CW spiral.

We assume that the unpinning constantly occurs at the phase $\varphi_u = 270^\circ$ because there, due to the parallel alignment of \hat{r}_t and \vec{E} , the ACW spiral experiences the maximum electric force opposing its tip rotation. Similarly, a CW spiral experiences the maximum electric force at the phase $\varphi_u = 90^\circ$. Mathematically, the condition can be expressed as $\vec{E} \cdot \hat{r}_t = E_{th}$. In general, for any electric field E greater than E_{th} the wave can be unpinned when the component of applied electric field (\vec{E}) along \hat{r}_t becomes equal to greater than E_{th} . i.e., $\vec{E} \cdot \hat{r}_t \geq E_{th}$. These assumptions will provide an unpinning phase window.

For an ACW spiral, it is given by,

$$\theta_E - 180^\circ + \sin^{-1}\left(\frac{E_{th}}{E}\right) \leq \varphi_u \leq \theta_E - \sin^{-1}\left(\frac{E_{th}}{E}\right) \quad (3.4)$$

In its course of rotation, an ACW spiral initially approaches the phase value,

$$\varphi_u = \theta_E - 180^\circ + \sin^{-1}\left(\frac{E_{th}}{E}\right) \quad (3.5)$$

So every ACW spiral, except those with $\varphi_0 \sim \varphi_u$, unpins at φ_u given by Eq.3.5. When the initial phase of the spiral is close to the expected unpinning phase (i.e., $\varphi_u - \Delta \leq \varphi_0 \leq \varphi_u + \Delta$), the wave unpins after a fixed delay of Δ (Fig.3.7,3.8).

$$\varphi_u = \varphi_0 + \Delta \quad (3.6)$$

where $\Delta = 30^\circ$ in experiments. However, φ_u is still within the upper bound of the provided window. This delay in unpinning can be related to the characteristic time for the diffusion of

ionic species in response to the applied field. This time of response must depend on the field strength and diffusion constant. In the case of $E = E_{th}$, Eq.3.5 will give $\varphi_u = 270^\circ$, which matches well with our observations in Fig.3.6b.

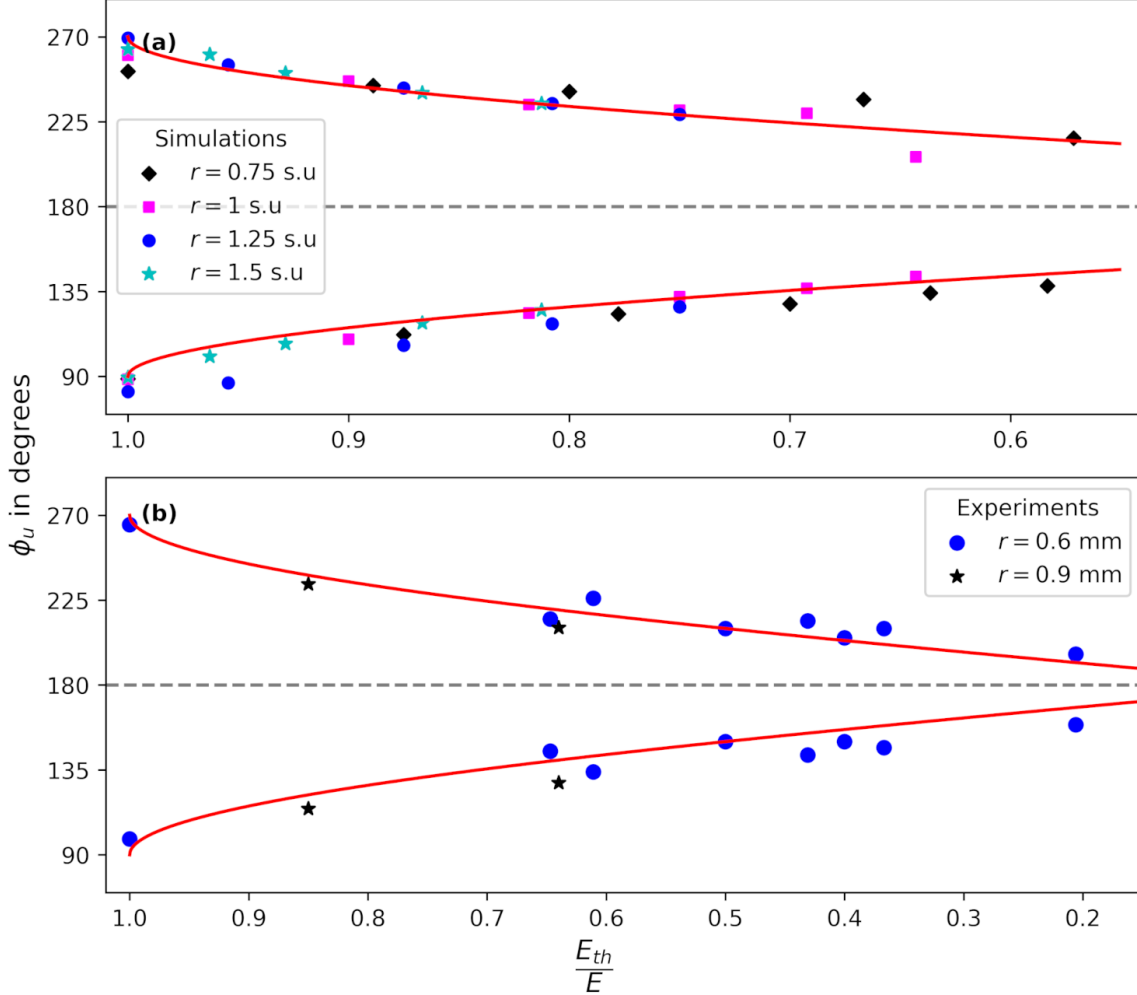


Figure 3.11: Unpinning phase varies with field strength: φ_u is plotted against the field strength ratio $\frac{E_{th}}{E}$ for spiral pinned to various obstacle sizes. The radius is measured in millimeters in experiments and space units in simulations. In both (a) simulation and (b) experiment, a solid red line indicates the values of φ_u calculated from the analytical formulae Eq.3.4 and Eq.3.7. For ACW and CW spirals, φ_u approaches 180° with the increase in field strength. , *i.e.*, An increase in the field strength results in an unpinning closer to the anode.

Similarly, for clockwise rotating spiral φ_u is,

$$\varphi_u = \theta_E + 180^\circ - \sin^{-1}\left(\frac{E_{th}}{E}\right) \quad (3.7)$$

The unpinning phases given by Eq.3.7 correspond to the mirror image of the unpinning phases obtained when the spiral was rotating in the anti-clockwise direction (Eq.3.5).

At $E = E_{th}$, Eq.3.7 gives $\varphi_u = 90^\circ$ as expected from Fig.3.6b and 3.6d.

As with the ACW spiral, here also when the initial phase of the spiral is close to this expected unpinning phase, (*i.e.*, $\varphi_u - \Delta \leq \varphi_0 \leq \varphi_u + \Delta$), then the wave unpins after a fixed delay of Δ .

$$\varphi_u = \varphi_0 - \Delta \quad (3.8)$$

For CW spiral, φ_u can vary up to $\theta_E + \sin^{-1}(\frac{E_{th}}{E})$.

It has been observed from the study that E_{th} increases with the obstacle radius (Fig.3.6a). Since φ_u depends on E_{th} , φ_u also increases with obstacle radius. For fixed field strength, unpinning will be delayed for a larger obstacle. Thus, the above equations relate the unpinning phase with the chirality, obstacle size, field strength, and field direction. In Fig.3.11, we plot φ_u of the spiral wave as a function of $(\frac{E_{th}}{E})$ by varying the obstacle size and field strength for a fixed θ_E . The maximum deviation from the predicted theoretical value is 15° in simulations and 10° in experiments.

As $(\frac{E_{th}}{E})$ decreases φ_u for an ACW spiral decreases and approaches 180° , *i.e.*, unpinning happens in the close vicinity of the anode. For spirals rotating in the CW direction, the plot between φ_u and $(\frac{E_{th}}{E})$ will show the opposite trend. When $E = E_{th}$, the wave unpins at 90° . As E increases, φ_u increases and approaches 180° .

3.4 Conclusions

This chapter reported a systematic study of the unpinning of spiral waves in a chemical excitable medium using a constant electric field. The unpinning is characterized by the unpinning phase, which is the angle of the spiral tip around the obstacle boundary at the time of unpinning. We measured the unpinning phase in the BZ reaction medium and the Oregonator model. For a given field strength, the spiral wave always unpins at a fixed phase while propagating away from the neighborhood of the anode. Except for a small range of initial phases, an anticlockwise (ACW) spiral unpins between 180° and 270° while a clockwise (CW) spiral unpins between 90° and 180° , for an electric field applied along the $+x$ -axis. Based on the assumption that unpinning is by the retarding force of the electric field, we estimated the unpinning phase, which is in good agreement with our measurements.

We performed unpinning by replacing the spherical bead with a cylindrical rod of the same diameter. With a spherical bead as the obstacle, the spiral pins to the great circle of the bead. The cylindrical rod is inserted vertically so that its top end is visible above the medium. In a two-dimensional system, the spiral on the gel surface gets pinned to both bead and rod identically. In our experiments, the spiral pinned to the rod unpinned exactly like a spiral unpinned from a bead. This observation ensures that our system is essentially two-dimensional.

The observation that the wave unpins as it moves away from the anode indicates that the electric force on the chemical wave depends on the propagation direction of the wave. In particular, if the wave moves along the direction of the field, it slows down, and if the field is in the opposite direction, it accelerates. An electric field along the $+x$ -axis accelerates an ACW spiral moving from 0° to 180° and decelerates when it moves from 180° to 360° . However, we do not observe the wave being dragged toward the anode as it approached the anode but instead slowed down as the wave moved away from it. The chemical waves in the BZ reaction involve three important chemical species: The Br^- ion, HBrO_2 , and the $\text{Fe}(\text{phen})_3^{3+}$. The Br^- ions, usually diffuse opposite to the wave, can make the wave move slowly if the wave is moving in the same direction as the field (Feeney et al. (1981)). Similarly, in a field opposite to the wave propagation, the Br^- ions move ahead of the wave, leading to wave acceleration. Our results show that the slow-down effect of the field is more pronounced than its ability to accelerate the wave. Slow down in the propagation of spiral wave when moving towards the negative electrode facilitates the unpinning of the spiral tip from the obstacle.

In the presence of an applied electric field, the core of a free spiral wave drifts toward the direction of the anode. However, the velocity of the spiral core has an additional component perpendicular to the direction of the field. The perpendicular component of the spiral drift depends on the chirality of the spiral (Agladze and De Kepper (1992)). Similarly, in the case of field-induced unpinning, the position of unpinning with respect to the field changes with the chirality of spiral rotation. The ‘electric force’ acting directly on the excitation wave is a unique feature of the chemical excitation wave. In physiological tissue, for example, though the excitation waves show similar dynamics, the electric field does not act directly on the wavefront. For example, in cardiac tissue, the field induces secondary excitation from

the boundaries of obstacles. When the secondary waves are generated within the vulnerable window of the spiral, the wave gets unpinned (Luther et al. (2011); Shajahan et al. (2016)). We have not observed such wave emission in the chemical medium; we are also unaware of any other excitable medium where the external field can directly apply a force on the excitation wave. In conclusion, we point out that the chemical excitation waves in the BZ reaction interact uniquely with an external electric field. Also, unpinning by a retarding electric force is not seen so far in any other excitable medium.

Chapter 4

Theory and experiments of spiral unpinning in the Belousov-Zhabotinsky reaction using a circularly polarized electric field

Summary

The mechanism of spiral wave unpinning in the BZ reaction with an applied circularly polarized electric field is investigated by varying the pacing ratio, initial spiral phase, and field strength. An electric force exerted in opposition to the spiral propagation by the applied field, while propagating away from the anode, induces unpinning. Based on the condition that the unpinning happens as the electric field component along the spiral propagation vector reaches the threshold, analytical formulae are derived for calculating the spiral unpinning phase. The unpinning occurs within the limits of the unpinning phase window calculated using the derived analytical formulae. The experimental observations are verified using the numerical simulations performed with the Oregonator model.

4.1 Introduction

We have seen from the previous chapters that applying an external electric field to the excitable systems, especially to the chemical and biological systems, can have a sensitive control over the wave dynamics (Feeney et al. (1981); Agladze and De Kepper (1992); Chen et al. (2006); Feng et al. (2014); Ji et al. (2013)). The variations in the chemical wave dy-

namics in an applied electric field are correlated with the oriented movement of ionic species in the medium. In the previous chapter, we have described, in detail, how an applied DC electric field can achieve the unpinning of pinned spirals from the inhomogeneities (Amrutha et al. (2022)). A slowdown in the spiral propagation due to the electric force leads to unpinning a pinned spiral tip in a DC electric field. The field vector is static in a DC field, and its orientation will not change with time. But, the spiral wave changes its phase according to its frequency. So, it is logical to think that a rotating field could provide better control over the spiral dynamics. In an applied rotating electric field, the spiral and the electric field exhibit relative rotation with specific individual frequencies.

It is possible to generate various polarized electric fields by changing the phase difference between the two applied AC electric fields. The resulting electric field will be circularly polarized if the phase difference is $\pm\pi/2$. A circularly polarized electric field (CPEF) is spatially uniform since it possesses constant amplitude and rotates in a particular direction with uniform frequency. Many of the numerical studies employed a CPEF to control the spiral dynamics. As in the case of a DC or an AC electric field, the spiral wave drifts in a CPEF, and a co-rotating CPEF induces maximum drift (Chen et al. (2006)). Numerical studies in reaction-diffusion models show that a co-rotating CPEF can synchronize the spiral frequency (Chen et al. (2009)) if the frequency of the CPEF is near that of the spiral. The synchronization is difficult to obtain if the CPEF is too fast or too slow. An applied CPEF breaks the chiral symmetry, and by adjusting the field frequency, a spiral with the same or opposite chirality can be selected. This phenomenon can be explained using frequency synchronization followed by the competition rule, that the faster waves always survive in excitable media (Li et al. (2013)). The only experimental study of CPEF in the BZ reaction is reported by Ji *et al.* (Ji et al. (2013)). The study explains the control of spiral turbulence obtained in the BZ reaction with CPEF based on frequency synchronization. The CPEF synchronizes some unstable spirals, and the prolonged field application helps develop well-formed spiral waves. All these control effects are possible only with a CPEF of frequency closer to the spiral frequency.

The unpinning so far reported using a CPEF in the reaction-diffusion models is based on the mechanism of wave emission from heterogeneities. Unpinning of spiral waves in cardiac models by WEH induced by the CPEF has been reported to have a higher success

rate and more application scope than a unidirectional electric field (UEF), even with a lower voltage (Feng et al. (2014); Punacha et al. (2020)). A CPEF induces spherical waves with frequencies higher than the pinned scroll wave in a three-dimensional system. Such higher-frequency spherical waves induced by CPEF can drive the pinned scroll wave out of the cardiac systems (Pan et al. (2016)).

So far, there are no reports on experiments of spiral unpinning using a rotating electric field. In this chapter, for the first time to our knowledge, the unpinning of a spiral wave with the circularly polarised electric field (CPEF) in the BZ reaction is reported. We will address the mechanism of spiral unpinning and formulate it analytically.

4.2 Methods

4.2.1 Experimental Methods

Our experiments were conducted in a ferroin-catalyzed BZ reaction with the same composition and concentration described in the second and third chapters. The single reaction layer of thickness 3 mm is taken in a glass petri dish of diameter 10 cm. The spiral generation and pinning procedure is explained in detail in the chapter Methods. A glass bead of diameter 1.2 mm is used as the pinning obstacle. An anticlockwise rotating circularly polarized electric field (CPEF) is applied using two pairs of copper electrodes as in Fig.4.1.

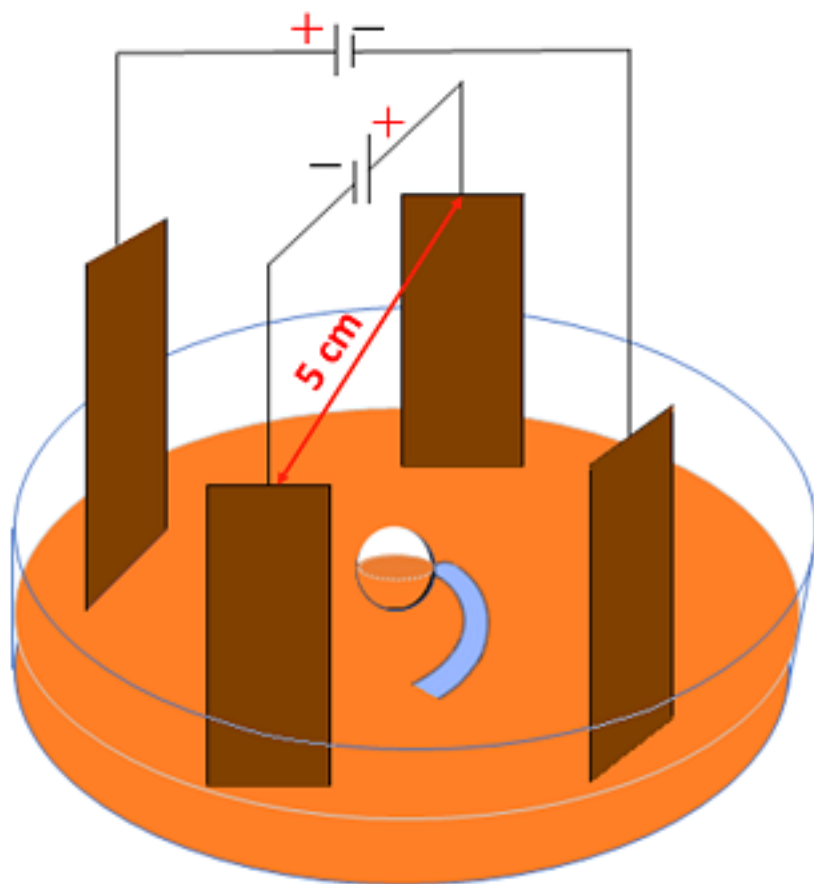


Figure 4.1: **Schematic diagram of the experimental system:** Positions of the two pairs of field electrodes with respect to the glass bead are shown schematically (not to scale).

Images of the reaction medium are recorded using a CCD camera at every 30s interval for 1 – 2 hours. Even though we mainly discuss the unpinning of a spiral pinned to a spherical bead, a comparative study with a spiral pinned to a cylindrical rod is included.

4.2.2 Numerical methods

According to the FKN mechanism, the variables u , v , and w in the three-variable Oregonator model (see Chapter 3 for details) represent the rescaled dimensionless equivalent of the concentrations of $HBrO_2$, oxidized catalyst, and Br^- ions respectively. Since w changes on the fastest time scale, $w(x, t)$ is always determined by the instantaneous values of u and v according to the relation $w = bv/(u + a)$. As a result, the three-variable Oregonator model is reduced to a two-variable system in u and v . The transport of the inhibitor Br^- ions is primarily responsible for the field-induced effects observed in the BZ reaction. The temporal evolution of the concentration of Br^- ions is anticorrelated to that of the autocatalytic component $HBrO_2$. The effect of the electric field on the variable Br^- is included in the

equation for u by the additional advection term. This advection term does not describe any real physical movement of $HBrO_2$ (Schmidt and Müller (1997)). The paper by Amrutha *et al.* (Amrutha *et al.* (2022)) reports an excellent agreement between the dynamics of spiral waves obtained using the three and two-variable Oregonator model.

So, here, the dynamical features of the BZ reaction are described using the two-variable Oregonator model. The model equations are as follows:

$$\frac{\partial u}{\partial t} = \frac{1}{\varepsilon} \left(u(1-u) - \frac{fv(u-q)}{u+q} \right) + D_u \nabla^2 u + M_u (\vec{E} \cdot \nabla u) \quad (4.1)$$

$$\frac{\partial v}{\partial t} = u - v + D_v \nabla^2 v + M_v (\vec{E} \cdot \nabla v). \quad (4.2)$$

where u , and v represent the re-scaled, dimensionless concentrations of $HBrO_2$, and Fe^{3+} respectively. The electric field \vec{E} is added as an advection term in the equations for u and v . The CPEF is represented as $\vec{E} = E_0 \sin(\frac{2\pi t}{T}) \hat{x} + E_0 \cos(\frac{2\pi t}{T}) \hat{y}$.

The model parameters are $q = 0.002$, $f = 1.4$ and $\varepsilon = 0.01$. $D_u = 1.0$ and $D_v = 0.6$ are the values of diffusion coefficients. The ionic mobilities of u and v are $M_u = 1.0$ and $M_v = -2.0$ respectively. The computation domain is 300 x 300 grids of size $dx = dy = 0.1$ spatial units (s.u). The numerical scheme is the explicit forward Euler method with a time step of $dt = 0.0001$. No-flux boundary conditions are imposed on the domain and the obstacle boundaries. An obstacle of radius $r = 10$ s.u is created by reducing the value of D_u to 0.0001 at the center. D_v and D_w are kept constant across the simulation domain. The phase-field approach sets no-flux boundary conditions at the obstacle boundary (Fenton *et al.* (2005)).

4.3 Results and Discussions

The location of the spiral tip on the obstacle is denoted by its phase, φ_s . The spiral phase at $t = 0$ s is represented as φ_0 (initial spiral phase), and the phase at the time of unpinning is φ_u (unpinning spiral phase). φ_s is measured anti-clockwise from the positive X-axis in degree by considering the obstacle center as the origin. The direction of the spiral tip rotation (\hat{r}_t) can be obtained by drawing a tangent at the respective phases. In experiments, φ_s is determined from the images using the software GIMP (GNU Image Manipulation Program). The resolution

in angle measurements is 6.67° for a bead of diameter 1.2 mm. In simulations, the point of intersection of the two contours $u = 1/2$ and $F(1/2, v) = 0$ is defined as the spiral tip. Here, F is given by the reaction term in the Eq.4.1 (Barkley (1991)).

4.3.1 Anti-clockwise spiral

We focused on the unpinning of an ACW spiral in an ACW CPEF.

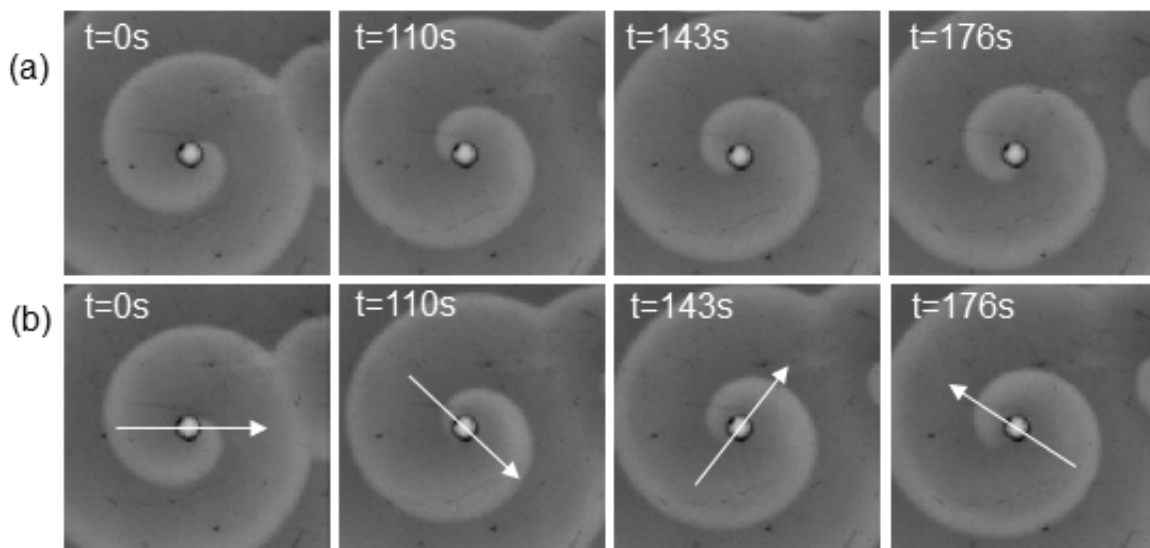


Figure 4.2: **Unpinning of an anti-clockwise rotating spiral using CPEF:** (a) An ACW rotating spiral pinned to a spherical bead of diameter 1.2 mm in the experiment. The natural period of pinned spiral tip $T_s = 297$ s. (b) A CPEF of strength $E_0 \simeq 1.38$ V/cm, and period $T_E = 125$ s applied to the medium unpins the spiral tip from the obstacle. The arrows show the direction of the applied CPEF.

As in the DC electric field (Amrutha et al. (2022)), the spiral can be unpinned with the CPEF only when the field strength E_0 equals a particular threshold value E_{th} . The significant difference from the DC electric field is that it is static there, but it is rotating here. Fig.4.2a gives the time sequence of field-free rotation of an ACW spiral wave and its unpinning with an ACW CPEF of strength $E_0 = E_{th}$. In experiments, the ACW spiral rotates with a period $T_s = 297$ s, and the period of the applied field is $T_E = 125$ s. Here, the field rotates with a higher frequency than the spiral ($T_s > T_E$). Hence, we say the pacing is overdrive. The ratio between the periods of the spiral and the field rotation is denoted as the pacing ratio; $p = T_s/T_E$. In terms of angular displacements,

$$p = \frac{\theta_E - \theta_0}{\varphi_u - \varphi_0} \quad (4.3)$$

where $\theta_0 = 0^\circ$ in the initial position of the field vector, and θ_E is the angle covered by the field vector by the time of unpinning. $(\phi_u - \phi_0)$ is the angle covered by the spiral during the time of unpinning.

To find out the mechanism behind the unpinning, we must examine the unpinning sequences, Fig.4.2b. It can be seen that the unpinning is initiated as the spiral starts to rotate toward the cathode after passing the anode. In Fig.4.2b, at $t = 110$ s, if we mark \hat{r}_t , it will align parallel to the field vector \vec{E} . So the electric force on the spiral will be in the opposite direction to \hat{r}_t , and hence its propagation slows down. If the applied field strength is equal to E_{th} , the opposing electric force leads to the unpinning of the tip from the obstacle. This condition is similar to the unpinning at E_{th} in a DC electric field (Amrutha et al. (2022)). Fig.4.3 schematically represents the above-explained mechanism of spiral unpinning in a CPEF.

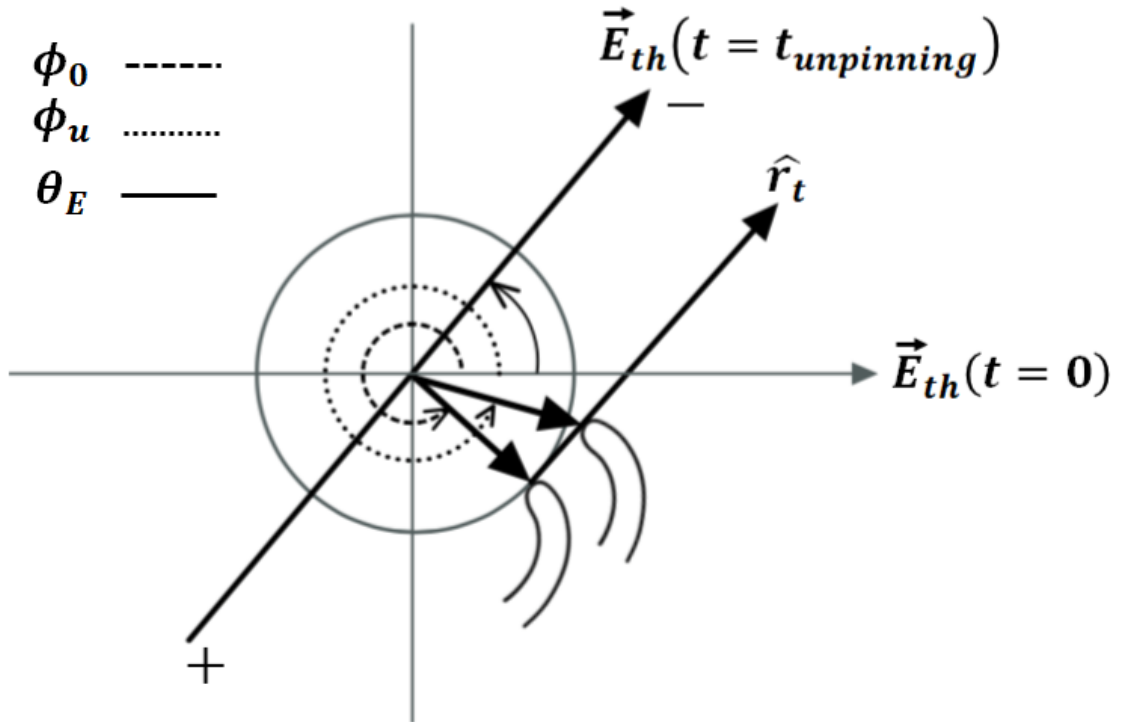


Figure 4.3: **Schematic diagram showing the mechanism of unpinning at $E_0 = E_{th}$:** ϕ_0 and ϕ_u are the phase of the spiral tip at $t = 0$ s and at the time of unpinning respectively. θ_E denotes the phase of the electric field \vec{E} and \hat{r}_t is the tangential vector of spiral rotation on the obstacle boundary. All phases are measured anticlockwise from the initial direction of the \vec{E} field. The wave unpins when the electric force is opposite to \hat{r}_t (or when \vec{E} and \hat{r}_t are parallel to each other). The tail of the resultant field vector \vec{E} marked with a + sign is mentioned as the anode, and the head with a - sign is the cathode.

So, the unpinning at $E_0 = E_{th}$ occurs when \vec{E} align parallel to \hat{r}_t . Following the mechanism at $E_0 = E_{th}$, the unpinning for a field strength greater than E_{th} must occur when the component of \vec{E} along \hat{r}_t reaches the critical threshold, E_{th} . *i.e.*, when the scalar product of \vec{E} and \hat{r}_t is equal to or greater than E_{th} . This condition gives a window of possible spiral unpinning phase φ_u as,

$$\theta_E - \pi + \sin^{-1}\left(\frac{E_{th}}{E}\right) \leq \varphi_u \leq \theta_E - \sin^{-1}\left(\frac{E_{th}}{E}\right) \quad (4.4)$$

which is the same as in a static DC field (Amrutha et al. (2022)). θ_E is a constant in the DC field. However, in a CPEF, θ_E is a function of the pacing ratio and the spiral phase according to the Eq.4.3. So, we can obtain φ_u in terms of φ_0 , p , E and E_{th} .

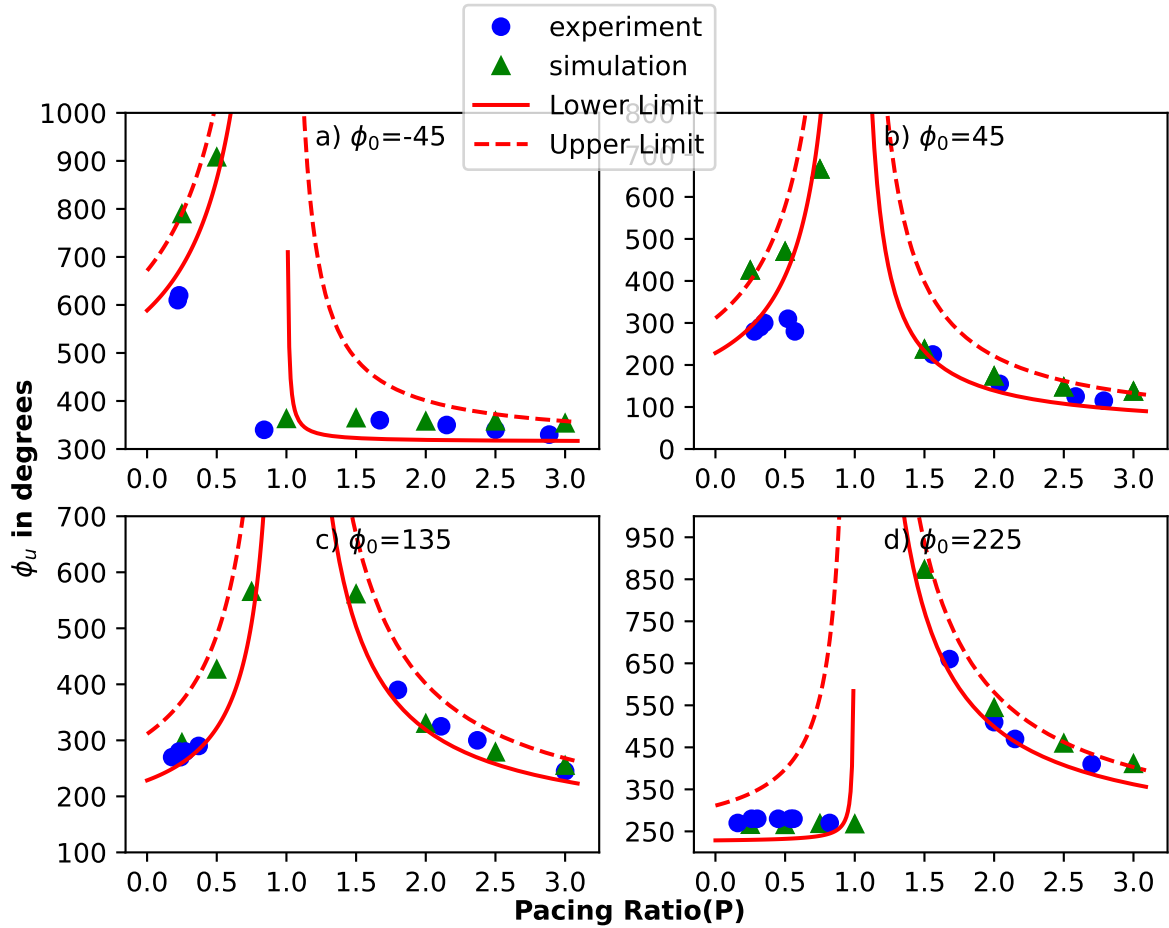


Figure 4.4: **Unpinning at $E_0 > E_{th}$ ($\sin^{-1}(\frac{E_{th}}{E_0}) = 48.95^\circ$):** Spiral waves with different φ_0 are unpinned in a CPEF with both under-drive ($p < 1$) and over-drive pacing ($p > 1$). The solid bottom line represents the lower limit of the range of possible φ_u -values given by the relation $\varphi_u = (p\varphi_0 + 48.95)/(p - 1)$ for over-drive pacing and $\varphi_u = (\pi - p\varphi_0 + 48.95)/(1 - p)$ for under-drive pacing. The upper limit of the range of possible φ_u -values, given by the relation $\varphi_u = (p\varphi_0 + \pi - 48.95)/(p - 1)$ for over-drive pacing and $\varphi_u = (2\pi - p\varphi_0 - 48.95)/(1 - p)$ for under-drive pacing, are represented by the top dashed line. Circles and triangles represent the experiment and simulation data, respectively.

For overdrive pacing with $p > 1$, the unpinning phase window is given by

$$\frac{p\varphi_0 + \sin^{-1}\left(\frac{E_{th}}{E_0}\right)}{p-1} \leq \varphi_u \leq \frac{p\varphi_0 + \pi - \sin^{-1}\left(\frac{E_{th}}{E_0}\right)}{p-1} \quad (4.5)$$

with a width $\Delta\varphi_u = \frac{\pi - 2\sin^{-1}\left(\frac{E_{th}}{E_0}\right)}{p-1}$.

For underdrive pacing *i.e.*, for $p < 1$, the unpinning phase window is

$$\frac{\pi + \sin^{-1}\left(\frac{E_{th}}{E_0}\right) - p\varphi_0}{1-p} \leq \varphi_u \leq \frac{2\pi - p\varphi_0 - \sin^{-1}\left(\frac{E_{th}}{E_0}\right)}{1-p} \quad (4.6)$$

The width of this window is $\Delta\varphi_u = \frac{\pi - 2\sin^{-1}\left(\frac{E_{th}}{E_0}\right)}{1-p}$. So, for a fixed E_0 , accurately choosing the p -value makes it possible to control the width of the unpinning phase window.

Fig.4.4 shows the unpinning phase window at $E_0 > E_{th}$ for different initial phases of the spiral. Here, the solid lines correspond to the lower limit, and the dashed lines correspond to the upper limit of the window according to Eq.4.5 and 4.6. The unpinning always happens at a phase within this range immediately after the required interaction between the spiral and the field.

At $E=E_{th}$ Eq.4.5 and 4.6 reduces to,

$$\varphi_u = \frac{p\varphi_0 + 90}{p-1}; p > 1 \quad (4.7a)$$

$$\varphi_u = \frac{270 - p\varphi_0}{1-p}; p < 1 \quad (4.7b)$$

In Fig.4.5, we plot the values of $(\varphi_u - \varphi_0)$ obtained in experiments as a function of the pacing ratio, p for different φ_0 at threshold field strength. The solid curves in Fig.4.5 represent the analytically predicted values (Eq.4.7). The observed values agree with the theoretical predictions.

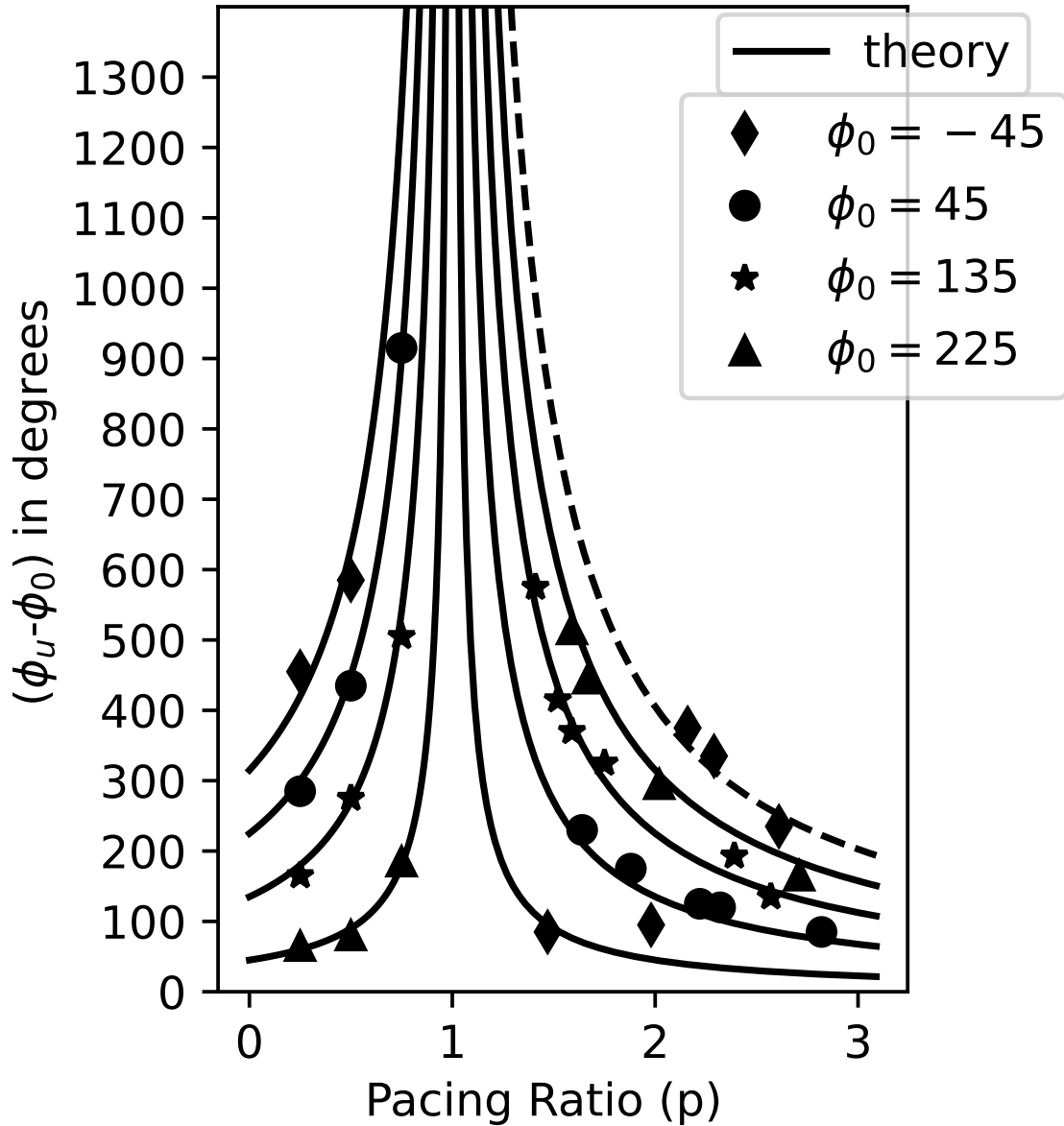


Figure 4.5: **Unpinning at $E_0 = E_{th}$** : For spirals having different ϕ_0 , the phase difference ($\phi_u - \phi_0$) is plotted with the pacing ratio, p in experiments. At overdrive pacing ($p > 1$), the red dashed lines on the top mark the theory curve for $\phi_0 = -45^\circ (315^\circ)$, corresponding to the second angular positions satisfying the unpinning mechanism. The solid red line at the bottom corresponds to the first set of angular positions satisfying the unpinning mechanism for $\phi_0 = -45^\circ (315^\circ)$.

It is evident from Fig.4.5 that ϕ_u explicitly depends on p and ϕ_0 . For example, in Fig.4.5 the spiral waves with $\phi_0 = 225^\circ$ unpin with a minimum $\Delta\phi \simeq 50^\circ$ for $p < 1$. However, the spirals with the same initial phase unpin with a larger phase difference $\Delta\phi \simeq 150^\circ$ for $p > 1$. If we consider some other ϕ_0 , the case will differ. It indicates that the unpinning is not instantaneous with the field application. Instead, it requires a minimum duration of interaction between the spiral and the field. So when the field starts with $\phi_0 = 225^\circ$, the spiral

experiences an opposing force from the beginning. Low pacing makes it possible to achieve the required interaction before the tip changes its orientation. However, with high pacing, the orientation changes quickly, and the process of unpinning is comparatively slow.

A comparison between unpinning in the case of spirals pinned to spherical bead and the cylindrical rod is given in Fig.4.6. It is clear from the figure that the unpinning is similar in both cases and is independent of the obstacle's shape.

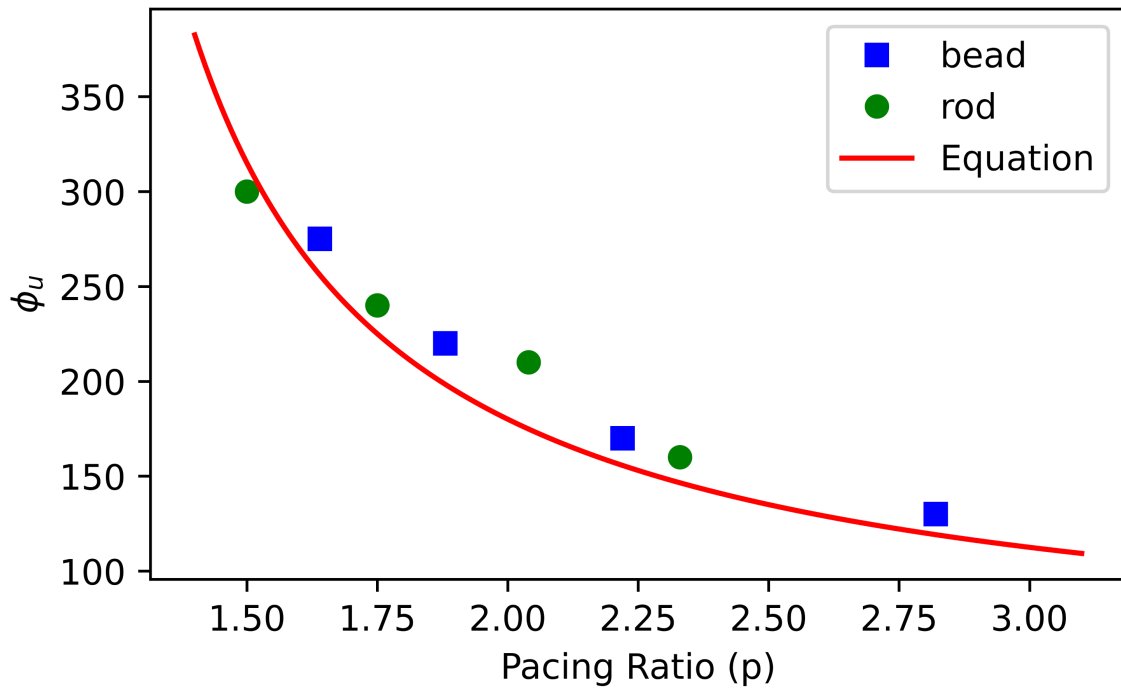


Figure 4.6: **Unpinning of spirals pinned to spherical bead and cylindrical rod:** ϕ_u is plotted against p , where p is greater than 1. Blue rectangles represent the unpinning from a bead, and green circles represent that from a rod. The red line represents the theory.

The variation in the unpinning phase with the initial phase is plotted in Fig.4.7a and Fig.4.7b by fixing the pacing ratio at 0.5 and 1.5, respectively. In DC, ϕ_u is constant with ϕ_0 except for $\phi_0 = \phi_u$, where ϕ_u is the lower bound of the unpinning phase window. When $\phi_0 = \phi_u$, spiral unpinned after a delay of around 30° . We got $\phi_u = \phi_0 + 30^\circ$. We assumed that the spiral could not instantaneously unpin with the applied electric field, but it requires a minimum interaction, which is why the delay occurs. The requirement of a minimum interaction time can be related to the time required for the diffusion of ions. Still, the unpinning happens within the upper bound of the window. The figures show that in a CPEF, ϕ_u varies with ϕ_0 . As ϕ_0 increases from -90° to 270° , ϕ_u decreases linearly for $p < 1$ and increases linearly

for $p > 1$. The point $\varphi_0 = 270^\circ$ acts as a point of resetting, so we have used the range -90° to 270° for φ_0 . According to formulae, at $\varphi_0 = 270^\circ$, φ_u is expected to be 270° . However, our observations show a delay in unpinning, similar to the case mentioned in the DC field.

In Fig.4.5, there are two theoretical curves for φ_u corresponding to $\varphi_0 = -45^\circ$ (315°). However, from the Eq.4.7a, at $E = E_{th}$ φ_u can have only a single value, represented by the solid line at the bottom. Instead, the unpinning happened at a subsequent φ_s after the expected φ_u , where the condition for unpinning is satisfied (dashed line in Fig.4.5). Such a significant change is most probable for high pacing ratios ($p > 2$).

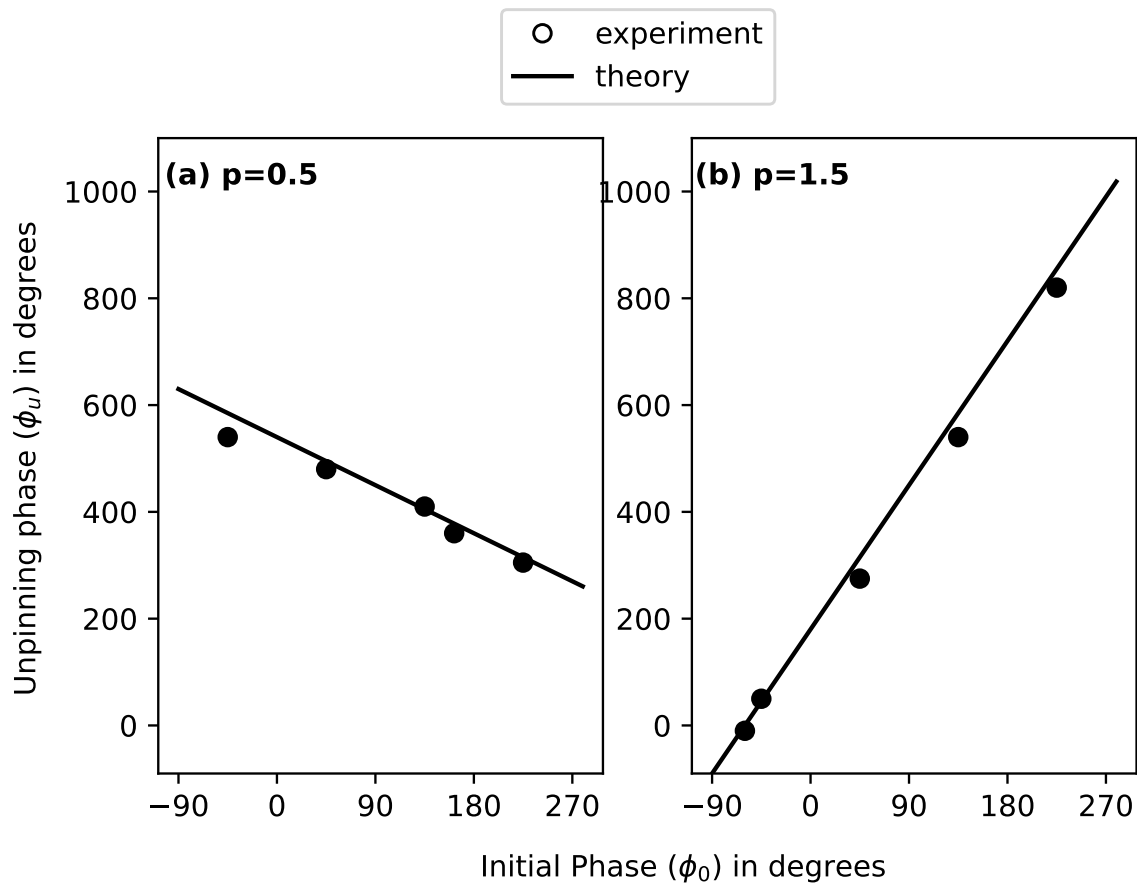


Figure 4.7: φ_u versus φ_0 : (a) The unpinning phase φ_u is plotted against φ_0 for $p = 0.5$ (underdrive pacing). (b) same as (a) but for $p = 1.5$ (overdrive pacing). In both cases φ_u varies linearly with φ_0 .

Suppose the time period of applied CPEF $T_E = T_s$. Then, the pacing ratio will be $p = 1$. We denote the case as resonant pacing. Here, the spiral and the CPEF would rotate with a fixed phase difference. According to the equations for φ_u , $p = 1$ will give infinity (Fig.4.5 and Fig.4.4). It means that unpinning is impossible for $p = 1$. It can be seen from Fig.4.4 and

4.5 that when $p=1$, the cases of unpinning are less. But in Fig.4.4, the spirals with $\varphi_0 = -45^\circ$ and 225° unpinned for $p = 1$. It implies that unpinning is possible with resonant pacing for particular values of φ_0 , which are marked in Fig.4.8.

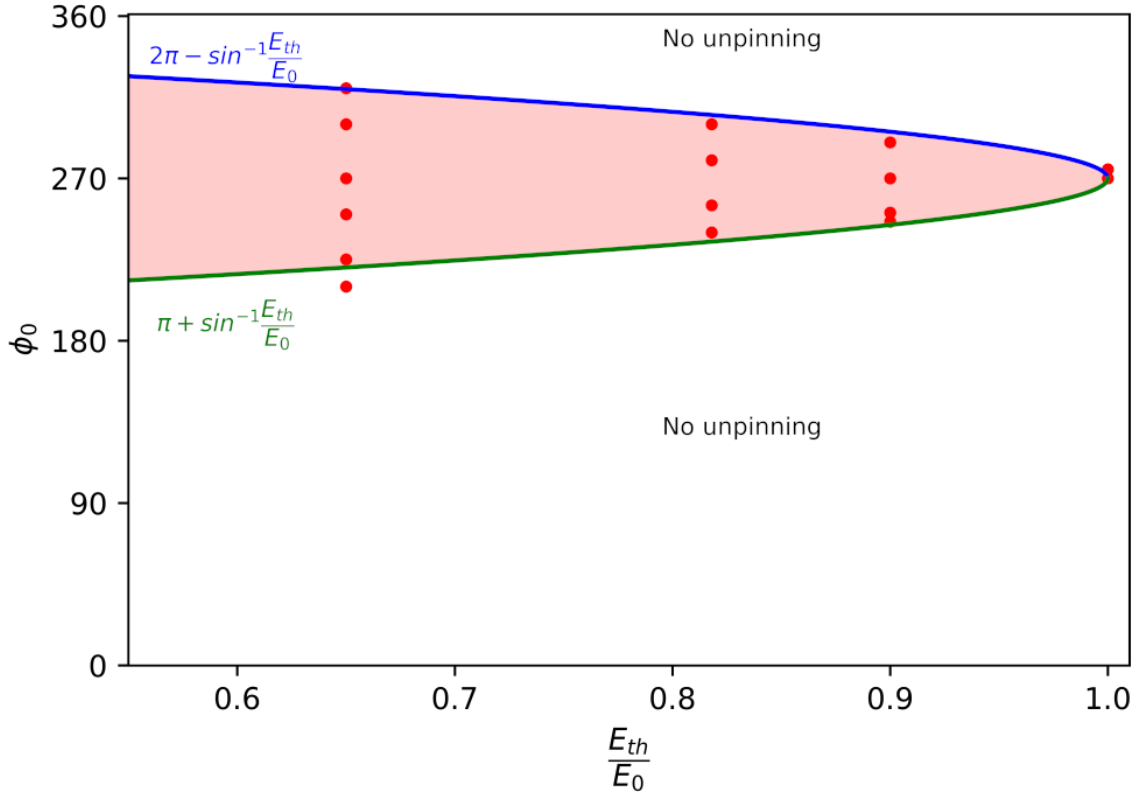


Figure 4.8: **Unpinning of spiral wave with pacing ratio, $p = 1$ for different field strength:** $\pi + \sin^{-1}(\frac{E_{th}}{E_0})$ and $2\pi - \sin^{-1}(\frac{E_{th}}{E_0})$ are the lower and upper limit of the range of possible φ_0 -values which gives successful unpinning for $p = 1$. The shaded region corresponds to the cases of successful unpinning.

For $p = 1$, unpinning happens if the following condition is satisfied.

$$\pi + \sin^{-1}\left(\frac{E_{th}}{E_0}\right) \leq \varphi_0 \leq 2\pi - \sin^{-1}\left(\frac{E_{th}}{E_0}\right) \quad (4.8)$$

This condition is reduced from the Eq.(4.5) and (4.6) by equating the numerator to zero. The observed φ_0 falls within the boundaries of the diagram (Fig.4.8) given by Eq.(4.8). The width of the possible φ_0 -values which results in unpinning is $\Delta\varphi_0 = \pi - 2 \sin^{-1}(\frac{E_{th}}{E_0})$. At $E_0 = E_{th}$, $\Delta\varphi_0 = 0$ and only spirals with $\varphi_0 = 270^\circ$ unpins. For $E_0 > E_{th}$, the unpinning is possible for a larger $\Delta\varphi_0$, with a maximum value of π . From Fig.4.4 and 4.8, it is clear that for a fixed E_{th} , the possibility of unpinning increases with an increase in the field strength.

4.3.2 Clockwise spiral

In the previous chapter, we have seen that the chirality of the rotating spiral influences the unpinning phase of the spiral. However, ACW and CW spirals behave mirror-symmetrically with a DC field. Studies on frequency synchronization (Chen et al. (2009)) and spiral drift (Chen et al. (2006)) using different polarized electric fields concluded that the relative rotation of the spiral and the field is an important parameter that defines the spiral dynamics. Only a co-rotating CPEF can synchronize the spiral and impose maximum spiral drift. Numerical studies show that the mechanism of spiral unpinning in the cardiac model differs with the relative rotation between the CPEF and the spiral (Punacha et al. (2020)). Here, we studied the unpinning of a CW spiral in an ACW CPEF. In this case, the CPEF and the spiral are doing counter-rotation.

Fig.4.9 gives the time sequence of field-free rotation of a CW spiral wave and its unpinning with a CPEF of strength $E_0 = E_{th}$. In experiments, the CW spiral rotates with a period $T_s = 287.14s$, and the period of the applied field is $T_E = 142.85s$. So, the pacing is overdrive, and the pacing ratio $p = 2.01$.

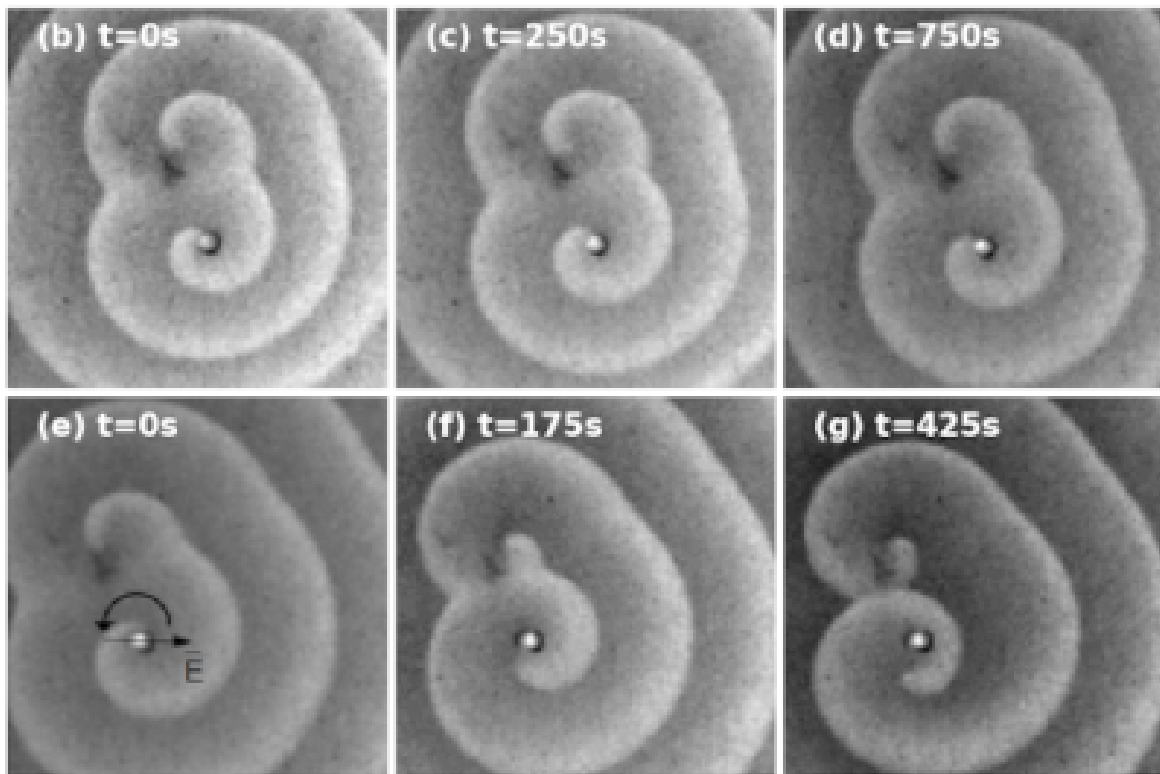


Figure 4.9: **Unpinning sequence of a CW spiral in an ACW CPEF:** The CW spiral rotates with a period $T_s = 287.14s$, and the period of the applied field is $T_E = 142.85s$.

The spiral phase difference ($\varphi_u - \varphi_0$) is plotted against the pacing ratio in the Fig.4.10. It is clear from the figures that the unpinning in every case occurred within a single spiral rotation. Except for $\varphi_u = 45^\circ$, the phase difference is less than 100° . *i.e.*, the unpinning is comparatively faster for counter-rotating spiral and CPEF.

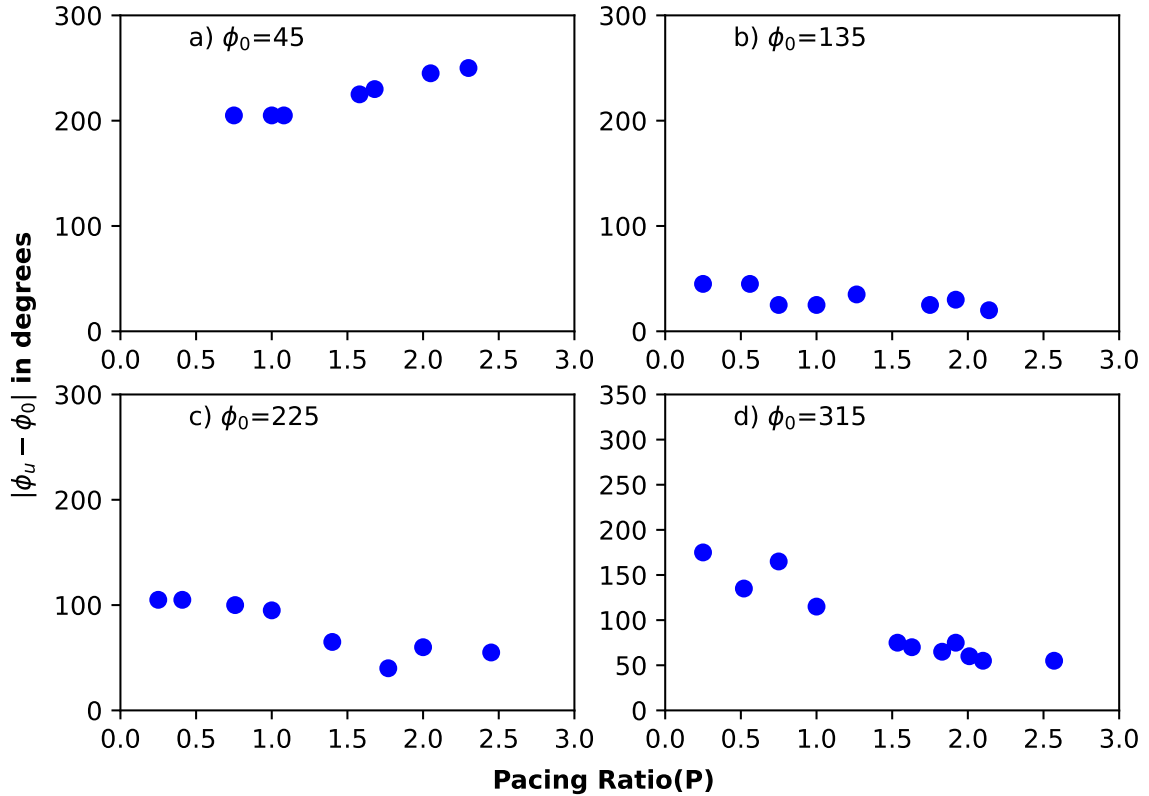


Figure 4.10: **Unpinning of CW spiral at $E=E_{th}$ with underdrive and overdrive pacing:** $|\varphi_u - \varphi_0|$ is plotted against p for different initial phases. The unpinning happens within one spiral rotation.

We have seen from Fig.4.8 that with resonant pacing, an ACW spiral (*i.e.*, a co-rotating spiral in our study) unpins only for particular initial phase values. However, a CW spiral (*i.e.*, a counter-rotating spiral in our study) with any initial phase value unpins with resonant pacing. It is evident from Fig.4.11 that the spiral phase difference ($\varphi_u - \varphi_0$) increases almost linearly with the initial spiral phase.

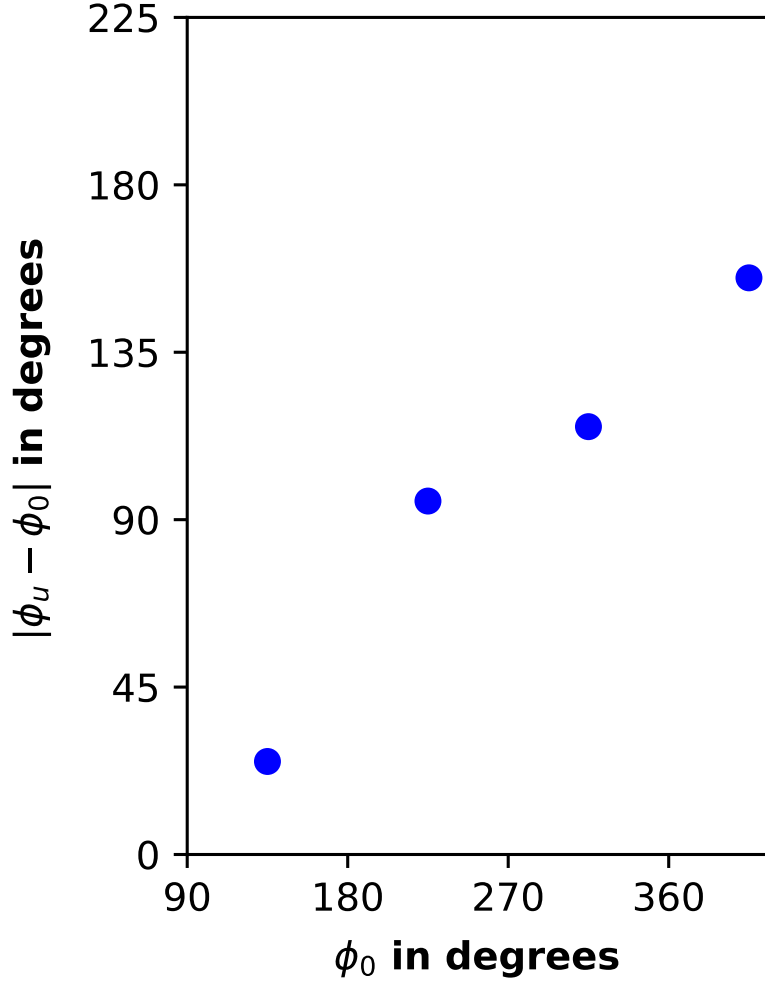


Figure 4.11: **Unpinning of CW spiral at E=Eth with resonant pacing ($p = 1$):** $|\phi_u - \phi_0|$ is plotted against initial phase, ϕ_0 . The unpinning happens with every ϕ_0 .

4.4 Conclusions

We have presented the first experimental studies of unpinning an excitation wave using a circularly polarized electric field. We observed unpinning with overdrive, underdrive, and resonant pacing in experiments and simulations of the BZ reaction. There does not exist a lower cut-off frequency of CPEF for unpinning. However, unpinning does not happen after a pacing ratio of $p=3$. It can be because of an extended refractory period of the medium compared to the time period of the CPEF. While ϕ_u is independent of ϕ_0 in the DC field, it depends linearly on the initial spiral phase in the CPEF.

The mechanism of unpinning a pinned wave in an excitable chemical medium differs from a similar process in other excitable media because of the charge on the chemical wavefront. The electric force induces retardation in the propagation of a pinned spiral, which eventually leads to the unpinning of the spiral if the field possesses a threshold amplitude. For any field strength greater than the threshold, the unpinning occurs when the electric field component along the tangential direction of spiral propagation reaches the critical threshold. Based on this condition, we can predict the unpinning phase, and the predicted values agree with those obtained in experiments and simulations.

The migration of negative bromide ions towards the anode causes retardation in the wave speed during the cycle of spiral rotation towards the cathode. The wave approaching the anode gets accelerated and decelerates as it leaves the anode. The spiral unpins only when it is being decelerated. Previous studies reported that the core size of a free-rotating spiral increases as it rotates toward the cathode and decreases as it rotates toward the anode (Agladze and De Kepper (1992)). When the core size is bigger than the size of the pinning obstacle, it is impossible to stay pinned. This could be why the unpinning happens as it rotates towards the cathode. This asymmetric interaction presents a unique situation. The anode can only 'catch' the spiral from behind while chasing it. If the anode fails to halt the spiral and overtakes it, the anode has to come back again to act on the spiral.

The unpinning demands a minimum interaction between the spiral and the field vector while the anode follows the spiral tip. For any field strength greater than the threshold, φ_u always comes within the unpinning phase window predicted by the analytical formulae. Unpinning happens at a spiral phase, immediately after the required interaction between the spiral and the field. According to the equations, φ_u depends on p , E , and φ_0 . These parameters fundamentally affect the interaction between the field vector and the spiral. Previous studies using a CPEF show that only a high-frequency CPEF can effectively control the rotating waves. However, in the BZ reaction, the unpinning is possible with a CPEF of lower frequency than the spiral wave. For a particular set of initial phases, unpinning is possible with resonant pacing ($p = 1$). With resonant pacing, unpinning is possible only when the initial position of the spiral is ahead of the anode as obtained from Eq.4.8. The variations in φ_0 with $\frac{E_{th}}{E}$ give a tongue-shaped diagram. The range of initial phases, which give unpinning with resonant pacing, increases with the applied field strength. Also, the width of the

unpinning phase increases with the field strength. It means an increase in the field strength increases the chances of unpinning. For a fixed field strength, the width of the unpinning phase window can be increased by properly choosing the pacing ratio, which is impossible with a unidirectional DC electric field.

A counter-rotating CPEF also follows the exact mechanism of unpinning explained for a co-rotating field. However, our observations indicate that unpinning is faster in a counter-rotating CPEF than in a co-rotating CPEF. Different from the case of a co-rotating spiral, with resonant pacing, the unpinning of the counter-rotating spiral occurs for all the initial spiral phase values.

Chapter 5

Conclusions

Summary

This chapter briefly describes the work carried out in this thesis. We discuss the scope for future studies in related research areas.

This work aims to study the dynamics and control of chemical excitation waves in the Belousov-Zhabotinsky (BZ) reaction with an external electric field. External control of excitation waves has interdisciplinary applications, including chemical computing, arrhythmia control in cardiac tissues, and self-propelled motion. The BZ reaction is one of the simple experimental models for studying the excitation wave dynamics. So, the excitation wave dynamics observed in other systems are expected to be qualitatively identical to that of the chemical waves. On the contrary, our studies show that the chemical excitation waves uniquely interact with an external electric field. We proposed to study the unpinning of rotating spiral waves using static and rotating electric fields in the BZ reaction. We have made considerable progress in the study, the results of which have been published in two international journals. The work presented in this thesis is summarised below.

In BZ experiments and simulations, we studied the unpinning of spiral waves with a constant DC electric field. To filter out the unpinning mechanism, we systematically measured the unpinning phase as a function of the chirality of spiral rotation, the initial phase of the spiral, the size of the pinning obstacle, the direction, and the strength of the applied electric field. The observations were intriguing: irrespective of these parameters, the unpinning always happens as the tip propagates away from the anode. We found that the spiral wave

always unpins at a fixed phase for a given field strength, except for a small range of initial phases. The tip unpins with a fixed delay when the initial phase is close to the unpinning phase.

We then presented the first experimental studies of unpinning an excitation wave using a circularly polarized electric field. The relative rotation of the spiral and the field resulted in more dynamic and exciting results. Here, we chose the rotational frequencies, initial spiral phase, and field strength as the control parameters for unpinning. The spiral unpinning as it lags behind the CPEF is identical to the observations in a DC field.

We have explained the mechanism of spiral unpinning based on the nature of the electric force on the wavefront. As the wave propagates away from the anode, it experiences an electric force opposite to its expected propagation due to the electromigration of the inhibitor bromide ions. This electric force retards the spiral propagation and induces unpinning. If the anode rotates behind the spiral, the CPEF could unpin the tip even with a lower or equal rotational frequency to that of the spiral. Based on the hypothesis, our theory accurately calculates the unpinning phase and agrees well with our observations in the static and rotating electric field. For a fixed field strength, the range of the unpinning phase can be increased by adequately choosing the pacing ratio in a CPEF, which is impossible with a unidirectional DC electric field.

Studies with different spiral chirality in the DC field have shown that the spirals with opposite chirality exhibit mirror-symmetrical unpinning with respect to the field. But in a rotating electric field, the relative rotation of the field and the spiral matters. We have performed a systematic study about the unpinning in a co-rotating field. Our trials with a counter-rotating field indicate that the unpinning is quicker than that in a co-rotating field. A detailed investigation of unpinning with a co-rotating and counter-rotating CPEF may lead to interesting observations.

From the studies conducted so far, it is clear that the response of a spiral wave to an applied field is not instantaneous. There is a delay between the field initiation and the spiral unpinning. The cause of the electric field effects in the BZ medium is the diffusion of mobile ions. Depending on the nature of the medium and the field, the characteristic time for

diffusion changes. We can relate the observed delay to the characteristic time for diffusion. A study governing the minimum period of effective interaction, which leads to unpinning in terms of diffusion, propagation speed, or field strength, can provide a better understanding of the electric field control of chemical wave dynamics. It could also find applications in the control of the self-propelled motion of the BZ droplets.

Moreover, all the studies in this thesis are restricted to a two-dimensional excitable system. By increasing the third dimension, *i.e.*, the height of the medium, it is possible to observe the scroll waves. The dynamics and control of three-dimensional excitation waves using an external electric field can be a new and promising field of research.

The ‘electric force’ acting directly on the excitation wave is a unique feature of the chemical excitation wave. Though the excitation waves show similar dynamics in physiological tissue, the field-induced unpinning in the cardiac system is based on the secondary wave emission from the obstacle boundary. We have not observed such wave emission in the chemical medium; we are also unaware of any other excitable medium where the external field can directly apply a force on the excitation wave. The electromigration of the mobile ions in the medium causes this unique behavior of the chemical wave. We have made considerable progress in understanding the electric field-induced unpinning of spiral waves in an excitable chemical medium. We hope our work will provide new insights into the control and applications of chemical waves.

Bibliography

- Agladze, K. and De Kepper, P. (1992). Influence of electric field on rotating spiral waves in the Belousov- Zhabotinskii reaction. *The Journal of Physical Chemistry*, 96(13):5239–5242.
- Agladze, K. and Steinbock, O. (2000). Waves and vortices of rust on the surface of corroding steel. *The Journal of Physical Chemistry A*, 104(44):9816–9819.
- Alonso, S., Bär, M., and Echebarria, B. (2016). Nonlinear physics of electrical wave propagation in the heart: a review. *Reports on Progress in Physics*, 79(9):096601.
- AM, Z. (1964). Periodic course of the oxidation of malonic acid in a solution (studies on the kinetics of belousov’s reaction). *Biofizika*, 9:306–311.
- Amemiya, T., Nakaiwa, M., Ohmori, T., and Yamaguchi, T. (1995). Chemical waves in mesoporous media. *Physica D: Nonlinear Phenomena*, 84(1-2):103–111.
- Amrutha, S., Sebastian, A., Sibeesh, P., Punacha, S., and Shajahan, T. (2022). Mechanism of spiral wave unpinning in the belousov–zhabotinsky reaction with a dc electric field. *The Journal of Physical Chemistry C*.
- Bánsági Jr, T., Leda, M., Toiya, M., Zhabotinsky, A. M., and Epstein, I. R. (2009). High-frequency oscillations in the belousov- zhabotinsky reaction. *The Journal of Physical Chemistry A*, 113(19):5644–5648.
- Barkley, D. (1991). A model for fast computer simulation of waves in excitable media. *Physica D: Nonlinear Phenomena*, 49(1-2):61–70.
- Behrens, S. H. and Grier, D. G. (2001). The charge of glass and silica surfaces. *The Journal of Chemical Physics*, 115(14):6716–6721.
- Belousov, B. (1973). Am zhabotinsky and a. n. zaikin. *J. Theor. Biol*, 40:45.
- Benini, O., Cervellati, R., and Fetto, P. (1996). The bz reaction: experimental and model studies in the physical chemistry laboratory. *Journal of Chemical Education*, 73(9):865.
- Benini, O., Cervellati, R., and Fetto, P. (1998). Experimental and mechanistic study of the bromomalonic acid/bromate oscillating system catalyzed by [fe (phen) 3] 2+. *International journal of chemical kinetics*, 30(4):291–300.
- Bray, W. C. (1921). A periodic reaction in homogeneous solution and its relation to catalysis. *Journal of the american chemical society*, 43(6):1262–1267.
- Chatterjee, M. and Sain, A. (2022). Dynamic surface patterns on cells. *The Journal of Chemical Physics*.

- Chen, J.-X., Zhang, H., and Li, Y.-Q. (2006). Drift of spiral waves controlled by a polarized electric field. *The Journal of Chemical Physics*, 124(1):014505.
- Chen, J.-X., Zhang, H., and Li, Y.-Q. (2009). Synchronization of a spiral by a circularly polarized electric field in reaction-diffusion systems. *The Journal of Chemical Physics*, 130(12):124510.
- Enderlein, J. and Kuhnert, L. (1996). Changing the dynamical behavior of nonlinear reaction diffusion systems by stochastic electric fields. *The Journal of Physical Chemistry*, 100(50):19642–19646.
- Feeney, R., Schmidt, S., and Ortoleva, P. (1981). Experiments on electric field-BZ chemical wave interactions: Annihilation and the crescent wave. *Physica D: Nonlinear Phenomena*, 2(3):536–544.
- Feng, X., Gao, X., Pan, D.-B., Li, B.-W., and Zhang, H. (2014). Unpinning of rotating spiral waves in cardiac tissues by circularly polarized electric fields. *Scientific reports*, 4(1):1–5.
- Fenton, F. H., Cherry, E. M., Karma, A., and Rappel, W.-J. (2005). Modeling wave propagation in realistic heart geometries using the phase-field method. *Chaos: An Interdisciplinary Journal of Nonlinear Science*, 15(1):013502.
- Field, R. J. (1985). *Oscillations and traveling waves in chemical systems*. Wiley.
- Field, R. J., Koros, E., and Noyes, R. M. (1972). Oscillations in chemical systems. ii. thorough analysis of temporal oscillation in the bromate-cerium-malonic acid system. *Journal of the American Chemical Society*, 94(25):8649–8664.
- Field, R. J. and Noyes, R. M. (1974). Oscillations in chemical systems. iv. limit cycle behavior in a model of a real chemical reaction. *The Journal of Chemical Physics*, 60(5):1877–1884.
- Ganaie, N. B. and Peerzada, G. (2009). Catalyst, co-ion and the media effect on the oscillatory behavior of resorcinol in the bz reaction. *Journal of the Brazilian Chemical Society*, 20:1262–1267.
- Ganapathisubramanian, N. and Noyes, R. M. (1982). Chemical oscillations and instabilities. part 49. additional complexities during oxidation of malonic acid in the belousov-zhabotinskii oscillating reaction. *The Journal of Physical Chemistry*, 86(26):5158–5162.
- Gruenert, G., Szymanski, J., Holley, J., Escuela, G., Diem, A., Ibrahim, B., Adamatzky, A., Gorecki, J., Dittrich, P., et al. (2013). Multi-scale modelling of computers made from excitable chemical droplets. *Int. J. Unconv. Comput.*, 9(3-4):237–266.
- Hamik, C. T., Manz, N., and Steinbock, O. (2001). Anomalous dispersion and attractive pulse interaction in the 1, 4-cyclohexanedione belousov-zhabotinsky reaction. *The Journal of Physical Chemistry A*, 105(25):6144–6153.
- Hu, L., Hu, G., and Xu, H. H. (2006). Kinetic determination of Ag^+ using a novel belousov-zhabotinskii oscillating system catalyzed by a macrocyclic complex. *Journal of Analytical Chemistry*, 61:1021–1025.

- Igarashi, Y., Gorecki, J., and Gorecka, J. N. (2006). Chemical information processing devices constructed using a nonlinear medium with controlled excitability. In *International Conference on Unconventional Computation*, pages 130–138. Springer.
- Jahnke, W., Skaggs, W., and Winfree, A. T. (1989). Chemical vortex dynamics in the belousov-zhabotinskii reaction and in the two-variable oregonator model. *The Journal of Physical Chemistry*, 93(2):740–749.
- Jahnke, W. and Winfree, A. T. (1991). Recipes for belousov-zhabotinsky reagents. *Journal of Chemical Education*, 68(4):320.
- Ji, L., Zhou, Y., Li, Q., Qiao, C., and Ouyang, Q. (2013). Experimental evidence of using a circularly polarized electric field to control spiral turbulence. *Physical Review E*, 88(4):042919.
- Jiménez, Z. A., Marts, B., and Steinbock, O. (2009). Pinned scroll rings in an excitable system. *Physical review letters*, 102(24):244101.
- Jiménez, Z. A., Zhang, Z., and Steinbock, O. (2013). Electric-field-controlled unpinning of scroll waves. *Physical Review E*, 88(5):052918.
- Körös, E. (1974). Monomolecular treatment of chemical oscillation. *Nature*, 251(5477):703–704.
- Körös, E., Burger, M., Friedrich, V., Ladányi, L., Nagy, Z., and Orbán, M. (1974). Chemistry of belousov-type oscillating reactions. In *Faraday Symposia of the Chemical Society*, volume 9, pages 28–37. Royal Society of Chemistry.
- Krüger, F., Nagy-Ungvárai, Z., and Müller, S. C. (1995). Influence of organic acids on oscillations and waves in the ferroin-catalyzed belousov-zhabotinsky reaction. *Physica D: Nonlinear Phenomena*, 84(1-2):95–102.
- Kumar, D. J. P., Borkar, C., and Dayal, P. (2021). Fast-moving self-propelled droplets of a nanocatalyzed belousov–zhabotinsky reaction. *Langmuir*, 37(43):12586–12595.
- Kurin-Csörgei, K., Zhabotinsky, A. M., Orbán, M., and Epstein, I. R. (1996). Bromate-1, 4-cyclohexanedione- ferroin gas-free oscillating reaction. 1. basic features and crossing wave patterns in a reaction- diffusion system without gel. *The Journal of Physical Chemistry*, 100(13):5393–5397.
- Li, B.-W., Cai, M.-C., Zhang, H., Panfilov, A. V., and Dierckx, H. (2014). Chiral selection and frequency response of spiral waves in reaction-diffusion systems under a chiral electric field. *The Journal of Chemical Physics*, 140(18):184901.
- Li, B.-W., Deng, L.-Y., and Zhang, H. (2013). Chiral symmetry breaking in a reaction-diffusion system. *Physical Review E*, 87(4):042905.
- Li, T.-C., Gao, X., Zheng, F.-F., Pan, D.-B., Zheng, B., and Zhang, H. (2017). A theory for spiral wave drift induced by ac and polarized electric fields in chemical excitable media. *Scientific Reports*, 7(1):1–9.
- Lim, Z. Y., Maskara, B., Aguel, F., Emokpae Jr, R., and Tung, L. (2006). Spiral wave attachment to millimeter-sized obstacles. *Circulation*, 114(20):2113–2121.

- Luther, S., Fenton, F. H., Kornreich, B. G., Squires, A., Bittihn, P., Hornung, D., Zabel, M., Flanders, J., Gladuli, A., Campoy, L., et al. (2011). Low-energy control of electrical turbulence in the heart. *Nature*, 475(7355):235–239.
- Mahanta, D., Das, N. P., and Dutta, S. (2018). Spirals in a reaction-diffusion system: dependence of wave dynamics on excitability. *Physical Review E*, 97(2):022206.
- Maselko, J. and Showalter, K. (1989). Chemical waves on spherical surfaces. *Nature*, 339(6226):609–611.
- Mikhailov, A. S. and Showalter, K. (2006). Control of waves, patterns and turbulence in chemical systems. *Physics Reports*, 425(2-3):79–194.
- Muñuzuri, A., Gómez-Gesteira, M., Pérez-Muñuzuri, V., Krinsky, V., and Pérez-Villar, V. (1993). Mechanism of the electric-field-induced vortex drift in excitable media. *Physical Review E*, 48(5):R3232.
- Munuzuri, A., Gómez-Gesteira, M., Pérez-Muñuzuri, V., Krinsky, V., and Pérez-Villar, V. (1994). Parametric resonance of a vortex in an active medium. *Physical Review E*, 50(5):4258.
- Noyes, R. M. (1972). R. 3. field, and e. k&es. *J. Amer. Chem. Soc.*, 95:1394.
- Oliver, S., Petteri, K., and Kenneth, S. (1996). Chemical wave logic gates. *The Journal of Physical Chemistry*, 100(49):18970–18975.
- Ostwald, W. (1899). *Abhandlungen der königlich sächsischen gesellschaft der wissenschaften zu leipzig*.
- Pan, D.-B., Gao, X., Feng, X., Pan, J.-T., and Zhang, H. (2016). Removal of pinned scroll waves in cardiac tissues by electric fields in a generic model of three-dimensional excitable media. *Scientific Reports*, 6(1):1–8.
- Pechenkin, A. (2018). Liesegang rings and the other periodic phenomena. In *The History of Research on Chemical Periodic Processes*, pages 9–28. Springer.
- Pérez-Muñuzuri, V., Aliev, R., Vasiev, B., and Krinsky, V. (1992). Electric current control of spiral wave dynamics. *Physica D: Nonlinear Phenomena*, 56(2-3):229–234.
- Porjai, P., Sutthiopad, M., Luengviriyi, J., Phantu, M., Müller, S. C., and Luengviriyi, C. (2016). Electrically forced unpinning of spiral waves from circular and rectangular obstacles. *Chemical Physics Letters*, 660:283–286.
- Prigogine, I. and Lefever, R. (1968). Symmetry breaking instabilities in dissipative systems. ii. *The Journal of Chemical Physics*, 48(4):1695–1700.
- Pumir, A., Nikolski, V., Hörning, M., Isomura, A., Agladze, K., Yoshikawa, K., Gilmour, R., Bodenschatz, E., and Krinsky, V. (2007). Wave emission from heterogeneities opens a way to controlling chaos in the heart. *Physical Review Letters*, 99(20):208101.
- Punacha, S., A, N. K., and Shajahan, T. K. (2020). Theory of unpinning of spiral waves using circularly polarized electric fields in mathematical models of excitable media. *Physical Review E*, 102(3):032411.

- Punacha, S., Berg, S., Sebastian, A., Krinski, V. I., Luther, S., and Shajahan, T. (2019). Spiral wave unpinning facilitated by wave emitting sites in cardiac monolayers. *Proceedings of the Royal Society A*, 475(2230):20190420.
- Rastogi, R., Singh, S., and Chand, P. (2004). Oscillatory characteristics of a b–z reacting system with xylose and oxalic acid as mixed substrate. *Chemical physics letters*, 385(5–6):403–408.
- Sadeghi, P., Dunphy, K., Punckt, C., and Rotermund, H. (2012). Inversion of pattern anisotropy during CO oxidation on pt (110) correlated with appearance of subsurface oxygen. *The Journal of Physical Chemistry C*, 116(7):4686–4691.
- Sawai, S., Thomason, P. A., and Cox, E. C. (2005). An autoregulatory circuit for long-range self-organization in dictyostelium cell populations. *Nature*, 433(7023):323–326.
- Schmidt, B. and Müller, S. C. (1997). Forced parallel drift of spiral waves in the Belousov-Zhabotinsky reaction. *Physical Review E*, 55(4):4390.
- Schmidt, S. and Ortoleva, P. (1977). A new chemical wave equation for ionic systems. *The Journal of Chemical Physics*, 67(8):3771–3776.
- Schmidt, S. and Ortoleva, P. (1979). Multiple chemical waves induced by applied electric field. *The Journal of Chemical Physics*, 71(2):1010–1015.
- Schmidt, S. and Ortoleva, P. (1981). Electric field effects on propagating bz waves: Predictions of an oregonator and new pulse supporting models. *The Journal of Chemical Physics*, 74(8):4488–4500.
- Sevcik, P. and Adamcikova, L. (1985). The oscillating belousov-zhabotinsky type reaction with saccharides. *The Journal of Physical Chemistry*, 89(24):5178–5179.
- Ševčíková, H. and Marek, M. (1983). Chemical waves in electric field. *Physica D: Nonlinear Phenomena*, 9(1-2):140–156.
- Ševčíková, H., Schreiber, I., and Marek, M. (1996). Dynamics of oxidation belousov-zhabotinsky waves in an electric field. *The Journal of Physical Chemistry*, 100(49):19153–19164.
- Shajahan, T. K., Berg, S., Luther, S., Krinski, V., and Bittihn, P. (2016). Scanning and resetting the phase of a pinned spiral wave using periodic far field pulses. *New Journal of Physics*, 18(4):043012.
- Shanks, N. (2001). Modeling biological systems: the belousov–zhabotinsky reaction. *Foundations of Chemistry*, 3(1):33–53.
- Sibeesh, P., Amrutha, S., and Shajahan, T. (2022). Variations in the scroll ring characteristics with the excitability and the size of the pinning obstacle in the bz reaction. In *Nonlinear Dynamics and Applications: Proceedings of the ICNDA 2022*, pages 1311–1317. Springer.
- Steinbock, O. and Müller, S. (1993). Light-controlled anchoring of meandering spiral waves. *Physical Review E*, 47(3):1506.

- Steinbock, O., Schütze, J., and Müller, S. (1992). Electric-field-induced drift and deformation of spiral waves in an excitable medium. *Physical Review Letters*, 68(2):248.
- Steinbock, O., Zykov, V., and Müller, S. C. (1993). Control of spiral-wave dynamics in active media by periodic modulation of excitability. *Nature*, 366(6453):322–324.
- Suematsu, N. J. and Nakata, S. (2018). Evolution of self-propelled objects: From the viewpoint of nonlinear science. *Chemistry—A European Journal*, 24(24):6308–6324.
- Sutthiopad, M., Luengviriyaya, J., Porjai, P., Phantu, M., Kanchanawarin, J., Müller, S. C., and Luengviriyaya, C. (2015). Propagation of spiral waves pinned to circular and rectangular obstacles. *Physical Review E*, 91(5):052912.
- Sutthiopad, M., Luengviriyaya, J., Porjai, P., Tomapatanaget, B., Müller, S. C., and Luengviriyaya, C. (2014). Unpinning of spiral waves by electrical forcing in excitable chemical media. *Physical Review E*, 89(5):052902.
- Szymanski, J., Gorecka, J. N., Igarashi, Y., Gizynski, K., Gorecki, J., Zauner, K.-P., Planque, M., et al. (2011). Droplets with information processing ability. *Int. J. Unconv. Comput.*, 7(3):185–200.
- Tam, W., Horsthemke, W., Noszticzius, Z., and Swinney, H. L. (1988). Sustained spiral waves in a continuously fed unstirred chemical reactor. *The Journal of chemical physics*, 88(5):3395–3396.
- Teng, R., Ren, L., Yuan, L., Wang, L., Gao, Q., and Epstein, I. R. (2019). Effect of reaction parameters on the wavelength of pulse waves in the belousov–zhabotinsky reaction–diffusion system. *The Journal of Physical Chemistry A*, 123(43):9292–9297.
- Vanag, V. K. and Epstein, I. R. (2008). Patterns of nanodroplets: the belousov-zhabotinsky-aerosol ot-microemulsion system. *Self-Organized Morphology in Nanostructured Materials*, pages 89–113.
- Vavilin, V., Gulak, P., Zhabotinskii, A., and Zaikin, A. (1969). Complex iron ions as catalysts for the autooscillating oxidation of malonic acid and its analogs with bromate. *Bulletin of the Academy of Sciences of the USSR, Division of chemical science*, 18:2467–2467.
- Winfrey, A. (1974). Two kinds of wave in an oscillating chemical solution. In *Faraday Symposia of the Chemical Society*, volume 9, pages 38–46. Royal Society of Chemistry.
- Winfrey, A. T. (1972). Spiral waves of chemical activity. *Science*, 175(4022):634–636.
- Winfrey, A. T. (1973). Scroll-shaped waves of chemical activity in three dimensions. *Science*, 181(4103):937–939.
- Winston, D., Arora, M., Maselko, J., Gáspár, V., and Showalter, K. (1991). Cross-membrane coupling of chemical spatiotemporal patterns. *Nature*, 351(6322):132–135.
- Wood, P. M. and Ross, J. (1985). A quantitative study of chemical waves in the belousov–zhabotinsky reaction. *The Journal of chemical physics*, 82(4):1924–1936.
- Yamaguchi, T., Kuhnert, L., Nagy-Ungvarai, Z., Müller, S., and Hess, B. (1991). Gel systems for the belousov-zhabotinskii reaction. *The Journal of Physical Chemistry*, 95(15):5831–5837.

- Zaikin, A. and Zhabotinsky, A. (1970). Concentration wave propagation in two-dimensional liquid-phase self-oscillating system. *Nature*, 225(5232):535–537.
- Zhabotinsky, A. and Zaikin, A. (1971). Oscillatory processes in biological and chemical systems. *Pushchino on Oka*, 2:279–283.
- Zhabotinsky, A. and Zaikin, A. (1973). Autowave processes in a distributed chemical system. *Journal of theoretical biology*, 40(1):45IN157–56IN361.
- Zhabotinsky, A. M. (1964). Periodical oxidation of malonic acid in solution (a study of the belousov reaction kinetics). *Biofizika*, 9:306–311.
- Zhang, Y. X., Foerster, P., and Ross, J. (1992). Origin of spontaneous wave generation in an oscillatory chemical system. *The Journal of Physical Chemistry*, 96(22):8898–8904.

List of publications

Peer Reviewed International Journal

- Amrutha, S. V., Sebastian, A., Sibeesh, P., Punacha, S., & Shajahan, T. K. (2022). Mechanism of Spiral Wave Unpinning in the Belousov–Zhabotinsky Reaction with a DC Electric Field. *The Journal of Physical Chemistry C*, 126(46), 19618-19626.
- SV, Amrutha, Anupama Sebastian, Puthiyapurayil Sibeesh, Shreyas Punacha, and T. K. Shajahan. Theory and experiments of spiral unpinning in the Belousov-Zhabotinsky reaction using a circularly polarized electric field. *Chaos* 33, 063157 (2023).

Peer Reviewed International Journal proceedings

- Sebastian, A., Amrutha, S. V., Punacha, S., & Shajahan, T. K. (2022). Dynamics of Chemical Excitation Waves Subjected to Subthreshold Electric Field in a Mathematical Model of the Belousov-Zhabotinsky Reaction. In *Nonlinear Dynamics and Applications* (pp. 1241-1249). Springer, Cham.
- Sibeesh, P., Amrutha, S. V., & Shajahan, T. K. (2022). Variations in the Scroll Ring Characteristics with the Excitability and the Size of the Pinning Obstacle in the BZ Reaction. In *Nonlinear Dynamics and Applications* (pp. 1311-1317). Springer, Cham.

International Conferences Presentations

- Conference on Nonlinear Systems and Dynamics (CNSD), School of Computational and Integrative Sciences, Jawaharlal Nehru University, New Delhi, October 11-14, 2018.
- 13th Conference on Nonlinear Systems & Dynamics (CNSD-2021), Sastra University (online), December 17-22, 2021.

CURRICULUM VITAE

Personal Data

Name : Amrutha S V

Permanent Address : Mrithyunjaya, Kaniyankunnu, PO Kozhummal

Pin code: 670521, Kerala, India.

Present Address: Type-III 301, NITK Quarters, NITK, Surathkal,

PO Srinivasnagar, Pin code: 575025

Marital Status : Married

Date of Birth :05-10-1991

Citizenship : Indian

email : svamrutha@gmail.com

Mobile : 8547060990

Sex : Female

Educational Details

- 2015 to 2023 - PhD in Physics, National Institute of Technology Karnataka, Surathkal, Field: Nonlinear Dynamics
Advisor: Dr. T K Shajahan
- 2014 - Master of Science in Physics from National Institute of Technology Karnataka with 1st Class (91.1%).
- 2012 - Bachelor of Science in Physics from University of Kannur with 1st Class (89%).
- 2009 - 12th from Kerala State Board with First Class (88%).
- 2007 - 10th from Kerala State Board with First Class (A+ in all the subjects).

Projects

-Synthesis and characterisation of calcium phosphate glasses with fly ash (MSc Project)

-Structural, thermodynamic and physical properties of materials using Molecular Dynamics (STIP 2013, IGCAR Kalpakkam)

-Determination of Planck's constant using LEDs (Bsc Project)

Awards and achievements

-2015 March

GATE-2015 , Graduate Aptitude Test in Engineering (GATE) in Physics with rank 265

-2014 May

Secured 1st rank with gold medal in MSc Physics from National Institute of Technology Karnataka

Scholarships

2017-2021: Senior Research Fellowship, Ministry of Human Resource Development, National Institute of Technology Karnataka, Surathkal, India.

2015-2020: Junior Research Fellowship, Ministry of Human Resource Development, National Institute of Technology Karnataka, Surathkal, India.

Computational Skills

- Operating System: Windows ,Ubuntu
- Programming Languages: Python
- Markup language:Latex
- Office Package: Word, Excel, Powerpoint
- Languages : Malayalam (mothertongue), English, Hindi

Research Intrests

- Nonlinear Dynamics
- Pattern formation in Excitable Media
- Spiral and Scroll Waves
- Low Voltage Defibrillation
- Computational Biology
- Cardiac Arrhythmias
- Neuroscience
- Self-propelled motion and microswimmers
- Chemical and Biological Excitable Systems
- Biophysics

Experience

2016-2017: Mentored Masters student project.

2015-2017: Teaching Assistant for B.Tech. Physics Course at NITK Surathkal.

2015-2016: Laboratory Teaching Assistant for M.Sc. Physics Laboratory at NITK Surathkal.

2015-2020: Laboratory Teaching Assistant for B.Tech. Physics Laboratory at NITK Surathkal.

Conferences

2018 - Conference on Nonlinear Systems and Dynamics, Jawaharlal Nehru University, New Mehrauli Road, Delhi.

2021- Conference on Nonlinear Systems and Dynamics (CNSD-2021), Centre for Nonlinear Science & Engineering, SEEE, SASTRA deemed University, Thanjavur

Research Publications

1. Amrutha, S. V., Sebastian, A., Sibeesh, P., Punacha, S., & Shajahan, T. K. (2022). Mechanism of Spiral Wave Unpinning in the Belousov–Zhabotinsky Reaction with a DC Electric

- Field. *The Journal of Physical Chemistry C*, 126(46), 19618-19626.
2. SV, Amrutha, Anupama Sebastian, Puthiyapurayil Sibeesh, Shreyas Punacha, and T. K. Shajahan. Theory and experiments of spiral unpinning in the Belousov-Zhabotinsky reaction using a circularly polarized electric field. *Chaos* 33, 063157 (2023).
 3. Sibeesh, P., Amrutha, S. V., & Shajahan, T. K. (2022). Variations in the Scroll Ring Characteristics with the Excitability and the Size of the Pinning Obstacle in the BZ Reaction. In *Nonlinear Dynamics and Applications* (pp. 1311-1317). Springer, Cham.
 4. Sebastian, A., Amrutha, S. V., Punacha, S., & Shajahan, T. K. (2022). Dynamics of Chemical Excitation Waves Subjected to Subthreshold Electric Field in a Mathematical Model of the Belousov-Zhabotinsky Reaction. In *Nonlinear Dynamics and Applications* (pp. 1241-1249). Springer, Cham.